Comput. Methods Appl. Mech. Engrg. 257 (2013) 221–247

Contents lists available at SciVerse ScienceDirect

Comput. Methods Appl. Mech. Engrg.

journal homepage: www.elsevier.com/locate/cma

Failure-Oriented Multi-scale Variational Formulation: Micro-structures with nucleation and evolution of softening bands

P.J. Sánchez [a,b,*], P.J. Blanco [c,d], A.E. Huespe [a], R.A. Feijóo [c,d]

[a] CIMEC-INTEC-UNL-CONICET, Güemes 3450, CP 3000 Santa Fe, Argentina
[b] GIMNI-UTN-FRSF, Lavaisse 610, CP 3000 Santa Fe, Argentina
[c] LNCC/MCTI Laboratório Nacional de Computação Científica, Getúlio Vargas 333, Petrópolis, Río de Janeiro, CEP: 25651-075, Brazil
[d] INCT-MACC Instituto Nacional de Ciência e Tecnologia em, Medicina Assistida por Computação Científica, Brazil

ARTICLE INFO

Article history:
Received 18 January 2012
Received in revised form 20 November 2012
Accepted 23 November 2012
Available online 5 December 2012

Keywords:
Multi-scale variational formulations
Strain localization bands
Heterogeneous material failure
Homogenized cohesive models

ABSTRACT

This contribution presents the theoretical foundations of a *Failure-Oriented Multi-scale variational Formulation* (*FOMF*) for modeling heterogeneous *softening-based* materials undergoing strain localization phenomena. The multi-scale model considers two coupled mechanical problems at different physical length scales, denoted as *macro* and *micro* scales, respectively. Every point, at the macro scale, is linked to a *Representative Volume Element* (*RVE*), and its constitutive response emerges from a consistent homogenization of the micro-mechanical problem.

At the macroscopic level, the initially continuum medium admits the nucleation and evolution of cohesive cracks due to progressive strain localization phenomena taking place at the microscopic level and caused by shear bands, damage or any other possible failure mechanism. A cohesive crack is introduced in the macro model once a specific macroscopic failure criterion is fulfilled.

The novelty of the present *Failure-Oriented Multi-scale Formulation* is based on a proper kinematical information transference from the *macro-to-micro* scales during the complete loading history, even in those points where macro cracks evolve. In fact, the proposed *FOMF* includes two multi-scale sub-models consistently coupled:

(i) a *Classical Multi-scale Model* (*ClaMM*) valid for the stable macro-scale constitutive response.
(ii) A novel *Cohesive Multi-scale Model* (*CohMM*) valid, once a macro-discontinuity surface is nucleated, for modeling the macro-crack evolution.

When a macro-crack is activated, two important kinematical assumptions are introduced: (i) a change in the rule that defines how the increments of generalized macro-strains are inserted into the micro-scale and (ii) the *Kinematical Admissibility* concept, from where proper *Strain Homogenization Procedures* are obtained. Then, as a consequence of the Hill–Mandel Variational Principle and the proposed kinematical assumptions, the *FOMF* provides an adequate homogenization formula for the stresses in the continuum part of the body, as well as, for the traction acting on the macro-discontinuity surface.

The assumed *macro-to-micro* mechanism of kinematical coupling defines a specific admissible *RVE*-displacement space, which is obtained by incorporating additional boundary conditions, *Non-Standard Boundary Conditions* (*NSBC*), in the new model. A consequence of introducing these *Non-Standard Boundary Conditions* is that they guarantee the existence of a physically admissible *RVE*-size, a concept that we call through the paper "*objectivity*" of the homogenized constitutive response.

Several numerical examples are presented showing the *objectivity* of the formulation, as well as, the capabilities of the new multi-scale approach to model material failure problems.

1. Introduction

Materials, in general, have an intrinsic heterogeneous nature. From a micro-structural point of view, they can be composed of a number of constituents and heterogeneities that govern the mechanical response of the material at the macro-structural level. For example, the evolution of inelastic/dissipative mechanisms, as well as the nucleation process of macroscopic failure phenomena, usually depends on the complex interaction between defects and heterogeneities at smaller length scales. Thus, suitable theoretical frameworks based on *Multi-scale* formulations arise as a powerful modeling tool to describe more general heterogeneous material

* Corresponding author at: CIMEC-INTEC-UNL-CONICET, Güemes 3450, CP 3000 Santa Fe, Argentina.
E-mail address: psanchez@intec.unl.edu.ar (P.J. Sánchez).

0045-7825/$ - see front matter © 2012 Elsevier B.V. All rights reserved.
http://dx.doi.org/10.1016/j.cma.2012.11.016

responses or, according to the particular interest of the present contribution, to understand more precisely the phenomenologies leading to material failure.

During the last decades, a great diversity of multi-scale methodologies for material modeling has been proposed and formulated from different perspectives, such as the approaches based on: the *Effective Medium* [8,24], the *Self-Consistent Models* [14,5], the *Variational Boundary Methods* [13,43], the *Homogenization Theory of Asymptotic Expansions* [35,10], among others. All these strategies have rigorous conceptual foundations and have been deduced using analytical or semi-analytical procedures. Nevertheless, they are restricted to micro-structures with simple topology of heterogeneities or adopt specific assumptions, limiting the scope of their applicability, specially if material failure is addressed.

In order to circumvent these limitations, multi-scale techniques based on the existence of a statistically *Representative Volume Element* (*RVE*), which is associated to the scale where the material heterogeneities are observable, have gained popularity [21–23]. A particular class of this *multi-scale* methodology uses two different scales: the "*macro*" and the "*micro*" scale, although generalizations for including additional length scales could be considered. In such approach, it is assumed that the constitutive behavior at the *macro-scale* is derived by means of two basic steps: (i) a specific insertion process of the macro strains into the *RVE* domain, which is interpreted as the prescribed action stimulating the micro mechanical problem; this step is sometimes called "*localization*" by some authors [9] and (ii) a variationally consistent homogenization procedure, or volumetric average, of the constitutive response at the micro-level. Specific kinematical constraints, as well as energetic equivalence principles, are additionally included in the model to obtain a consistent mechanical framework.

In this kind of approach, the notion of constitutive equation is a concept that is only defined at the micro-structural level (*RVE*-level). Meanwhile, at the macro-level, the material response is a consequence of the micro mechanical behavior and the adopted model to transfer the information between scales. From this perspective, the constitutive model defined in the micro-mechanical problem turns out to be a particularly important ingredient in the multi-scale formulation.

Regarding the following two general local continuum constitutive relation categories that can be adopted to describe the micro-mechanical response:

- Constitutive relations derived from associative flow rules and hardening-based inelastic evolutions models, here called for simplicity *Standard* or *Generalized Associative Materials*.
- Constitutive relations based on non-associative flow rules or strain softening models, generally adopted for describing degradation mechanisms and failure,

and inspired in the issues addressed in this paper; the fundamental difference between them is attributed to the intrinsic ability of the *Softening*-based material models to induce strain localization into narrow bands. These strain localization bands are the precursor to the development of strong discontinuities, which can be associated with cracks, shear bands, etc. On the contrary, the *Standard or Generalized* materials completely inhibit the development of strain localization bands.

A number of well-established two-scale *RVE*-based approaches using *Generalized/Associative Materials* has been proposed in the literature, see for example [21,23,40,41,29] and references cited therein. We call this family of approaches: the "*Classical Multi-scale Model* (*ClaMM*)". However, in their present form, they cannot be applied to problems involving material failure because they give inconsistent results, as will be shown in the following.

Adoption of materials with softening, for modeling failure at the micro-mechanical level as a mechanism inducing degradation at the macro-level, introduces some theoretical issues which should be particularly considered in the development of multi-scale formulations. Aside from the well-known fact that continuum onstitutive equations with softening have to be regularized, we mention that:

- Material softening induces dissimilar mechanical regimes in the *RVE* domain, such as *loading* into strain localization bands and *unloading* in the remaining domain. Under favorable kinematical conditions, this strain-localization phenomenon can evolve throughout the *RVE* and, eventually, nucleate a bifurcation mode at the macro scale. Hence, the traditional assumptions of *Classical Multi-scale Models* by which a macro-strain is uniformly distributed into the micro-cell, as well as, the standard stress homogenization procedure extended over the entire *RVE* domain, have a debatable physical meaning and need to be reformulated.
- Strain localization phenomena induce a "*size-effect*" in the micro-cell response, a well-known behavior in the context of structural analysis [2]. A consequence of this, in the Classical Multi-scale setting, is that the stress homogenized response becomes sensitive with respect to the micro-cell size [11]. Then, some action must be adopted to remove this deficient behavior.

From these observations, an alternative class of multi-scale models should be developed whenever strain localization phenomena are considered. Pursuing this objective, recent contributions have been proposed. For instance, Belytschko and co-workers [4,39] presented a specific stress homogenization procedure excluding, from the integration domain where the stresses are averaged, the zones where strain localization is detected. They called this methodology the "*Multi-scale Aggregating Discontinuities*" model. By construction, the so obtained homogenized mechanical response keeps the material stability. A connection between the micro-cell domain measure and the finite element size at the macro-level is introduced.

A second-order (gradient-based) computational homogenization scheme has been proposed by Kouznetsova and co-authors [16–18]. Recently, this model has been adapted for the analysis of strain localization problems introducing a generalized periodicity boundary condition, that is aligned with the direction of the localization band developed in the micro scale domain [6].

An alternative technique for modeling the constitutive response of a "*pre-existent*" macro-adhesive discontinuity is due to Matouš and co-workers [20,19]. They postulated a multi-scale model based on the existence of a *volumetric* heterogeneous *RVE*, linked to the macroscopic adhesive-interface. A limitation of their approach is that the thickness of the assumed *RVE* is associated with the physical thickness of the macro-adhesive surface. They do not give a procedure to determine the *RVE* cell size in more general problems. An additional limitation of this model is that it cannot be trivially extended to nucleate discontinuities from an initially continuum medium. Thus, according to the authors, the discontinuity surfaces must be predefined in the body.

Verhoosel et al. [42] developed a method for determining the homogenized macro cohesive model derived from micro-structures with possible nucleation of micro-cohesive cracks and adhesive micro-interfaces. Nguyen et al. [26] have extended this proposal to include micro-cells with a damaged material model regularized with an enhanced gradient approach. They also introduced the notion of "*failure zone averaging technique*", where the homogenized procedure for micro-stresses is only extended over the *RVE* active damaged sub-domain. Although the so-called

"*failure zone averaging technique*" seems to have a consistent physical meaning, this concept is presented as an "*a priori*" mechanical definition and there is no clear relation established between the imposed macro and micro kinematics. The authors show, through numerical experimentation, the existence of objective macro responses, with respect to the *RVE*-size.

Up to the authors' knowledge, a unified framework based exclusively in physical/modeling arguments, and not only on numerical ones, where the adopted hypotheses and derived consequences are well established and fully justified, has not yet been completely developed in the context of material failure multi-scale modeling. This subject remains an open issue at present and this paper addresses some contributions in this direction.

In this contribution we present a *Failure-Oriented Multi-scale Formulation* (*FOMF*) that uses a specific insertion of macro-strains into the micro scale domain [34]. The *Insertion Operator* is incorporated in the kinematical description of the *RVE* and it is used to introduce the concept of *Kinematical Admissibility* between the strains at macro and micro levels. Then, following a purely variational framework, a number of associated mechanical consequences are derived, as for example the micro-equilibrium problem and the stress homogenization procedure. The *FOMF* comprehends two multi-scale sub-models sequentially coupled in a consistent manner: (i) a *Classical Multi-scale Model* (*ClaMM*) and (ii) a new *Cohesive Multi-scale Model* (*CohMM*). A number of distinguishing features of the *FOMF* are shown in detail in the body of the paper and they are summarized as follows:

(I) We systematically follow a well established variational methodology.
(II) All developments are based on "*kinematical hypotheses*".
(III) The generalized stress homogenization procedures arise as a "*consequence*" of the formulation, as a dual concept from the adopted kinematical hypotheses (ruled by the *Insertion Operator*) and consistent with the Hill–Mandel principle. Thus, they are not an "*a priori*" definition. Furthermore, this generalized stress homogenization procedure is characterized by an integration over specific *RVE* sub-domains, and not over the entire micro-cell.
(IV) The topology of the *RVE* sub-domain, where the strain localization takes place, emerges from the evolution of the mechanical problem. It depends on the complexities of the underlying micro-structure and the loading history.
(V) The proposed formulation is able to nucleate a macro cohesive crack, and model its evolution, from an initially classical macro-continuum medium. Therefore, the *classical* or *standard* multi-scale model represents a particular case of the proposed multi-scale formulation.
(VI) The micro-mechanical problem is solved considering new kinematical constraints, imposed through additional boundary conditions that naturally emerge in the present formulation. *By construction*, they assure the *objectivity* of the model with respect to the *RVE*-size.

Since our interest in this paper is to highlight the fundamental aspects of the formulation, additional topics such as: the constitutive softening regularization model adopted at the *RVE*-level, the classical displacement boundary conditions defined in the *RVE* describing the Taylor, Linear or Periodic models among others, are not discussed in detail in this manuscript.

The remainder of this document is structured as follows. In Section 2, the governing equations for a macro-mechanical problem, in which failure mechanisms in the form of cohesive cracks can nucleate and evolve, are discussed. The need for two homogenization rules is shown: a classical model for the stress–strain response during the macroscopic pre-bifurcation stage and a new one, giving a traction-separation cohesive model for the evolution of macroscopic displacement discontinuities. Such discontinuities are activated after detecting a macroscopic bifurcation point, and this is discussed in Section 2.2. Section 3 is devoted to reviewing the foundations of *Classical Multi-scale Models* (*ClaMM*). Some general operators, useful for the subsequent developments, are introduced. In Section 4, a new variational formulation is discussed in detail. We show that, following the same basic theoretical steps used in the context of *ClaMM* and introducing additional ingredients, a well-posed model, called *Cohesive Multi-scale Model* (*CohMM*) which captures objective cohesive responses from a degraded/localized *RVE*, is obtained. Section 5 presents several numerical examples showing the mechanical consistency of the complete multi-scale formulation here proposed (*FOMF*). In Section 6 the important role played by the kinematical restriction imposed on the boundary of the strain localization domain, named in the paper as *NSBC*, is highlighted through several examples. Conclusions are exposed in Section 7. For the sake of completeness, Appendix A is devoted to a brief description concerning the numerical techniques used for the *FOMF* implementation into a finite element code.

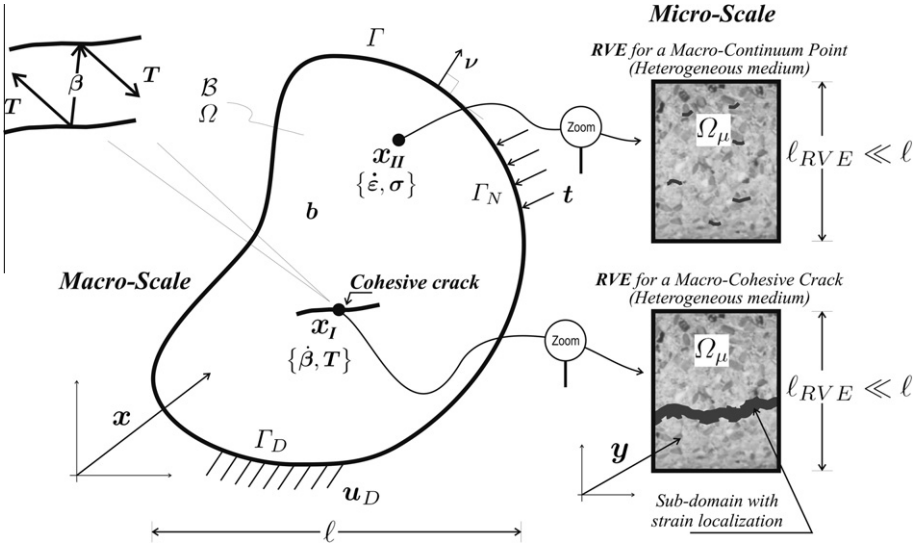

Fig. 1. Multi-scale (macro–micro) model idealization for failure analysis.

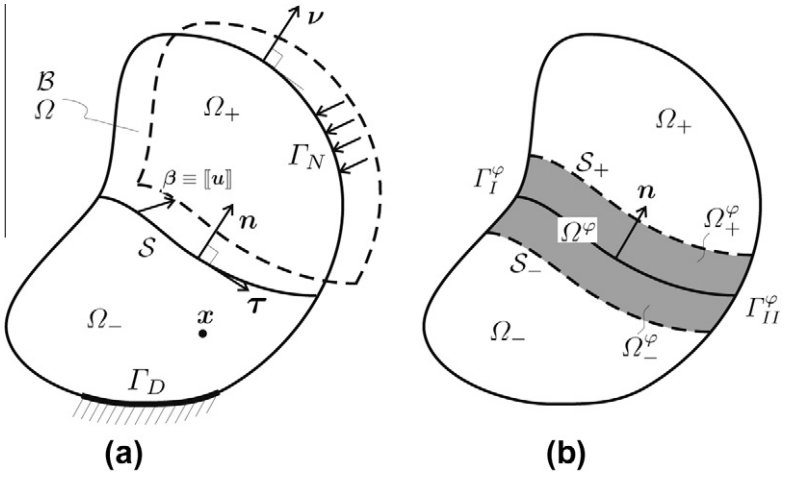

Fig. 2. Basic ingredients and nomenclature defining a mechanical problem exhibiting strong discontinuities across the material surface $\mathcal{S}$.

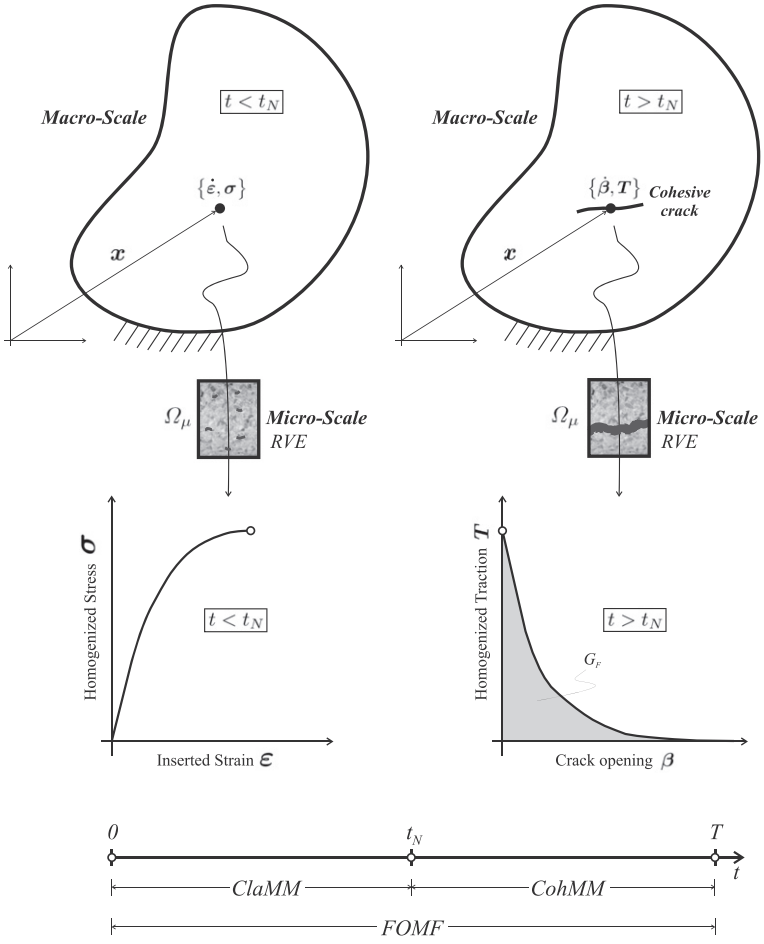

Fig. 3. Schematic representation of the whole constitutive response provided by the proposed *Failure-Oriented Multi-scale Formulation (FOMF)*.

2. Macro-model with cohesive crack for modeling material failure

In the subsequent paragraphs, the main features of the macro-mechanical equilibrium problem, along with the associated set of governing equations, are presented. The purpose of this Section is to provide the reader a comprehensive presentation of the coupled macro–micro multi-scale formulation. The model is fully determined with the developments addressed in the forthcoming Sections 3 and 4. A summary of the multi-scale formulation developed in this Section is presented in Box 1.

2.1. Preliminaries

The following premises define the basic assumptions of the model:

(i) Quasi-static problems are considered. A monotonically increasing pseudo-time variable $t \in [0,T]$, which belongs to the pre-established interval of analysis $[0,T]$, is used to account for the evolution of the non-linear material response.
(ii) Infinitesimal strain theory is assumed. Then, Ω denotes the reference configuration of the body $\mathcal{B}$ defined as an open bounded set in $\mathbb{R}^{\text{ndim}}$, "ndim" refers to the spatial dimension of the problem. A material point of $\mathcal{B}$, at the macro-scale, is denoted: "$\boldsymbol{x}$", see Fig. 1. In the following, we use the prefix "macro-$(\bullet)$" to denote the fields depending on $\boldsymbol{x}$ and omitting, for the sake of simplicity, this functional dependence.
(iii) $\mathcal{B}$ undergoes a loading process given by body forces per unit of volume, $\boldsymbol{b}$, and external tractions per unit of surface area, $\boldsymbol{t}$. As usual, Γ symbolizes the piece-wise smooth boundary of Ω, which can be split into two sub-sets Γ_D and Γ_N, where predefined values of displacements, $\boldsymbol{u}_D$, and traction, $\boldsymbol{t}$, are prescribed, respectively. Besides we have: $\Gamma_D \cup \Gamma_N = \Gamma$, $\Gamma_D \cap \Gamma_N = \emptyset$, and $\boldsymbol{v}$ is the outward unit vector normal to Γ, as shown in Fig. 1.
(iv) Initially, the macro-scale is idealized as a homogeneous *continuum* body where displacements, $\boldsymbol{u}$, macro-strains, $\boldsymbol{\varepsilon}$, and macro-stresses, $\boldsymbol{\sigma}$, characterize the mechanical state of the continuum medium. However, since softening-based materials are considered for the definition of the micro-scale problem, an alternative macro-mechanical scenario can arise. A strain localization mode can nucleate and develop in $\boldsymbol{x}$ after a critical condition is fulfilled. This critical condition is governed by the progressive accumulation of micro-failure mechanisms. The strain localized macro-modes can represent shear bands, fractures/cracks, slip surfaces, etc., depending on the considered problem. A fundamental assumption of the present formulation is that the mechanical phenomenology associated to these failure modes are adequately represented, at the macro-scale, by the inclusion of a "*Cohesive Crack*" [7,1,15].
(v) Every point $\boldsymbol{x} \in \Omega$ is linked to the micro-scale through a heterogeneous *RVE*. The same concept exists for those points $\boldsymbol{x}$ that belong to the macro-crack. Thus, it arises a mechanical representation of the displacement jumps and cohesive forces characterizing the "discontinuity interface" through a "volumetric" micro-cell domain, see Fig. 1.
(vi) For simplicity, it is assumed that the macro-cracks do not intersect neither the Dirichlet boundary Γ_D nor the non-homogeneous Neumann boundary Γ_N. In addition, the macro-cracks do not intersect each other.

The *Cohesive Crack* concept introduces, in the macro mechanical formulation, two features which cannot be reproduced by means of the standard (stress–strain) mechanical description: (i) the activation of a new independent kinematical field, accounting for displacement discontinuities through the faces of the crack (commonly known as *Strong Discontinuity Kinematics*), and (ii) an additional generalized stress variable $\boldsymbol{T}$, called the *Cohesive Traction vector* or the *Cohesive Generalized Force*, conjugated to the displacement discontinuity field. Once a macro cohesive crack is activated at point $\boldsymbol{x}$, it is not possible to return to the classical continuum description. The constitutive response of the crack is governed, exclusively, by the so-called cohesive model (traction-jump model) which, in turn, is determined from a specific stress homogenization procedure performed in the micro scale.

Remark 2.1. In the context of softening material modeling, we postulate that a physically admissible RVE does exist. We adopt the classical definition of RVE given in the literature (see for example [25]) in which, a micro-cell is a RVE whenever it has the property of material statistical representativeness with respect to micro-structural patterns.

In the present context of analysis, the essential key point to determine the RVE, and thus its existence, lies on the fact that a well-posed multi-scale model does exist, in the sense that a sequence of increasing micro-cell sizes furnishes a convergent macroscopic homogenized response. Standard multi-scale techniques fail to reach this goal, obscuring the notion of the existence of a physically admissible RVE for softening-based materials [11].

From this point of view, in the following development of the model, speaking of RVE, Micro-Cell or Unit-Cells is immaterial. These terms are here used only to keep in mind the existence of an underlying heterogeneous material micro-structure.

2.2. Failure criterion at the macro scale

A criterion to decide "*when*" and "*how*" a cohesive cracks has to be inserted, or activated, in the initially continuum medium, is an ingredient to be defined in the present formulation. The failure criterion here adopted is derived from the *RVE Homogenized* mechanical state. It specifies the following two attributes of the macro-crack:

- the nucleation pseudo-time $t_N \in [0,T]$, defined as the instant at which an admissible mechanical condition for the development of a bifurcation mode, at the macro-level, is reached for the first time during the load history;
– the orientation of the discontinuity surface given by the unit vector $\boldsymbol{n}$ orthogonal to the crack direction.

For this purpose, the classical bifurcation analysis based on the spectral properties of the *Localization Tensor*, is considered [32,30,33]. This criterion determines the mechanical conditions under which a strain rate discontinuity, across a given material interface, is admissible.

Defining the jump, or discontinuity, operator across a material surface $\mathcal{S}$ with normal vector $\boldsymbol{n}$ as follows:

$$[\![(\bullet)]\!] = (\bullet)|_{(\boldsymbol{x}+d\boldsymbol{x})} - (\bullet)|_{(\boldsymbol{x}-d\boldsymbol{x})} \quad \forall \boldsymbol{x} \in \mathcal{S};\ d\boldsymbol{x} \text{ parallel to the } \boldsymbol{n}\text{-direction and } ||d\boldsymbol{x}|| \to \boldsymbol{0} \tag{1}$$

then, the Maxwell's kinematical compatibility condition establishes that a discontinuity in the strain rate $[\![\dot{\boldsymbol{\varepsilon}}]\!]$ has the following structure:

$$[\![\dot{\boldsymbol{\varepsilon}}]\!] = \dot{\boldsymbol{\gamma}} \otimes^s \boldsymbol{n} \tag{2}$$

where $\dot{\boldsymbol{\gamma}}$ is an arbitrary (pseudo-) velocity vector and the symbol $\otimes^s$ denotes the external symmetric dyadic product.

We admit the existence of a *strain-localization* band inside which the strain rate, $\dot{\boldsymbol{\varepsilon}}_B$, experiences a jump with respect to the strain rate in the surrounding continuum medium, $\dot{\boldsymbol{\varepsilon}}_C$, and such that: $\dot{\boldsymbol{\varepsilon}}_B = \dot{\boldsymbol{\varepsilon}}_C + [\![\dot{\boldsymbol{\varepsilon}}]\!]$. Additionally, an incrementally linear strain rate-stress rate behavior at the macro-scale is assumed to exist as a result of the homogenization procedure:

$$\dot{\boldsymbol{\sigma}} = \boldsymbol{C}(\boldsymbol{\varepsilon}^{(t)})\, \dot{\boldsymbol{\varepsilon}} \tag{3}$$

where the symbol $\boldsymbol{\varepsilon}^{(t)}$ denotes the history of the strains up to the instant "t" and $\boldsymbol{C}$ represents the homogenized tangent constitutive operator which, for general non-linear models, depends on $\boldsymbol{\varepsilon}^{(t)}$ (see Section 3.4). Then, the traction continuity condition across $\mathcal{S}$ implies:

$$[\![\dot{\boldsymbol{\sigma}}]\!]\boldsymbol{n} = [\![\dot{\boldsymbol{T}}]\!] = \dot{\boldsymbol{T}}_B - \dot{\boldsymbol{T}}_C = \left(\boldsymbol{C}(\boldsymbol{\varepsilon}^{(t)})\, [\![\dot{\boldsymbol{\varepsilon}}]\!]\right)\boldsymbol{n} = \boldsymbol{0} \tag{4}$$

where the term $[\![\dot{\boldsymbol{\sigma}}]\!]\boldsymbol{n} = \dot{\boldsymbol{T}}_B - \dot{\boldsymbol{T}}_C$ represents the jump between the (rate of) traction inside the strain-localization band, $\dot{\boldsymbol{T}}_B$, and the (rate of) traction in the continuum part of the body, $\dot{\boldsymbol{T}}_C$. Note that (4) has been derived by assuming the same incremental constitutive behavior, *loading-regime*, on both sides of the surface $\mathcal{S}$.

Taking into account (2) and considering the minor symmetries of $\boldsymbol{C}$, expression (4) yields:

$$\left[\left(\boldsymbol{C}(\boldsymbol{\varepsilon}^{(t)})\,\boldsymbol{n}\right)\dot{\boldsymbol{\gamma}}\right]\boldsymbol{n} = \boldsymbol{Q}(\boldsymbol{\varepsilon}^{(t)},\boldsymbol{n})\,\dot{\boldsymbol{\gamma}} = \boldsymbol{0} \tag{5}$$

where the definition of the so-called *Localization Tensor* $\boldsymbol{Q}(\boldsymbol{\varepsilon}^{(t)},\boldsymbol{n})$ is introduced. Non trivial solutions for the system (5), with $\dot{\boldsymbol{\gamma}} \neq \boldsymbol{0}$, can be obtained only if $\boldsymbol{Q}$ is singular:

$$\det\ \left(\boldsymbol{Q}(\boldsymbol{\varepsilon}^{(t)},\boldsymbol{n})\right) = 0 \tag{6}$$

Eq. (6) is a necessary condition for the existence of discontinuous strain rate modes in the body, and can also be interpreted as a necessary condition for the activation of velocity discontinuities across a material surface $\mathcal{S}$ with normal $\boldsymbol{n}$ [27,3].

The failure criterion here adopted postulates that the nucleation of a macro-crack is determined once the instability condition (6) is verified for the first time ($t = t_N$) during the loading history. The criterion also determines the normal vector to the localization direction $\boldsymbol{n}$. In particular, when $\boldsymbol{C}$ possesses major symmetries, the solution of (6) has two conjugate eigenvectors: $\boldsymbol{n}$ and the initial opening (pseudo-) velocity direction $\dot{\boldsymbol{\gamma}}_i$ [28]. The solution of the nucleation problem (6) is denoted as: $\mathbb{S}_N = \{t_N, \boldsymbol{n}, \dot{\boldsymbol{\gamma}}_i\}$.

2.3. Macroscopic kinematical description with strong discontinuities

When a non-trivial solution $\mathbb{S}_N = \{t_N, \boldsymbol{n}, \dot{\boldsymbol{\gamma}}_i\}$ of the problem (6) is detected at point $\boldsymbol{x}$, a cohesive crack along the surface denoted $\mathcal{S}$, is there inserted. Once the crack is active, its orientation remains fixed for all $t > t_N$. The nucleation and evolution of a crack requires a specific kinematical description which is presented in this Section.

Let us consider the mechanical problem of a body $\mathcal{B}$, in its configuration Ω, exhibiting a discontinuity in the displacement field across the surface $\mathcal{S}$ ($\mathcal{S} \subset \Omega$) with a unit normal vector $\boldsymbol{n}$, see Fig. 2(a). In two-dimensional cases, as depicted in the same figure, for each point $\boldsymbol{x} \in \mathcal{S}$ it is possible to define a local cartesian system $\{\boldsymbol{n}, \boldsymbol{\tau}\}$. $\mathcal{S}$ divides Ω in two sub-domains: Ω_+ and Ω_-, according to the direction of $\boldsymbol{n}$ (with $\boldsymbol{n}$ pointing to Ω_+).

For subsequent developments, we define Ω^φ as an arbitrary sub-domain of Ω ($\Omega^\varphi \subset \Omega$) including the interface discontinuity $\mathcal{S}$ ($\mathcal{S} \subset \Omega^\varphi$), with piece-wise smooth boundary Γ^φ which can be split as: $\Gamma^\varphi = \mathcal{S}_+ \cup \mathcal{S}_- \cup \Gamma^\varphi_I \cup \Gamma^\varphi_{II}$, see Fig. 2(b). Also, note that $\mathcal{S}$ divides Ω^φ in two sub-domains Ω^φ_+ and Ω^φ_- ($\boldsymbol{n}$ pointing towards Ω^φ_+). The (outward) unit vectors $\boldsymbol{n}_+$, $\boldsymbol{n}_-$, $\boldsymbol{n}_I$ and $\boldsymbol{n}_{II}$ are normal to the boundaries $\mathcal{S}_+$, $\mathcal{S}_-$, Γ^φ_I and Γ^φ_{II} of Ω^φ, respectively.

After the insertion of the macro-crack, a strong discontinuity develops on $\mathcal{S}$. Let us consider the total macro-displacement field $\boldsymbol{u}$ and the arbitrary smooth vectorial function $\boldsymbol{\beta}$, defined in $\Omega \times [t_N, T] \to \mathbb{R}^{\text{ndim}}$, which is such that:

$$\boldsymbol{\beta}(\boldsymbol{x},t) := [[\boldsymbol{u}]](\boldsymbol{x},t) \quad \forall \boldsymbol{x} \in \mathcal{S} \quad \text{and} \quad (\nabla_{\boldsymbol{x}}\boldsymbol{\beta})\,\boldsymbol{n} = \boldsymbol{0} \quad \forall \boldsymbol{x} \in \Omega \tag{7}$$

Thus, $\boldsymbol{\beta}$ represents the displacement jump in $\mathcal{S}$. Following to [38], the discontinuous macro-displacement field can be written as the addition of two terms:

$$\boldsymbol{u}(\boldsymbol{x},t) = \overbrace{\overline{\boldsymbol{u}}(\boldsymbol{x},t)}^{\text{continuous}} + \overbrace{\mathcal{M}_{\mathcal{S}}(\boldsymbol{x})\,\boldsymbol{\beta}(\boldsymbol{x},t)}^{\text{discontinuous}}; \quad \forall \boldsymbol{x} \in \Omega \tag{8}$$

where $\overline{\boldsymbol{u}}(\boldsymbol{x},t)$ is a smooth function in Ω and is called the continuous displacement term, and $\mathcal{M}_{\mathcal{S}}(\boldsymbol{x})$ is a prescribed function, constant in time, usually called the *Unit Jump function* and defined as follows, see Fig. 2(b):

$$\mathcal{M}_{\mathcal{S}}(\boldsymbol{x}) := \mathcal{H}_{\mathcal{S}}(\boldsymbol{x}) - \varphi(\boldsymbol{x}); \quad \mathcal{H}_{\mathcal{S}}(\boldsymbol{x}) = \begin{cases} 0 & \forall \boldsymbol{x} \in \Omega_- \\ 1 & \forall \boldsymbol{x} \in \Omega_+ \end{cases}; \quad \varphi(\boldsymbol{x}) = \begin{cases} 0 & \forall \boldsymbol{x} \in \Omega_- \setminus \Omega^\varphi_- \\ 1 & \forall \boldsymbol{x} \in \Omega_+ \setminus \Omega^\varphi_+ \end{cases} \tag{9}$$

$\mathcal{H}_{\mathcal{S}}(\boldsymbol{x}) : \Omega \to \mathbb{R}$ is the Heaviside step function shifted to the discontinuity surface $\mathcal{S}$ and $\varphi(\boldsymbol{x}) : \Omega \to \mathbb{R}$ is a sufficiently smooth and arbitrary function with the two requirements showed in Eq. (9)-right. From equations (9) $\mathcal{M}_{\mathcal{S}}(\boldsymbol{x})$ has compact support and it coincides with Ω^φ ($\mathcal{M}_{\mathcal{S}}(\boldsymbol{x}) \equiv 0\ \forall \boldsymbol{x} \in \Omega \setminus \Omega^\varphi$).

In view of the above definitions, the strain tensor $\boldsymbol{\varepsilon}$, compatible with Eq. (8), is expressed as:

$$\begin{aligned} \boldsymbol{\varepsilon} &= \nabla^s_{\boldsymbol{x}}\boldsymbol{u} = \nabla^s_{\boldsymbol{x}}\overline{\boldsymbol{u}} + \mathcal{M}_{\mathcal{S}}\nabla^s_{\boldsymbol{x}}\boldsymbol{\beta} - \boldsymbol{\beta}\otimes^s\nabla_{\boldsymbol{x}}\varphi = \boldsymbol{\varepsilon}_R(\overline{\boldsymbol{u}},\boldsymbol{\beta}); \\ &\quad \forall \boldsymbol{x} \in \Omega \setminus \mathcal{S} \end{aligned} \tag{10}$$

where $\nabla^s_{\boldsymbol{x}}$ is the symmetric gradient operator. Note that the expression $\boldsymbol{\varepsilon}_R(\overline{\boldsymbol{u}},\boldsymbol{\beta})$ is a regular bounded term. Considering the compact support of $\boldsymbol{\beta}$, $\mathcal{M}_{\mathcal{S}}$ and φ, from expression (10), we have: $\boldsymbol{\varepsilon} = \nabla^s_{\boldsymbol{x}}\overline{\boldsymbol{u}};\ \forall \boldsymbol{x} \in \Omega \setminus \Omega^\varphi$.

For the macro-points located in $\mathcal{S}$, we introduce the notion of *generalized strain* which, in this case, is characterized by: (i) the vector $\boldsymbol{\beta}$ in $\mathcal{S}$ with normal $\boldsymbol{n}$ and (ii) the regular counterpart $\boldsymbol{\varepsilon}_R$, see Eq. (10). Then, generalized strains in $\mathcal{S}$ are characterized through the list of variables: $\{\boldsymbol{\varepsilon}_R, \boldsymbol{\beta}, \boldsymbol{n}\}$.

Kinematically admissible discontinuous macro-displacements $\boldsymbol{u}$, are described by the elements $(\overline{\boldsymbol{u}}, \boldsymbol{\beta})$ of the linear manifold $\mathcal{U}$, which is defined as:

$$\mathcal{U} \equiv \left\{ (\overline{\boldsymbol{u}}, \boldsymbol{\beta})\ ;\ \overline{\boldsymbol{u}} \in \mathbf{H}^1(\Omega),\ \boldsymbol{\beta} \in \mathbf{H}^1(\Omega) \text{ and } \overline{\boldsymbol{u}}|_{\Gamma_D} = \boldsymbol{u}_D \right\} \tag{11}$$

where $\boldsymbol{H}^1(\bullet)$ is the vectorial space of functions whose first derivative is square-integrable. In the present context, the vector space $\mathcal{V}$ characterizing the virtual kinematically admissible actions (velocities), denoted by $\hat{\boldsymbol{u}} = \hat{\overline{\boldsymbol{u}}} + \mathcal{M}_{\mathcal{S}}\hat{\boldsymbol{\beta}}$, reads:

$$\mathcal{V} \equiv \left\{ (\hat{\overline{\boldsymbol{u}}}, \hat{\boldsymbol{\beta}});\ \hat{\overline{\boldsymbol{u}}} \in \mathbf{H}^1(\Omega),\ \hat{\boldsymbol{\beta}} \in \mathbf{H}^1(\Omega) \text{ and } \hat{\overline{\boldsymbol{u}}}|_{\Gamma_D} = \boldsymbol{0} \right\} \tag{12}$$

2.4. Variational equilibrium problem at the macro-level

In problems with nucleation and evolution of cohesive cracks, the equilibrium at the macro level is described by means of the *Principle of Virtual Power (PVP)*, as follows:

> Given prescribed values of body forces $\boldsymbol{b}$ and predefined tractions $\boldsymbol{t}$; find the kinematically admissible displacement field $(\overline{\boldsymbol{u}}, \boldsymbol{\beta}) \in \mathcal{U}$, such that:
>
> $$\begin{aligned} &\int_{\Omega\setminus\mathcal{S}} \boldsymbol{\sigma}(\overline{\boldsymbol{u}},\boldsymbol{\beta}) \cdot \hat{\boldsymbol{\varepsilon}}_R\, d\Omega + \int_{\mathcal{S}} \boldsymbol{T}(\overline{\boldsymbol{u}},\boldsymbol{\beta}) \cdot \hat{\boldsymbol{\beta}}\, d\mathcal{S} \\ &- \int_{\Omega\setminus\mathcal{S}} \boldsymbol{b} \cdot (\hat{\overline{\boldsymbol{u}}} + \mathcal{M}_{\mathcal{S}}\hat{\boldsymbol{\beta}})\, d\Omega - - \int_{\Gamma_N} \boldsymbol{t} \cdot \hat{\overline{\boldsymbol{u}}}\, d\Gamma = 0; \quad \forall (\hat{\overline{\boldsymbol{u}}}, \hat{\boldsymbol{\beta}}) \in \mathcal{V} \end{aligned} \tag{13}$$

where the first integral term is the internal virtual power in the continuous part of the solid, and the second one is the internal virtual power of the cohesive crack, noting that this term is present in the formulation whenever the failure criterion presented in Section 2.2 has been fulfilled. In both terms, $\hat{\boldsymbol{\varepsilon}}_R = \boldsymbol{\varepsilon}_R(\hat{\overline{\boldsymbol{u}}}, \hat{\boldsymbol{\beta}})$ and $\hat{\boldsymbol{\beta}}$ represent the virtual kinematically admissible *generalized-strains*. On the other hand, the third and fourth terms in (13) are the external virtual power.

In order to completely define the mechanical problem at the macro-scale, constitutive relations for the stress field, $\boldsymbol{\sigma}$, and for the cohesive traction, $\boldsymbol{T}$, need to be prescribed. In this contribution it is assumed that each one of this constitutive relations is obtained using specific multi-scale formulations that are defined in the following Sections. In general, we consider non-linear material responses, where the functionals of the *stress-like* macro-quantities $\boldsymbol{\sigma}$ and $\boldsymbol{T}$, at time t, depend on the history of the *strain-like* macro-variables up to the time t, here denoted as: $\boldsymbol{\varepsilon}_R^{(t)}$ and $\boldsymbol{\beta}^{(t)}$.

Defining the history of the generalized strains in the spatial domains and time intervals by means of:

$$\boldsymbol{\varepsilon}_R^{(t)}(\boldsymbol{x},t); \quad \forall \boldsymbol{x} \in \Omega \setminus \mathcal{S} \text{ and } \forall t \in [0,T] \tag{14}$$

$$\{\boldsymbol{\varepsilon}_R^{(t)}(\boldsymbol{x},t), \boldsymbol{\beta}^{(t)}(\boldsymbol{x},t)\}; \quad \forall \boldsymbol{x} \in \mathcal{S} \text{ and } \forall t \in [t_N,T] \tag{15}$$

the generalized stress functionals can be written as follows:

$$\boldsymbol{\sigma} = \mathcal{F}(\boldsymbol{\varepsilon}_R^{(t)}) = \mathcal{F}^*(\boldsymbol{\varepsilon}_R^{(t-dt)}, d\boldsymbol{\varepsilon}_R); \quad \forall \boldsymbol{x} \in \Omega \setminus \mathcal{S}; \quad \forall t \in [0,T] \tag{16}$$

$$\boldsymbol{T} = \mathcal{T}(\boldsymbol{\varepsilon}_R^{(t)}, \boldsymbol{\beta}^{(t)}) = \mathcal{T}^*(\boldsymbol{\varepsilon}_R^{(t-dt)}, \boldsymbol{\beta}^{(t-dt)}, d\boldsymbol{\varepsilon}_R, d\boldsymbol{\beta}); \quad \forall \boldsymbol{x} \in \mathcal{S}; \quad \forall t \in [t_N,T] \tag{17}$$

where the symbols $\boldsymbol{\varepsilon}_R^{(t-dt)}$ and $\boldsymbol{\beta}^{(t-dt)}$ stand for the history of the generalized strains up to time $(t-dt)$ and $d(\bullet)$ represents the infinitesimal increments at t. The last terms in the right side of both equations explicitly introduce, in the arguments of the stress functionals, the kinematically admissible strain increments $d\boldsymbol{\varepsilon}_R$ and $d\boldsymbol{\beta}$, at t. Also, the generalized stresses can be written in incremental form:

$$\boldsymbol{\sigma} = \boldsymbol{\sigma}_{t-dt} + d\boldsymbol{\sigma}; \quad \boldsymbol{T} = \boldsymbol{T}_{t-dt} + d\boldsymbol{T} \tag{18}$$

where the sub-indices identify the pseudo-time at which the variables are evaluated. From now on, and in order to simplify the notation, we remove the sub-indices when variables are evaluated at the present time "t".

Remark 2.2. From a thermodynamical point of view, $\boldsymbol{T}$ only produces virtual power through the kinematically admissible variations $\hat{\boldsymbol{\beta}}$, i.e. $\boldsymbol{T}$ is conjugate to $\hat{\boldsymbol{\beta}}$. Thus, the regular component $\boldsymbol{\varepsilon}_R$, in the argument of function (17), works as a parameter when the virtual power of cohesive forces is evaluated. In Section 4 we exploit this feature.

2.5. The whole constitutive response via a Failure-Oriented Multi-scale Formulation (FOMF)

From the perspective of the variational formulation, the solution of the equilibrium problem at the macro-level requires the definition of two different constitutive multi-scale models. Each one is enunciated as follows:

- A *Classical Multi-scale Model* (*ClaMM*) for the regular domain in the macro-scale (refer to Section 3 for more details):
  - $\forall \boldsymbol{x} \in \Omega \setminus \mathcal{S}$ and $\forall t \in [0,T]$,
  - given the history of regular strains $\boldsymbol{\varepsilon}_R^{(t-dt)}$ and the strain increment $d\boldsymbol{\varepsilon}_R$, obtain the associated increment of macroscopic stress $d\boldsymbol{\sigma}$.
- A *Cohesive Multi-scale Model* (*CohMM*) for the points in the macro-crack (refer to Section 4 for additional details):
  - $\forall \boldsymbol{x} \in \mathcal{S}$ and $\forall t \in [t_N,T]$,
  - given the history of generalized strains $\left\{\boldsymbol{\varepsilon}_R^{(t-dt)}, \boldsymbol{\beta}^{(t-dt)}\right\}$ and the generalized strain increment $\{d\boldsymbol{\varepsilon}_R, d\boldsymbol{\beta}\}$, obtain the associated increment of macroscopic cohesive traction $d\boldsymbol{T}$.

The *FOMF* approach proposed in this contribution is based on a consistent mechanical coupling between the two sub-models: *ClaMM* and *CohMM*. In order to clarify ideas, Fig. 3 sketches the whole homogenized constitutive response of a macro-point $\boldsymbol{x}$ which, at $t = t_N$, nucleates a cohesive crack.

The basic ingredients defining the macro-mechanical problem with nucleation and evolution of cohesive cracks are summarized in Box 1, while both sub-models, the *ClaMM* and *CohMM*, are described in the two following sections.

3. Classical Multi-scale variational Model (*ClaMM*)

Following the similar axiomatic framework described in [40,41,29], the foundations of the so-called *Classical Multi-scale Model* (*ClaMM*) are here summarized. In addition, we introduce the definitions and nomenclature of new operators, that are useful in the subsequent developments of Section 4. We remark, as a particular aspect in this Section, the effect that the kinematical assumptions and the Hill–Mandel Principle have on the resulting stress homogenization rule and the equilibrium problem at micro-level.

The *ClaMM* results an important ingredient of the complete proposed multi-scale methodology. It is used to obtain the macro homogenized constitutive response in the following two situations, see the item 4.1 in Box 1 and also Fig. 3:

(i) in those points where, according to the criterion discussed in Section 2.2, no crack formation is detected during the entire load history;
(ii) during the period of stable homogenized material response in the points where, eventually at a posterior time, a crack is inserted.

From the previous explanations, the kinematics at macro-level, in the present context of analysis, is only characterized by the regular strain component $\boldsymbol{\varepsilon}_R$.

As it is well known, material models with softening characterizing the micro-structural constituents, require a "regularization" of the constitutive theories to keep the mechanical problem well-posed. Depending on the specific technique used to perform this regularization, some particular aspects of the following *ClaMM* can be described through different approaches. To avoid unnecessary details that would obscure the following presentation, we adopt a regularization strategy based on the "*Smeared Crack Approach*" to fracture (*SCA*) [31], which uses a standard continuum mechanical description at the micro-scale level and regularizes the softening parameter according to the fracture energy and a predefined characteristic length. However, the foundations of the proposed multi-scale formulation works well with different regularization strategies, such as: non-local schemes, gradient/higher-order models as well as strong discontinuity techniques with cohesive laws. In other word, the methodology is flexible for adopting different regularization strategies in the RVE.

Box 1: Macro-mechanical problem with strong discontinuities. Basic concepts and ingredients

1.***Kinematics:***

$$\boldsymbol{u} = \overline{\boldsymbol{u}} + \mathcal{M}_{\mathcal{S}}\,\boldsymbol{\beta} \quad ; \quad \forall \boldsymbol{x} \in \Omega$$
$$\boldsymbol{\varepsilon} = \boldsymbol{\varepsilon}_R = \nabla^s_{\boldsymbol{x}}\overline{\boldsymbol{u}} + \mathcal{M}_{\mathcal{S}}\,\nabla^s_{\boldsymbol{x}}\boldsymbol{\beta} - \nabla_{\boldsymbol{x}}\varphi \otimes^s \boldsymbol{\beta} \quad ; \quad \forall \boldsymbol{x} \in \Omega/\mathcal{S}$$
$$(\overline{\boldsymbol{u}}, \boldsymbol{\beta}) \in \mathcal{U}\,;\ \mathcal{U} \equiv \left\{(\overline{\boldsymbol{u}}, \boldsymbol{\beta});\ \overline{\boldsymbol{u}} \in \mathbf{H}^1(\Omega),\ \boldsymbol{\beta} \in \mathbf{H}^1(\Omega) \text{ and } \overline{\boldsymbol{u}}|_{\Gamma_D} = \boldsymbol{u}_D\right\}$$

1. *Virtual kinematically admissible actions (velocities):*

$$\hat{\boldsymbol{u}} = \hat{\overline{\boldsymbol{u}}} + \mathcal{M}_{\mathcal{S}}\,\hat{\boldsymbol{\beta}}$$
$$(\hat{\overline{\boldsymbol{u}}}, \hat{\boldsymbol{\beta}}) \in \mathcal{V};\ \mathcal{V} \equiv \left\{(\hat{\overline{\boldsymbol{u}}}, \hat{\boldsymbol{\beta}});\ \hat{\overline{\boldsymbol{u}}} \in \mathbf{H}^1(\Omega),\ \hat{\boldsymbol{\beta}} \in \mathbf{H}^1(\Omega) \text{ and } \hat{\overline{\boldsymbol{u}}}|_{\Gamma_D} = \mathbf{0}\right\}$$

2.***Variational Equilibrium Problem:***

Given $\boldsymbol{b}$ and $\boldsymbol{t}$; find $(\overline{\boldsymbol{u}}, \boldsymbol{\beta}) \in \mathcal{U}$ such that :

$$\int_{\Omega\setminus\mathcal{S}} \boldsymbol{\sigma} \cdot \nabla^s_{\boldsymbol{x}}(\hat{\overline{\boldsymbol{u}}} + \mathcal{M}_{\mathcal{S}}\hat{\boldsymbol{\beta}})\, d\Omega + \int_{\mathcal{S}} \boldsymbol{T} \cdot \hat{\boldsymbol{\beta}}\, d\mathcal{S} - \int_{\Omega\setminus\mathcal{S}} \boldsymbol{b} \cdot (\hat{\boldsymbol{u}} + \mathcal{M}_{\mathcal{S}}\hat{\boldsymbol{\beta}})\, d\Omega - \int_{\Gamma_N} \boldsymbol{t} \cdot \hat{\overline{\boldsymbol{u}}}\, d\Gamma = 0; \quad \forall (\hat{\overline{\boldsymbol{u}}}, \hat{\boldsymbol{\beta}}) \in \boldsymbol{\mathcal{V}}$$

3.***Constitutive response via the Failure-Oriented Multi-scale Formulation (FOMF):***

4.1 $\forall \boldsymbol{x} \in \Omega/\mathcal{S}$ and $\forall t \in [0, T]$: Given $\boldsymbol{\varepsilon}_R^{(t-dt)}$ and $d\boldsymbol{\varepsilon}_R$; find $d\boldsymbol{\sigma}$,

via a *Classical Multi-scale Model* (*ClaMM*), refer to Section 3 and Box 2. Update stresses: $\boldsymbol{\sigma} = \boldsymbol{\sigma}_{t-dt} + d\boldsymbol{\sigma}$

4.2 $\forall \boldsymbol{x} \in \mathcal{S}$ and $\forall t \in [t_N, T]$: Given $\{\boldsymbol{\varepsilon}_R^{(t-dt)}, \boldsymbol{\beta}^{(t-dt)}\}$ and $\{d\boldsymbol{\varepsilon}_R, d\boldsymbol{\beta}\}$; find $d\boldsymbol{T}$,

via the *Cohesive Multi-scale Model* (*CohMM*), refer to Section 4 and Box 3. Update tractions: $\boldsymbol{T} = \boldsymbol{T}_{t-dt} + d\boldsymbol{T}$

4.***Cohesive crack nucleation criterion:***

Find $\mathbb{S}_N = \{t_N, \boldsymbol{n}, \dot{\gamma}_i\}$, verifying the singularity of the *Localization Tensor* $\boldsymbol{Q}(\boldsymbol{\varepsilon}^{(t)}, \boldsymbol{n})$:

$\det\left(\boldsymbol{Q}(\boldsymbol{\varepsilon}^{(t)}, \boldsymbol{n})\right) = 0; \quad \forall \boldsymbol{x} \in \Omega/\mathcal{S}$ and $\forall \boldsymbol{n} \in \mathbb{R}^{\text{ndim}}$

where $\boldsymbol{Q}(\boldsymbol{\varepsilon}^{(t)}, \boldsymbol{n})\,\dot{\boldsymbol{\gamma}} = [(\boldsymbol{C}(\boldsymbol{\varepsilon}^{(t)})\,\boldsymbol{n})\,\dot{\boldsymbol{\gamma}}]\,\boldsymbol{n},\ \forall \dot{\boldsymbol{\gamma}} \in \mathbb{R}^{\text{ndim}}$

and $\boldsymbol{C}(\boldsymbol{\varepsilon}^{(t)})$ is the *Homogenized Tangent Constitutive Tensor*, obtained via a *Classical Multi – scale Model* (*ClaMM*)

3.1. Kinematical description at the micro-cell level

Let us consider a reference configuration Ω_μ ($\Omega_\mu \subset \mathbb{R}^{\text{ndim}}$) of the heterogeneous micro-cell $\mathcal{B}_\mu$ having a piece-wise smooth boundary Γ_μ, see Fig. 1. A specific reference system is introduced to describe the mechanical problem at the micro-scale. Points in $\mathcal{B}_\mu$ are denoted "$\boldsymbol{y}$" ($\boldsymbol{y} \in \Omega_\mu$).

Macro-fields depend on "$\boldsymbol{x}$", whereas those defined at the micro-scale depend on "$\boldsymbol{y}$". For the sake of simplicity, all functional dependencies on "$\boldsymbol{y}$" are omitted, while the sub-index $(\bullet)_\mu$ denotes the variables defined in $\mathcal{B}_\mu$. Additionally, we use the prefix "micro-$(\bullet)$" for the fields defined at the micro-scale.

Let $\boldsymbol{\varepsilon}_R = \nabla^s_{\boldsymbol{x}}\boldsymbol{u} = \boldsymbol{\varepsilon}_R(\overline{\boldsymbol{u}}, \boldsymbol{\beta})$ be the regular component of the strain at the point $\boldsymbol{x} \in \Omega \setminus \mathcal{S}$, see Eq. (10). We define the total micro-strain field, $\boldsymbol{\varepsilon}_\mu$, as the addition of two contributions:

$$\boldsymbol{\varepsilon}_\mu = \mathcal{I}_{\boldsymbol{y}}(\boldsymbol{\varepsilon}_R) + \tilde{\boldsymbol{\varepsilon}}_\mu \tag{19}$$

where the first term represents the (*macro-to-micro*) *insertion* of the regular macro-strain into the *RVE*, and the second term is the micro-strain fluctuation field given by $\tilde{\boldsymbol{\varepsilon}}_\mu = \nabla^s_{\boldsymbol{y}}\tilde{\boldsymbol{u}}_\mu$, with $\tilde{\boldsymbol{u}}_\mu$ being the fluctuation of the micro-displacement field. From now on, the supra-symbol $(\tilde{\bullet})$ denotes fluctuations in $\mathcal{B}_\mu$.

The *Insertion Operator* $\mathcal{I}_{\boldsymbol{y}}(\bullet)$ maps a symmetric second order tensor, defined at the macro-scale, into a symmetric second order tensor field in the micro-cell domain. In addition, $\mathcal{I}_{\boldsymbol{y}}(\bullet)$ is a linear application, thus it can be expressed in the form:

$$\mathcal{I}_{\boldsymbol{y}}(\bullet) \equiv \boldsymbol{I}(\boldsymbol{y})\,(\bullet) \tag{20}$$

with $\boldsymbol{I}(\boldsymbol{y})$ being a fourth order tensor micro-field, that must be properly defined.

Using the incremental format introduced in the previous Section, and the property (20), we can alternatively write Eq. (19) as follows:

$$d\boldsymbol{\varepsilon}_\mu = \boldsymbol{I}(\boldsymbol{y})\, d\boldsymbol{\varepsilon}_R + \nabla^s_{\boldsymbol{y}} d\tilde{\boldsymbol{u}}_\mu \tag{21}$$

We say that $d\boldsymbol{\varepsilon}_\mu$ is "*Kinematically Admissible*" in Ω_μ, for a given $\boldsymbol{I}(\boldsymbol{y})(\bullet)$, if it satisfies:

$$\int_{\Omega_\mu} d\boldsymbol{\varepsilon}_\mu\, d\Omega_\mu = \int_{\Omega_\mu} \boldsymbol{I}(\boldsymbol{y})\, d\boldsymbol{\varepsilon}_R\, d\Omega_\mu \tag{22}$$

In the *Classical Multi-scale Formulation*, the *Insertion Operator* is defined as the identity operator, such that for each point $\boldsymbol{y} \in \Omega_\mu$, it can be characterized by the *fourth order identity tensor*: $\mathbb{I}$. Then, $d\boldsymbol{\varepsilon}_R$ is homogeneously inserted into Ω_μ, and Eq. (21), results:

$$d\boldsymbol{\varepsilon}_\mu = d\boldsymbol{\varepsilon}_R + \nabla^s_{\boldsymbol{y}} d\tilde{\boldsymbol{u}}_\mu \tag{23}$$

Under this condition, the Eq. (22) yields:

$$d\boldsymbol{\varepsilon}_R = \frac{1}{|\Omega_\mu|}\int_{\Omega_\mu} d\boldsymbol{\varepsilon}_\mu \, d\Omega_\mu \tag{24}$$

with $|\Omega_\mu|$ being the measure of Ω_μ.

Replacing $d\boldsymbol{\varepsilon}_\mu$, defined in (21), in (24) and using standard mathematical manipulation, Eq. (24) results equivalent to the following kinematical constraint at the micro-cell level:

$$\int_{\Gamma_\mu} d\widetilde{\boldsymbol{u}}_\mu \otimes^s \boldsymbol{v}_\mu \, d\Gamma_\mu = \boldsymbol{0} \tag{25}$$

where $\boldsymbol{v}_\mu$ is the outward unit vector normal to the boundary Γ_μ. Prescription (25) defines what is known as the *Minimally Constrained Vector Space of kinematically admissible incremental displacement fluctuations* at the *RVE*-level: $\widetilde{\mathcal{U}}_\mu$. We establish that $d\widetilde{\boldsymbol{u}}_\mu$ is admissible if $d\widetilde{\boldsymbol{u}}_\mu \in \widetilde{\mathcal{U}}_\mu$, where $\widetilde{\mathcal{U}}_\mu$ is defined as:

$$\widetilde{\mathcal{U}}_\mu \equiv \left\{ d\widetilde{\boldsymbol{u}}_\mu;\ d\widetilde{\boldsymbol{u}}_\mu \in \mathbf{H}^1(\Omega_\mu) \text{ and } \int_{\Gamma_\mu} d\widetilde{\boldsymbol{u}}_\mu \otimes^s \boldsymbol{v}_\mu \, d\Gamma_\mu = \boldsymbol{0} \right\} \tag{26}$$

from where we can define the minimally constrained vector space $\mathcal{V}_\mu$ of virtual kinematically admissible actions (velocities), $\hat{\boldsymbol{u}}_\mu$, as follows:

$$\mathcal{V}_\mu \equiv \left\{ \hat{\boldsymbol{u}}_\mu;\ \hat{\boldsymbol{u}}_\mu \in \mathbf{H}^1(\Omega_\mu) \text{ and } \int_{\Gamma_\mu} \hat{\boldsymbol{u}}_\mu \otimes^s \boldsymbol{v}_\mu \, d\Gamma_\mu = \boldsymbol{0} \right\} \tag{27}$$

Summarizing, we have: $d\widetilde{\boldsymbol{u}}_\mu \in \widetilde{\mathcal{U}}_\mu$ and $\hat{\boldsymbol{u}}_\mu \in \mathcal{V}_\mu \equiv \widetilde{\mathcal{U}}_\mu$.

Taking into account (21) and (27), it is also possible to introduce the concept of virtual kinematically admissible (rate of) micro-strain $\hat{\boldsymbol{\varepsilon}}_\mu$:

$$\hat{\boldsymbol{\varepsilon}}_\mu = \boldsymbol{I}(\boldsymbol{y})\,\hat{\boldsymbol{\varepsilon}}_R + \nabla^s_{\boldsymbol{y}} \hat{\boldsymbol{u}}_\mu; \quad \forall \hat{\boldsymbol{\varepsilon}}_R \text{ and } \forall \hat{\boldsymbol{u}}_\mu \in \mathcal{V}_\mu \tag{28}$$

$\hat{\boldsymbol{\varepsilon}}_R$ being a virtual kinematically admissible (rate of) macro-regular strain.

Remark 3.1. Expression (24) is widely known as the Strain Homogenization Principle. In the present framework, we remark the fact that expression (24) is not a Principle, but a condition derived from the Kinematical Admissibility concept, introduced in (22). Then, alternative multi-scale models can be derived by adopting different Insertion Operators $\mathcal{I}_{\boldsymbol{y}}$ that lead to Strain Homogenization Procedures not coinciding with (24).

Remark 3.2. From (26), alternative Classical Multi-scale Models can be defined by adopting different sub-spaces of the minimally constrained vector space $\widetilde{\mathcal{U}}_\mu$ (and $\mathcal{V}_\mu$), such as: the Taylor or homogeneous strain model, the Linear or affine RVE-boundary displacement model, the Periodic RVE-boundary displacement fluctuations model. Moreover, it can be proved that the formulation with minimum kinematical restrictions, given by the definition (26), represents the so-called Uniform boundary Traction model [40].

3.2. The Hill–Mandel Variational Principle of macro-homogeneity

In order to guarantee the energetic consistency between the macro and micro scales, the Hill–Mandel Variational Principle is assumed. This principle establishes an equivalence between the virtual internal power at the macro-scale and the homogenized virtual internal power at the micro-scale:

$$\boldsymbol{\sigma} \cdot \hat{\boldsymbol{\varepsilon}}_R = \frac{1}{|\Omega_\mu|}\int_{\Omega_\mu} \boldsymbol{\sigma}_\mu \cdot \hat{\boldsymbol{\varepsilon}}_\mu \, d\Omega_\mu; \quad \forall \hat{\boldsymbol{\varepsilon}}_R \text{ and } \forall \hat{\boldsymbol{\varepsilon}}_\mu \text{ kinematically admissible} \tag{29}$$

where $\boldsymbol{\sigma}_\mu$ is the stress tensor field in the micro-scale. Alternatively, writing $\boldsymbol{\sigma}$ and $\boldsymbol{\sigma}_\mu$ in term of stress increments, as shown in expression (18)left, and considering that the variational equation (29) is satisfied throughout the history, this Variational Principle reads:

$$d\boldsymbol{\sigma} \cdot \hat{\boldsymbol{\varepsilon}}_R = \frac{1}{|\Omega_\mu|}\int_{\Omega_\mu} d\boldsymbol{\sigma}_\mu \cdot \hat{\boldsymbol{\varepsilon}}_\mu \, d\Omega_\mu; \quad \forall \hat{\boldsymbol{\varepsilon}}_R \text{ and } \forall \hat{\boldsymbol{\varepsilon}}_\mu \text{ kinematically admissible} \tag{30}$$

Inserting (28) into (30), and after some algebra, the Hill–Mandel Variational Principle is expressed as:

$$\left[d\boldsymbol{\sigma} - \frac{1}{|\Omega_\mu|}\int_{\Omega_\mu} (\boldsymbol{I}(\boldsymbol{y}))^T \, d\boldsymbol{\sigma}_\mu \, d\Omega_\mu \right] \cdot \hat{\boldsymbol{\varepsilon}}_R - \frac{1}{|\Omega_\mu|}\int_{\Omega_\mu} d\boldsymbol{\sigma}_\mu \cdot \nabla^s_{\boldsymbol{y}} \hat{\boldsymbol{u}}_\mu \, d\Omega_\mu = 0; \quad \forall \hat{\boldsymbol{\varepsilon}}_R \text{ and } \forall \hat{\boldsymbol{u}}_\mu \in \mathcal{V}_\mu \tag{31}$$

where $(\boldsymbol{I}(\boldsymbol{y}))^T$ represents the transpose of the *Insertion Tensor* $\boldsymbol{I}(\boldsymbol{y})$. In the present context: $(\boldsymbol{I}(\boldsymbol{y}))^T = \boldsymbol{I}(\boldsymbol{y}) = \mathbb{I}$.

3.2.1. First consequence of the Hill–Mandel Principle: the homogenized mechanical response

From expression (31), considering arbitrary variations of $\hat{\boldsymbol{\varepsilon}}_R$ and fixing to zero $\hat{\boldsymbol{u}}_\mu$, it is derived the so-called *micro-to-macro Stress-Homogenization Operator* $\mathcal{H}(\bullet)$:

$$\mathcal{H}(d\boldsymbol{\sigma}_\mu) = d\boldsymbol{\sigma} = \frac{1}{|\Omega_\mu|}\int_{\Omega_\mu} (\boldsymbol{I}(\boldsymbol{y}))^T \, d\boldsymbol{\sigma}_\mu \, d\Omega_\mu \tag{32}$$

which, for the particular case of the *ClaMM*, it results in the conventional stress homogenization procedure:

$$\mathcal{H}(d\boldsymbol{\sigma}_\mu) = d\boldsymbol{\sigma} = \frac{1}{|\Omega_\mu|}\int_{\Omega_\mu} d\boldsymbol{\sigma}_\mu \, d\Omega_\mu \tag{33}$$

Note that the *Insertion Operator*, $\mathcal{I}_{\boldsymbol{y}}(\bullet)$, plays a fundamental role in the characterization of the *Stress Homogenization Operator* $\mathcal{H}(\bullet)$, see Eq. (32). Any change in $\mathcal{I}_{\boldsymbol{y}}(\bullet)$, i.e. changes of the kinematical description, would introduce modification in the stress homogenization process to hold the energetic consistency, the Hill–Mandel Principle in this case. We exploit this concept in Section 4.

3.2.2. Second consequence of the Hill–Mandel Principle: the RVE equilibrium problem

Alternatively, considering arbitrary variations $\hat{\boldsymbol{u}}_\mu$ and fixing to zero the variations $\hat{\boldsymbol{\varepsilon}}_R$ in expression (31), it is derived the *RVE* equilibrium problem that is written in a variational format as follows:

> Given the history of the regular strains $\boldsymbol{\varepsilon}_R^{(t-dt)}$ and a kinematically admissible increment $d\boldsymbol{\varepsilon}_R$; find the incremental micro-displacement fluctuation field $d\widetilde{\boldsymbol{u}}_\mu \in \widetilde{\mathcal{U}}_\mu$, such that:
>
> $$\int_{\Omega_\mu} d\boldsymbol{\sigma}_\mu \cdot \nabla^s_{\boldsymbol{y}} \hat{\boldsymbol{u}}_\mu \, d\Omega_\mu = 0; \quad \forall \hat{\boldsymbol{u}}_\mu \in \mathcal{V}_\mu \tag{34}$$

Eq. (34) prescribes a self-equilibrated micro-stress field, which can be understood as a reaction to the imposed generalized loading system induced by $\mathcal{I}_{\boldsymbol{y}}(d\boldsymbol{\varepsilon}_R)$.

Remark 3.3. From the topics discussed in the present Section, the conceptual guidelines for the formal treatment of a kinematical and variationally consistent multi-scale formulation can be summarized in three basics steps:

(1) Postulate the kinematical description at the micro-level by introducing the definition of the strain tensor field $\boldsymbol{\varepsilon}_\mu$ through the selection of the Insertion Operator $\mathcal{I}_{\boldsymbol{y}}(\bullet)$.
(2) Apply the (incremental) Kinematical Admissibility concept, Eq. (22), from where a Strain Homogenization Procedure emerges.
(3) Postulate the energetic equivalence between the macro and micro scales through the Hill–Mandel Variational Principle.

Once defined this theoretical framework and following purely variational arguments, both mechanical ingredients: (i) the homogenized stresses, i.e. the definition of the Stress-Homogenization Operator $\mathcal{H}(\bullet)$, and (ii) the RVE mechanical equilibrium equations, emerge as "direct consequences" of the formulation.

Assumptions of purely kinematical character, such as those described in points (1) and (2) above, guide our proposal to generalize the Classical Multi-scale Formulation for modeling material failure problems.

3.3. Constitutive model at the micro-scale

In general, the stress state in the *RVE*, $\boldsymbol{\sigma}_\mu$, depends on the history of the micro-strains through a given constitutive functional of the type:

$$\boldsymbol{\sigma}_\mu = \mathcal{F}_\mu\left(\boldsymbol{\varepsilon}_\mu^{(t)}\right) \tag{35}$$

For the problems addressed in this work, the functional $\mathcal{F}_\mu$ describes a generic dissipative inviscid material model with regularized softening, not necessarily derived from a convex potential.

3.4. Homogenized tangent constitutive tensor

The linearization of the macro-homogenized constitutive response defines the so-called *Homogenized Tangent Constitutive Tensor* $\boldsymbol{C}$. Evaluation of $\boldsymbol{C}$ is necessary for two reasons: (i) numerical procedures to solve the fully coupled non-linear macro–micro multi-scale problem, generally requires its computation and (ii) as it is explained in Section 2.2 and based on this tensor, we define a material stability criterion in order to determine the instant when a cohesive crack is introduced in a point $\boldsymbol{x}$ at the macro-level. The last item motivates this Section.

Let us consider the conventional definition of the constitutive tangent operator, which can be expressed as:

$$\boldsymbol{C}(\boldsymbol{\varepsilon}^{(t)}) = \left.\frac{D\boldsymbol{\sigma}}{D\boldsymbol{\varepsilon}_R}\right|_{\boldsymbol{\varepsilon}_R} = \left.\frac{D\, d\boldsymbol{\sigma}}{D\, d\boldsymbol{\varepsilon}_R}\right|_{\boldsymbol{\varepsilon}_R} \tag{36}$$

where $\frac{D}{D\boldsymbol{\varepsilon}_R}(\bullet)$ denotes the "total derivative" with respect to $\boldsymbol{\varepsilon}_R$. Then, regarding the dependence of $d\boldsymbol{\sigma}$ with $d\boldsymbol{\sigma}_\mu$ through expression (33), jointly with the definition of $\boldsymbol{\sigma}_\mu$ in (35) and $\boldsymbol{\varepsilon}_\mu$ in (21), the expression (36) can be rewritten as follows:

$$\boldsymbol{C} = \left.\frac{D\, d\boldsymbol{\sigma}}{D\, d\boldsymbol{\varepsilon}_R}\right|_{\boldsymbol{\varepsilon}_R} = \underbrace{\frac{1}{|\Omega_\mu|}\int_{\Omega_\mu} \boldsymbol{C}_\mu \, d\Omega_\mu}_{\text{Taylor Contribution}} + \underbrace{\frac{1}{|\Omega_\mu|}\int_{\Omega_\mu} \boldsymbol{C}_\mu \, \frac{\partial d\widetilde{\boldsymbol{\varepsilon}}_\mu}{\partial d\boldsymbol{\varepsilon}_R}|_{\boldsymbol{\varepsilon}_R} \, d\Omega_\mu}_{\text{Fluctuation contribution}}$$
$$= \boldsymbol{C}_T + \widetilde{\boldsymbol{C}} \tag{37}$$

where $\boldsymbol{C}_\mu = \left.\frac{\partial d\boldsymbol{\sigma}_\mu}{\partial d\boldsymbol{\varepsilon}_\mu}\right|_{\boldsymbol{\varepsilon}_R}$ represents the tangent constitutive tensor for each point $\boldsymbol{y}$, at the *RVE*-level, which depends on the functional $\mathcal{F}_\mu$, see Eq. (35). From expression (37), two terms contribute to the homogenized tangent constitutive tensor $\boldsymbol{C}$: the first one called the Taylor term, $\boldsymbol{C}_T$, and the second one called the fluctuation contribution $\widetilde{\boldsymbol{C}}$. The Taylor component $\boldsymbol{C}_T$ is determined through direct averaging of the micro-constitutive tangent tensors $\boldsymbol{C}_\mu$. The computation of the fluctuation component $\widetilde{\boldsymbol{C}}$ is here summarized for a cartesian system with base vectors $(\boldsymbol{e}_1, \boldsymbol{e}_2, \boldsymbol{e}_3)$. It is given by:

$$\widetilde{\boldsymbol{C}} = \left[\frac{1}{|\Omega_\mu|}\int_{\Omega_\mu} (\boldsymbol{C}_\mu)_{ijpq}\, (\nabla^s_{\boldsymbol{y}} \Delta\widetilde{\boldsymbol{u}}_{kl})_{pq}\right] \boldsymbol{e}_i \otimes \boldsymbol{e}_j \otimes \boldsymbol{e}_k \otimes \boldsymbol{e}_l \tag{38}$$

where $\Delta\widetilde{\boldsymbol{u}}_{kl}$ is the *Tangential Displacement Fluctuation* vector determined by solving one linear system of equations for each macro-strain component $(\boldsymbol{e}_k \otimes^s \boldsymbol{e}_l)$, with $k, l = 1, 2, 3$. This set of variational linear problems is enunciated as follows: for $k, l = 1, 2, 3$ find $\Delta\widetilde{\boldsymbol{u}}_{kl} \in \mathcal{V}_\mu$ such that:

$$\int_{\Omega_\mu} \boldsymbol{C}_\mu \, \nabla^s_{\boldsymbol{y}} \Delta\widetilde{\boldsymbol{u}}_{kl} \cdot \nabla^s_{\boldsymbol{y}} \hat{\boldsymbol{u}}_\mu \, d\Omega_\mu = -\left[\int_{\Omega_\mu} \boldsymbol{C}_\mu \, (\boldsymbol{e}_k \otimes^s \boldsymbol{e}_l) \cdot \nabla^s_{\boldsymbol{y}} \hat{\boldsymbol{u}}_\mu \, d\Omega_\mu\right];$$
$$\forall \hat{\boldsymbol{u}}_\mu \in \mathcal{V}_\mu \tag{39}$$

Additional details about this derivation can be found in [40,29].

A summary of this Section is presented in Box 2, where the basic ingredients defining the *ClaMM* are shown.

4. Cohesive Multi-scale variational Model (*CohMM*)

The variational multi-scale formulation presented in this Section is envisaged for the modeling of the macroscopic post-critical stage of materials whose micro-structure undergoes degradation and failure. According to the methodology proposed in this contribution, a cohesive-crack is inserted in a macro-point $\boldsymbol{x}$ when the stress–strain state fulfills the criterion discussed in Section 2.2. In this case, the *Homogenized Cohesive-type Constitutive Relation*, developed in this Section, defines the corresponding constitutive response of the point $\boldsymbol{x}$.

We show that, following the same systematic approach of the previous Section (see in particular the Remark 3.3), and incorporating some rational kinematical ingredients, a variationally consistent framework can be established for modeling material failure in a multi-scale setting. The following developments describe, in detail, the item 4.2 in Box 1.

4.1. Kinematical description of the RVE

Let us focus our attention in the pseudo-time interval $t > t_N$, with t_N being the instant when the macro-crack nucleation criterion is first fulfilled at a certain point $\boldsymbol{x}$. An increment of the "*generalized*" macro-strain is characterized by a kinematically admissible increment of the displacement jump $d\boldsymbol{\beta}$ across the macro-crack $\mathcal{S}$ with normal $\boldsymbol{n}$, and by an increment of the regular counterpart $d\boldsymbol{\varepsilon}_R$. Thus, the kinematics in $\boldsymbol{x}$ is determined by: $\{d\boldsymbol{\varepsilon}_R, d\boldsymbol{\beta}, \boldsymbol{n}\}$.

Similarly to the *ClaMM*, the incremental micro-strain field, $d\boldsymbol{\varepsilon}_\mu$, can be described as the addition of two contributions:

$$d\boldsymbol{\varepsilon}_\mu = \mathcal{I}^*_{\boldsymbol{y}}(d\boldsymbol{\varepsilon}_R, d\boldsymbol{\beta}) + d\widetilde{\boldsymbol{\varepsilon}}_\mu \tag{40}$$

involving an adequate definition of the *Insertion Operator* $\mathcal{I}^*_{\boldsymbol{y}}$, which depends on $\boldsymbol{y}$, and a fluctuation component: $d\widetilde{\boldsymbol{\varepsilon}}_\mu := \nabla^s_{\boldsymbol{y}} d\widetilde{\boldsymbol{u}}_\mu$. With similar arguments to those given in the previous Section, only the regular component, $d\boldsymbol{\varepsilon}_R$, is uniformly inserted in Ω_μ. Then, expression (40) can be rewritten as follows:

$$d\boldsymbol{\varepsilon}_\mu = d\boldsymbol{\varepsilon}_R + \mathcal{I}^L_{\boldsymbol{y}}(d\boldsymbol{\beta}) + \nabla^s_{\boldsymbol{y}} d\widetilde{\boldsymbol{u}}_\mu \tag{41}$$

and the kinematical description reduces to define the new operator $\mathcal{I}^L_{\boldsymbol{y}}(\bullet)$, which establishes "*how*" the localized macro-mode is inserted into the *RVE*, such that it is consistent with the physical phenomenology of material failure at the micro-scale.

We denote Ω^L_μ $(\Omega^L_\mu \subset \Omega_\mu)$ the sub-domain where the micro-strain field, $\boldsymbol{\varepsilon}_\mu$, localizes. The criterion that defines Ω^L_μ, at the nucleation time t_N, is described in Section 4.3. It is postulated that an increment of the localized macro-kinematics, characterized by the elements $\{d\boldsymbol{\beta}, \boldsymbol{n}\}$, is uniformly inserted into Ω^L_μ, instead of being uniformly inserted into Ω_μ. Then, the "*macro-to-micro*" kinematical information transference is defined through the so-called *Failure-Oriented Insertion Operator* $\mathcal{I}^L_{\boldsymbol{y}}(\bullet)$:

$$\mathcal{I}^L_{\boldsymbol{y}}(d\boldsymbol{\beta}) = \phi^L_\mu(\boldsymbol{y}) \frac{d\boldsymbol{\beta} \otimes^s \boldsymbol{n}}{\ell_M} \quad \forall \boldsymbol{y} \in \Omega_\mu; \quad \phi^L_\mu(\boldsymbol{y}) = \begin{cases} \frac{|\Omega_\mu|}{|\Omega^L_\mu|} = \frac{\ell_M}{\ell_\mu} & \forall \boldsymbol{y} \in \Omega^L_\mu \\ 0 & \text{otherwise} \end{cases} \tag{42}$$

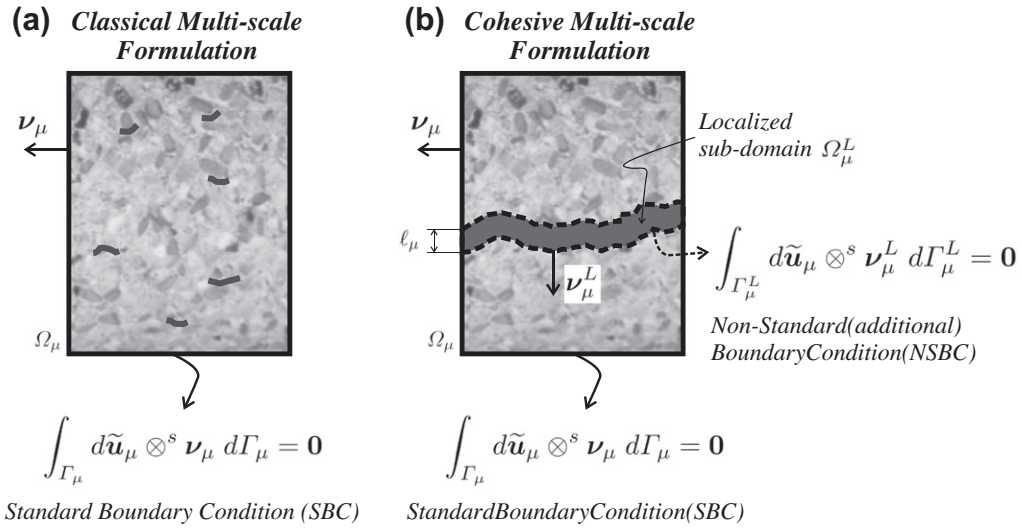

Fig. 4. Minimal Kinematical Constraints (boundary conditions) to be imposed on the micro-cell: (a) *Classical Multi-scale Model (ClaMM)*, (b) *Cohesive Multi-scale Model (CohMM)*.

where $\phi_\mu^L(\boldsymbol{y})$ is a collocation function and ℓ_μ represents the thickness where the strain localization process takes place, see Fig. 4. Furthermore, ℓ_M is a length parameter that, from the definition of $\phi_\mu^L(\boldsymbol{y})$, results:

$$\ell_M = \ell_\mu \frac{|\Omega_\mu|}{|\Omega_\mu^L|} \tag{43}$$

Remark 4.1. In the present methodology ℓ_M results immaterial, as we show in the following. Contrarily, ℓ_μ plays a very important and fundamental role in the mathematical formulation. Let us consider the so called Irwin's characteristic length of the material: $\ell_{ch} = EG_F/\sigma_u^2$ (where E is the Young's modulus, G_F the fracture energy and σ_u represents an ultimate limit stress). As exposed by Bazant and Planas [2], this physical parameter, ℓ_{ch}, is related to the width of the localization band in softening materials. Then, ℓ_μ could be associated with ℓ_{ch}. However, from the modelling point of view, it is convenient to differentiate both parameters, such that, even for a given material with fixed ℓ_{ch}, a localization bandwidth ℓ_μ, can be taken depending on the adopted model for regularizing the material softening. Typically, for example, considering a smeared crack approach at the RVE level, ℓ_μ should be associated to the finite element size, while the ratio ℓ_μ/ℓ_{ch} is used to define an intrinsic softening modulus of the continuum that regularizes the material response during the softening regime. Alternatively, by adopting a strong discontinuity model [27], it can be considered that: $\ell_\mu \to 0$ while ℓ_{ch} remains fixed.

In the present formulation, and from Remark 4.1, the parameter ℓ_μ, is called the localization bandwidth at the *RVE* finite element discretization level.

Since the *Failure-Oriented Insertion Operator* $\mathcal{I}_{\boldsymbol{y}}^L(\bullet)$ is linear, expression (42) can be rewritten as:

$$\mathcal{I}_{\boldsymbol{y}}^L(d\boldsymbol{\beta}) \equiv \boldsymbol{I}^L(\boldsymbol{y}) \, d\boldsymbol{\beta} = \begin{cases} \frac{d\boldsymbol{\beta}\otimes^s \boldsymbol{n}}{\ell_\mu} & \forall \boldsymbol{y} \in \Omega_\mu^L \\ \mathbf{0} & \text{otherwise} \end{cases} \tag{44}$$

where $\boldsymbol{I}^L(\boldsymbol{y})$ is a third order tensor field, that maps vectors $(d\boldsymbol{\beta})$ into symmetric second order tensors of the form given by (44). Note that, irrespective of the micro-cell size, for a given value of the macro displacement jump increment $d\boldsymbol{\beta}$, $\mathcal{I}_{\boldsymbol{y}}^L(\bullet)$ imposes "*identical*" micro-strains into the localized sub-domain Ω_μ^L.

The tensor $\boldsymbol{I}^L(\boldsymbol{y})$ has the following property: let $\boldsymbol{\Sigma}$ be a symmetric second order tensor and $\boldsymbol{\omega}$ an arbitrary vector, then:

$$\boldsymbol{\Sigma}\cdot\boldsymbol{I}^L(\boldsymbol{y})\,\boldsymbol{\omega} = \left(\boldsymbol{I}^L(\boldsymbol{y})\right)^T\boldsymbol{\Sigma}\cdot\boldsymbol{\omega} = \begin{cases} \frac{1}{\ell_\mu}\boldsymbol{\Sigma}\boldsymbol{n}\cdot\boldsymbol{\omega} & \forall \boldsymbol{y}\in\Omega_\mu^L \\ \mathbf{0} & \text{otherwise} \end{cases} \quad \forall \boldsymbol{\omega}\in\mathbb{R}^{\text{ndim}} \tag{45}$$

Hence $\left(\boldsymbol{I}^L(\boldsymbol{y})\right)^T$ is such that:

$$\left(\boldsymbol{I}^L(\boldsymbol{y})\right)^T\boldsymbol{\Sigma} = \begin{cases} \frac{1}{\ell_\mu}\boldsymbol{\Sigma}\boldsymbol{n} & \forall \boldsymbol{y}\in\Omega_\mu^L \\ \mathbf{0} & \text{otherwise} \end{cases} \tag{46}$$

We define that $d\boldsymbol{\varepsilon}_\mu$, given by (41) and (44), is *Kinematically Admissible* if it fulfills the following two constraints:

$$\int_{\Omega_\mu} \overbrace{\left[d\boldsymbol{\varepsilon}_R + \mathcal{I}_{\boldsymbol{y}}^L(d\boldsymbol{\beta})\right]}^{\mathcal{I}_{\boldsymbol{y}}^s(d\boldsymbol{\varepsilon}_R, d\boldsymbol{\beta})} d\Omega_\mu = \int_{\Omega_\mu} d\boldsymbol{\varepsilon}_\mu \, d\Omega_\mu \tag{47}$$

$$\int_{\Omega_\mu^L} \underbrace{\left[d\boldsymbol{\varepsilon}_R + \mathcal{I}_{\boldsymbol{y}}^L(d\boldsymbol{\beta})\right]}_{\mathcal{I}_{\boldsymbol{y}}^s(d\boldsymbol{\varepsilon}_R, d\boldsymbol{\beta})} d\Omega_\mu^L = \int_{\Omega_\mu^L} d\boldsymbol{\varepsilon}_\mu \, d\Omega_\mu^L \tag{48}$$

which, considering (42) and (44), are equivalent to:

$$d\boldsymbol{\varepsilon}_R + \frac{d\boldsymbol{\beta}\otimes^s\boldsymbol{n}}{\ell_M} = \frac{1}{|\Omega_\mu|}\int_{\Omega_\mu} d\boldsymbol{\varepsilon}_\mu \, d\Omega_\mu \tag{49}$$

$$d\boldsymbol{\varepsilon}_R + \frac{d\boldsymbol{\beta}\otimes^s\boldsymbol{n}}{\ell_\mu} = \frac{1}{|\Omega_\mu^L|}\int_{\Omega_\mu^L} d\boldsymbol{\varepsilon}_\mu \, d\Omega_\mu^L \tag{50}$$

In the present formulation, equations (49) and (50) define the *Strain Homogenization Procedures*. Notice the similarities between (49) and (50) and the strain homogenization formula (24), of the previous Section.

Considering the definitions (41) and (42), and after simple mathematical manipulation, expression (49) results equivalent to the following kinematical restriction on the micro-displacement fluctuation increments $d\widetilde{\boldsymbol{u}}_\mu$:

$$\int_{\Gamma_\mu} d\widetilde{\boldsymbol{u}}_\mu \otimes^s \boldsymbol{v}_\mu \, d\Gamma_\mu = \mathbf{0} \tag{51}$$

Eq. (51) represents the *conventional* kinematical constraint, already analyzed in the context of *ClaMM*. Therefore, we call this expression

the "*Standard Boundary Condition* (*SBC*)" for the proposed multi-scale formulation.

Similarly, in view of (41) and (44), the strain homogenization procedure (50) imposes an additional kinematical constraint on $d\widetilde{\boldsymbol{u}}_\mu$, given by:

$$\int_{\Gamma_\mu^L} d\widetilde{\boldsymbol{u}}_\mu \otimes^s \boldsymbol{v}_\mu^L \, d\Gamma_\mu^L = \boldsymbol{0} \tag{52}$$

where Γ_μ^L is the boundary of Ω_μ^L and $\boldsymbol{v}_\mu^L$ its outward unit normal vector. Observe that Eq. (52) naturally emerges from the adopted kinematical assumptions and induces kinematical boundary conditions to be applied on the new boundary Γ_μ^L. Hereafter, expression (52) is called the "*Non-Standard Boundary Condition* (*NSBC*)". It is interesting to observe here that the kinematical boundary condition *NSBC* to be prescribed over the new boundary Γ_μ^L is of the same type of the kinematical boundary condition *SBC* applied over the boundary of the *RVE*, Γ_μ. Furthermore, from the theoretical point of view they do not need to be identical. See the examples in Section 5.4 and 5.6.

Box 2: Classical Multi-scale Model (ClaMM): given $\boldsymbol{\varepsilon}_R^{(t-dt)}$ and $d\boldsymbol{\varepsilon}_R$; find $d\boldsymbol{\sigma}$ and $\boldsymbol{C}$ (Equations governing the stable material response of a macro-point)

1.***Kinematics:***

$$d\boldsymbol{\varepsilon}_\mu = \mathcal{I}_{\boldsymbol{y}}(d\boldsymbol{\varepsilon}_R) + d\widetilde{\boldsymbol{\varepsilon}}_\mu = d\boldsymbol{\varepsilon}_R + \nabla_{\boldsymbol{y}}^s d\widetilde{\boldsymbol{u}}_\mu; \quad \forall \boldsymbol{y} \in \Omega_\mu$$
$$\mathcal{I}_{\boldsymbol{y}}(\bullet) \equiv \boldsymbol{I}(\boldsymbol{y})(\bullet) = (\bullet); \quad \forall \boldsymbol{y} \in \Omega_\mu$$

1.a *Kinematical Admissibility Concept and Strain Homogenization Procedure:*

$$\int_{\Omega_\mu} \mathcal{I}_{\boldsymbol{y}}(d\boldsymbol{\varepsilon}_R)\, d\Omega_\mu = \int_{\Omega_\mu} d\boldsymbol{\varepsilon}_\mu \, d\Omega_\mu \quad \Rightarrow \quad d\boldsymbol{\varepsilon}_R = \frac{1}{|\Omega_\mu|}\int_{\Omega_\mu} d\boldsymbol{\varepsilon}_\mu \, d\Omega_\mu$$
$$d\widetilde{\boldsymbol{u}}_\mu \in \widetilde{\mathcal{U}}_\mu;\ \widetilde{\mathcal{U}}_\mu \equiv \left\{ d\widetilde{\boldsymbol{u}}_\mu;\ d\widetilde{\boldsymbol{u}}_\mu \in \mathbf{H}^1(\Omega) \text{ and } \int_{\Gamma_\mu} d\widetilde{\boldsymbol{u}}_\mu \otimes^s \boldsymbol{v}_\mu \, d\Gamma_\mu = \boldsymbol{0} \right\}$$

1.b *Virtual kinematically admissible actions (velocities):*

$$\hat{\boldsymbol{u}}_\mu \in \mathcal{V}_\mu;\ \mathcal{V}_\mu \equiv \left\{ \hat{\boldsymbol{u}}_\mu;\ \hat{\boldsymbol{u}}_\mu \in \mathbf{H}^1(\Omega) \text{ and } \int_{\Gamma_\mu} \hat{\boldsymbol{u}}_\mu \otimes^s \boldsymbol{v}_\mu \, d\Gamma_\mu = \boldsymbol{0} \right\}$$
$$\hat{\boldsymbol{\varepsilon}}_\mu = \mathcal{I}_{\boldsymbol{y}}(\hat{\boldsymbol{\varepsilon}}_R) + \nabla_{\boldsymbol{y}}^s \hat{\boldsymbol{u}}_\mu; \quad \forall \hat{\boldsymbol{\varepsilon}}_R \text{ and } \forall \hat{\boldsymbol{u}}_\mu \in \mathcal{V}_\mu$$

2.***Hill-Mandel Variational Principle of Macro-Homogeneity:***

$$d\boldsymbol{\sigma} \cdot \hat{\boldsymbol{\varepsilon}}_R = \frac{1}{|\Omega_\mu|}\int_{\Omega_\mu} d\boldsymbol{\sigma}_\mu \cdot \hat{\boldsymbol{\varepsilon}}_\mu \, d\Omega_\mu \quad ; \quad \forall \hat{\boldsymbol{\varepsilon}}_R \text{ and } \forall \hat{\boldsymbol{\varepsilon}}_\mu \text{ kinematically admissible}$$

2.a *First consequence of the Hill-Mandel Principle: Stress Homogenization Operator* $\mathcal{H}(\bullet)$

$$\mathcal{H}(d\boldsymbol{\sigma}_\mu) = \frac{1}{|\Omega_\mu|}\int_{\Omega_\mu} (\boldsymbol{I}(\boldsymbol{y}))^T \, d\boldsymbol{\sigma}_\mu \, d\Omega_\mu = \frac{1}{|\Omega_\mu|}\int_{\Omega_\mu} d\boldsymbol{\sigma}_\mu \, d\Omega_\mu = d\boldsymbol{\sigma}$$

2.b *Second consequence of the Hill-Mandel Principle: Micro-Equilibrium problem*

Given $\boldsymbol{\varepsilon}_R^{(t-dt)}$ and $d\boldsymbol{\varepsilon}_R$; find $d\widetilde{\boldsymbol{u}}_\mu \in \widetilde{\mathcal{U}}_\mu$ such that :

$$\int_{\Omega_\mu} d\boldsymbol{\sigma}_\mu \cdot \nabla_{\boldsymbol{y}}^s \hat{\boldsymbol{u}}_\mu \, d\Omega_\mu = 0 \qquad \forall \hat{\boldsymbol{u}}_\mu \in \mathcal{V}_\mu$$

3.***Constitutive Model at the micro-scale:***

$$\boldsymbol{\sigma}_\mu = \mathcal{F}_\mu(\boldsymbol{\varepsilon}_\mu^{(t)})$$

4.***Homogenized Tangent Constitutive Tensor:***

$$\boldsymbol{C} = \boldsymbol{C}_T + \widetilde{\boldsymbol{C}}$$

4.a *Taylor contribution*

$$\boldsymbol{C}_T = \frac{1}{|\Omega_\mu|}\int_{\Omega_\mu} \boldsymbol{C}_\mu \, d\Omega_\mu$$

4.b *Fluctuation contribution*

For $k, l = 1, 2, 3$; find $\Delta\widetilde{\boldsymbol{u}}_{kl} \in \mathcal{V}_\mu$ such that :

$$\int_{\Omega_\mu} \boldsymbol{C}_\mu \nabla_{\boldsymbol{y}}^s \Delta\widetilde{\boldsymbol{u}}_{kl} \cdot \nabla_{\boldsymbol{y}}^s \hat{\boldsymbol{u}}_\mu \, d\Omega_\mu = -\left[\int_{\Omega_\mu} \boldsymbol{C}_\mu \, (\boldsymbol{e}_k \otimes^s \boldsymbol{e}_l) \cdot \nabla_{\boldsymbol{y}}^s \hat{\boldsymbol{u}}_\mu \, d\Omega_\mu \right]; \quad \forall \hat{\boldsymbol{u}}_\mu \in \mathcal{V}_\mu$$
$$\widetilde{\boldsymbol{C}} = \left[\frac{1}{|\Omega_\mu|}\int_{\Omega_\mu} (\boldsymbol{C}_\mu)_{ijpq} \, (\nabla_{\boldsymbol{y}}^s \Delta\widetilde{\boldsymbol{u}}_{kl})_{pq} \, d\Omega_\mu \right] \boldsymbol{e}_i \otimes \boldsymbol{e}_j \otimes \boldsymbol{e}_k \otimes \boldsymbol{e}_l$$

Remark 4.2. The distinguishing features of the present CohMM approach are threefold: (i) the nature of the adopted Insertion Operator $\mathcal{I}^L_{\boldsymbol{y}}(\bullet)$ defined in expression (42), (ii) the "Kinematical Admissibility" concept given by expressions (47), (48) and (iii) the additional derived kinematical constraints given by expression (52). These features represent the most salient differences between the present model and existing multi-scale formulations accounting for failure and strain localization.

The set of Eqs. (51) and (52) defines what we call the *Minimally Constrained Vector Space* of *kinematically admissible incremental displacement fluctuations* in the *RVE*: $\widetilde{\mathcal{U}}^L_\mu$. Formally, the micro-field $d\widetilde{\boldsymbol{u}}_\mu$ is kinematically admissible if $d\widetilde{\boldsymbol{u}}_\mu \in \widetilde{\mathcal{U}}^L_\mu$:

$$\widetilde{\mathcal{U}}^L_\mu \equiv \left\{ d\widetilde{\boldsymbol{u}}_\mu;\ d\widetilde{\boldsymbol{u}}_\mu \in \mathbf{H}^1(\Omega_\mu), \quad \int_{\Gamma_\mu} d\widetilde{\boldsymbol{u}}_\mu \otimes^s \boldsymbol{v}_\mu \, d\Gamma_\mu = \mathbf{0} \quad \text{and} \right.$$
$$\left. \int_{\Gamma^L_\mu} d\widetilde{\boldsymbol{u}}_\mu \otimes^s \boldsymbol{v}^L_\mu \, d\Gamma^L_\mu = \mathbf{0} \right\} \tag{53}$$

Then, the minimally constrained vector space $\boldsymbol{\mathcal{V}}^L_\mu$ of virtual kinematically admissible actions (velocities), $\hat{\boldsymbol{u}}_\mu$, can be defined as:

$$\boldsymbol{\mathcal{V}}^L_\mu \equiv \left\{ \hat{\boldsymbol{u}}_\mu;\ \hat{\boldsymbol{u}}_\mu \in \mathbf{H}^1(\Omega_\mu), \quad \int_{\Gamma_\mu} \hat{\boldsymbol{u}}_\mu \otimes^s \boldsymbol{v}_\mu \, d\Gamma_\mu = \mathbf{0} \quad \text{and} \quad \int_{\Gamma^L_\mu} \hat{\boldsymbol{u}}_\mu \otimes^s \boldsymbol{v}^L_\mu \, d\Gamma^L_\mu = \mathbf{0} \right\} \tag{54}$$

from where: $\widetilde{\mathcal{U}}^L_\mu \equiv \boldsymbol{\mathcal{V}}^L_\mu$. Furthermore, it follows that:

$$\boldsymbol{\mathcal{V}}^L_\mu \subset \boldsymbol{\mathcal{V}}_\mu \tag{55}$$

where $\boldsymbol{\mathcal{V}}_\mu$ has been defined in expression (27).

Considering (41), (44) and (54), it is also possible to introduce the concept of virtual kinematically admissible micro-strain $\hat{\boldsymbol{\varepsilon}}_\mu$:

$$\hat{\boldsymbol{\varepsilon}}_\mu = \boldsymbol{I}^L(\boldsymbol{y})\,\hat{\boldsymbol{\beta}} + \nabla^s_{\boldsymbol{y}}\hat{\boldsymbol{u}}_\mu = \phi^L_\mu(\boldsymbol{y})\,\frac{\hat{\boldsymbol{\beta}}\otimes^s \boldsymbol{n}}{\ell_M} + \nabla^s_{\boldsymbol{y}}\hat{\boldsymbol{u}}_\mu; \quad \forall\,\hat{\boldsymbol{\beta}} \text{ and } \forall\,\hat{\boldsymbol{u}}_\mu \in \boldsymbol{\mathcal{V}}^L_\mu \tag{56}$$

where $\hat{\boldsymbol{\beta}}$ is a virtual kinematically admissible macro-displacement jump defined in $\mathcal{S}$. Comparing Eq. (41) with (56), it can be noticed that, for $t > t_N$, $d\boldsymbol{\varepsilon}_R$ does not induce virtual actions in the micro-scale.

In Fig. 4, we compare the *Minimal Kinematical Constraints* that are imposed on a generic *RVE* using both, the *ClaMM* and the *CohMM* approaches. As we show in Section 4.2, the additional restriction (52) gives *mechanical consistency* to the formulation, in the sense that the homogenized response results *objective* with respect to the *RVE*-size.

The *Standard Boundary Condition* (51) is included in the model from the beginning of the analysis. Meanwhile, the *Non-Standard Boundary Condition* (52) is introduced once the sub-domain Ω^L_μ is properly defined, i.e. after fulfilling the macro-crack nucleation criterion at $t = t_N$. In this context, the adopted "*incremental*" framework plays a fundamental role because it allows for a time continuous kinematical transition, from the *ClaMM* to the new *CohMM*, which is adapted for the treatment of generalized kinematics (strain and macro-discontinuities). The topology of Ω^L_μ has to be established according to the micro-cell mechanical state at t_N. In Section 4.3, we propose a kinematical criterion to define the geometry and boundaries of Ω^L_μ.

Remark 4.3. Alternative Failure-Oriented Multi-scale sub-models can be adopted by taking sub-spaces of $\widetilde{\mathcal{U}}^L_\mu$ and $\boldsymbol{\mathcal{V}}^L_\mu$, such as: (i) the Taylor model, (ii) the Linear or Affine model and (iii) the Periodic model. Note also that, any alternative combination between the multi-scale sub-models derived from the Standard Boundary Condition (51) and those derived from the Non-Standard Boundary Condition (52), are also possible. From this perspective, expression (52) represents the most flexible Kinematical Constraint.

Henceforth, we follow the same conceptual steps and variational arguments discussed in the context of the *ClaMM*. Thus, once the kinematics of the multi-scale model has been defined, the Hill–Mandel Principle is postulated and its variational consequences are derived. This fact evidences the kinematical character of the assumptions incorporated in the present multi-scale framework, justifying the comments in the items (I) and (II) listed in the introductory Section.

4.2. The Hill–Mandel Variational Principle of macro-homogeneity

In order to guarantee energetic consistency, the Hill–Mandel Variational Principle of Macro-Homogeneity is postulated. For the present case we adapt this Principle to deal with the generalized stresses, $\boldsymbol{T}$, and generalized virtual displacement, $\hat{\boldsymbol{\beta}}$, which are defined at the macro-level. Thus, the macro internal virtual power per unit of crack area is given by:

$$P^{int}_{\mathcal{S}} = \boldsymbol{T}\cdot\hat{\boldsymbol{\beta}} \tag{57}$$

Then, for $t > t_N$, the Hill–Mandel Principle is written as follows:

$$\boldsymbol{T}\cdot\hat{\boldsymbol{\beta}} = \frac{\ell_M}{|\Omega_\mu|}\int_{\Omega_\mu} \boldsymbol{\sigma}_\mu \cdot \hat{\boldsymbol{\varepsilon}}_\mu \, d\Omega_\mu; \quad \forall\,\hat{\boldsymbol{\beta}},\ \forall\,\hat{\boldsymbol{\varepsilon}}_\mu \text{ kinematically admissible} \tag{58}$$

where the right hand side term represents the *RVE* total internal virtual power per unit of area of a *RVE* characteristic surface, orthogonal to the vector $\boldsymbol{n}$, and representative of the failure domain in Ω_μ. The area of this surface is given by: $|\Omega_\mu|/\ell_M$.

Considering that the variational equation (58) is satisfied during the previous loading history, see the remark (4.5) below, and the definition of virtual micro-strain $\hat{\boldsymbol{\varepsilon}}_\mu$ from (56), the Hill–Mandel Principle can be expressed in an incremental form, as follows:

$$\left[d\boldsymbol{T} - \frac{\ell_M}{|\Omega_\mu|}\int_{\Omega_\mu} \left(\boldsymbol{I}^L(\boldsymbol{y})\right)^T d\boldsymbol{\sigma}_\mu \, d\Omega_\mu \right]\cdot\hat{\boldsymbol{\beta}} - \frac{\ell_M}{|\Omega_\mu|}\int_{\Omega_\mu} d\boldsymbol{\sigma}_\mu \cdot \nabla^s_{\boldsymbol{y}}\hat{\boldsymbol{u}}_\mu \, d\Omega_\mu = 0;$$
$$\forall\,\hat{\boldsymbol{\beta}},\ \forall\,\hat{\boldsymbol{u}}_\mu \in \boldsymbol{\mathcal{V}}^L_\mu \tag{59}$$

4.2.1. First consequence of the Hill–Mandel Principle: the Failure-Oriented homogenized mechanical response

From the variational equation (59), by taking arbitrary variations $\hat{\boldsymbol{\beta}}$ and $\hat{\boldsymbol{u}}_\mu \equiv \mathbf{0}$, it is derived the *micro-to-macro Failure-Oriented Stress Homogenization Operator* $\boldsymbol{\mathcal{H}}^L(\bullet)$:

$$d\boldsymbol{T} = \boldsymbol{\mathcal{H}}^L(d\boldsymbol{\sigma}_\mu) = \frac{\ell_M}{|\Omega_\mu|}\int_{\Omega_\mu} \left(\boldsymbol{I}^L(\boldsymbol{y})\right)^T d\boldsymbol{\sigma}_\mu \, d\Omega_\mu; \quad \text{for } t > t_N \tag{60}$$

and by recalling the property of the tensor $\left(\boldsymbol{I}^L(\boldsymbol{y})\right)^T$, given by expression (46), this *Operator* reads:

$$\boldsymbol{\mathcal{H}}^L(d\boldsymbol{\sigma}_\mu) = \frac{1}{|\Omega^L_\mu|}\int_{\Omega^L_\mu} d\boldsymbol{\sigma}_\mu \, \boldsymbol{n} \, d\Omega^L_\mu; \quad \text{for } t > t_N \tag{61}$$

Observe that the homogenization of the stresses at the micro-level, Eqs. (60) and (61), is not an "*a priori*" mechanical definition, but it arises as a consequence of the adopted admissible kinematics, defined through the operator $\mathcal{I}^L_{\boldsymbol{y}}(\bullet)$, and the Hill–Mandel Principle.

The expression (60) is a *Non-Standard* homogenization procedure for stresses. It has two distinctive features with respect to the classical stress homogenization approach defined in Eq. (33):

(i) the homogenization is performed considering the contribution from points $\boldsymbol{y} \in \Omega^L_\mu$, according to the definition of the adopted insertion operator $\mathcal{I}^L_{\boldsymbol{y}}(\bullet)$, and
(ii) the homogenization is performed with the incremental traction $d\boldsymbol{\sigma}_\mu\boldsymbol{n}$.

The previous considerations give a full justification for the point (III) enunciated in the introductory Section.

Remark 4.4. The present stress homogenization procedure ensures an objective connection between $d\boldsymbol{T}$ and $d\boldsymbol{\beta}$, irrespective of the RVE-size. Observe that the application of the additional Non-Standard Boundary Condition (52) associates the increments of the generalized strains, $d\boldsymbol{\beta}$, with the strains inserted into Ω^L_μ, since: $\int_{\Omega^L_\mu} d\widetilde{\boldsymbol{\varepsilon}}_\mu \, d\Omega^L_\mu = \mathbf{0}$.

This remark justifies the item (VI) listed in the introduction Section.

4.2.2. Second consequence of the Hill–Mandel Principle: the RVE equilibrium problem

From expression (59), by adopting $\hat{\boldsymbol{\beta}} \equiv \mathbf{0}$ and arbitrary variations $\hat{\boldsymbol{u}}_\mu$, it is derived the variational equilibrium at the micro-level, which is enunciated as follows:

Given the history of macro-generalized strains $\{\boldsymbol{\varepsilon}_R^{(t-dt)}, \boldsymbol{\beta}^{(t-dt)}\}$ and kinematically admissible increments $\{d\boldsymbol{\varepsilon}_R, d\boldsymbol{\beta}\}$; find the incremental micro-displacement fluctuation field $d\widetilde{\boldsymbol{u}}_\mu \in \widetilde{\mathcal{U}}_\mu^L$, such that:

$$\int_{\Omega_\mu} d\boldsymbol{\sigma}_\mu \cdot \nabla_{\boldsymbol{y}}^s \hat{\boldsymbol{u}}_\mu \, d\Omega_\mu = 0; \quad \forall \hat{\boldsymbol{u}}_\mu \in \mathcal{V}_\mu^L \text{ and for } t > t_N \tag{62}$$

The variational equation (62) determines that the incremental micro stress field, $d\boldsymbol{\sigma}_\mu$, is self-equilibrated. This stress is the reaction to the imposed generalized loading system induced by the application of the generalized macro-strain increments, $d\boldsymbol{\varepsilon}_R$ and $\mathcal{I}_{\boldsymbol{y}}^L(d\boldsymbol{\beta})$, in Ω_μ and Ω_μ^L, respectively. Moreover, notice that the variational equilibrium problem is subjected to special kinematical restrictions according to the definitions of $\widetilde{\mathcal{U}}_\mu^L$ and $\mathcal{V}_\mu^L$, expressed in (53) and (54)), which are consistent with the two strain homogenization procedures (49) and (50).

For convenience, the relevant expressions defining the *CohMM* are summarized in Box 3. Note the similarities and differences between the main ingredients of Boxes 2 and 3.

Remark 4.5. The derivation of Eq. (59) in terms of increments, from expression (58), requires the time continuity of macro-tractions in $\mathcal{S}$. Particularly, this requirement has to be fulfilled at $t = t_N$. This is a delicate issue which motivates the specific selection of the domain Ω_μ^L described in the following Section 4.3. This time continuity condition can be expressed as follows:

$$\boldsymbol{T}^{\text{ClaMM}} = \boldsymbol{T}^{\text{CohMM}} \quad \text{for } t = t_N \tag{63}$$

where $\boldsymbol{T}^{\text{ClaMM}}$ is the traction vector in $\mathcal{S}$ evaluated with the ClaMM formulation:

$$\boldsymbol{T}^{\text{ClaMM}} = \frac{1}{|\Omega_\mu|} \int_{\Omega_\mu} \boldsymbol{\sigma}_\mu \boldsymbol{n} \, d\Omega_\mu \tag{64}$$

and $\boldsymbol{T}^{\text{CohMM}}$ is the traction vector in $\mathcal{S}$ evaluated with the CohMM formulation:

$$\boldsymbol{T}^{\text{CohMM}} = \frac{1}{|\Omega_\mu^L|} \int_{\Omega_\mu^L} \boldsymbol{\sigma}_\mu \boldsymbol{n} \, d\Omega_\mu^L \tag{65}$$

Box 3: Cohesive Multi-scale Model (CohMM): given $\{\boldsymbol{\varepsilon}_R^{(t-dt)}, \boldsymbol{\beta}^{(t)}\}$ and $\{d\boldsymbol{\varepsilon}_R, d\boldsymbol{\beta}\}$; find $d\boldsymbol{T}$ (Expressions valid for the points belonging to the macro-cohesive cracks)

1.***Kinematics:***

$$d\boldsymbol{\varepsilon}_\mu = \overbrace{d\boldsymbol{\varepsilon}_R + \mathcal{I}_{\boldsymbol{y}}^L(d\boldsymbol{\beta})}^{\mathcal{I}_{\boldsymbol{y}}^s(d\boldsymbol{\varepsilon}_R, d\boldsymbol{\beta})} + d\widetilde{\boldsymbol{\varepsilon}}_\mu = d\boldsymbol{\varepsilon}_R + \phi_\mu^L(\boldsymbol{y}) \frac{d\boldsymbol{\beta} \otimes^s \boldsymbol{n}}{\ell_M} + \nabla_{\boldsymbol{y}}^s d\widetilde{\boldsymbol{u}}_\mu; \quad \forall \boldsymbol{y} \in \Omega_\mu$$

$$\phi_\mu^L(\boldsymbol{y}) = \begin{cases} \frac{|\Omega_\mu|}{|\Omega_\mu^L|} = \frac{\ell_M}{\ell_\mu} & \forall \boldsymbol{y} \in \Omega_\mu^L \\ 0 & \text{otherwise} \end{cases}$$

$$\mathcal{I}_{\boldsymbol{y}}^L(\bullet) \equiv \boldsymbol{I}^L(\boldsymbol{y}) \, (\bullet) = \phi_\mu^L(\boldsymbol{y}) \frac{(\bullet) \otimes^s \boldsymbol{n}}{\ell_M}; \quad \forall \boldsymbol{y} \in \Omega_\mu$$

1.a *Kinematical Admissibility Concept and Strain Homogenization Procedures:*

$$\int_{\Omega_\mu} \left[d\boldsymbol{\varepsilon}_R + \mathcal{I}_{\boldsymbol{y}}^L(d\boldsymbol{\beta}) \right] d\Omega_\mu = \int_{\Omega_\mu} d\boldsymbol{\varepsilon}_\mu \, d\Omega_\mu \quad \Rightarrow \quad d\boldsymbol{\varepsilon}_R + \frac{d\boldsymbol{\beta} \otimes^s \boldsymbol{n}}{\ell_M} = \frac{1}{|\Omega_\mu|} \int_{\Omega_\mu} d\boldsymbol{\varepsilon}_\mu \, d\Omega_\mu$$

$$\int_{\Omega_\mu^L} \left[d\boldsymbol{\varepsilon}_R + \mathcal{I}_{\boldsymbol{y}}^L(d\boldsymbol{\beta}) \right] d\Omega_\mu^L = \int_{\Omega_\mu^L} d\boldsymbol{\varepsilon}_\mu \, d\Omega_\mu^L \quad \Rightarrow \quad d\boldsymbol{\varepsilon}_R + \frac{d\boldsymbol{\beta} \otimes^s \boldsymbol{n}}{\ell_\mu} = \frac{1}{|\Omega_\mu^L|} \int_{\Omega_\mu^L} d\boldsymbol{\varepsilon}_\mu \, d\Omega_\mu^L$$

$$d\widetilde{\boldsymbol{u}}_\mu \in \widetilde{\mathcal{U}}_\mu^L; \; \widetilde{\mathcal{U}}_\mu^L \equiv \left\{ d\widetilde{\boldsymbol{u}}_\mu; \; d\widetilde{\boldsymbol{u}}_\mu \in \mathbf{H}^1(\Omega), \; \int_{\Gamma_\mu} d\widetilde{\boldsymbol{u}}_\mu \otimes^s \boldsymbol{v}_\mu \, d\Gamma_\mu = \mathbf{0} \text{ and } \int_{\Gamma_\mu^L} d\widetilde{\boldsymbol{u}}_\mu \otimes^s \boldsymbol{v}_\mu^L \, d\Gamma_\mu^L = \mathbf{0} \right\}$$

1.b *Virtual kinematically admissible actions (velocities):*

$$\hat{\boldsymbol{u}}_\mu \in \mathcal{V}_\mu^L; \; \mathcal{V}_\mu^L \equiv \left\{ \hat{\boldsymbol{u}}_\mu; \; \hat{\boldsymbol{u}}_\mu \in \mathbf{H}^1(\Omega), \; \int_{\Gamma_\mu} \hat{\boldsymbol{u}}_\mu \otimes^s \boldsymbol{v}_\mu \, d\Gamma_\mu = \mathbf{0} \text{ and } \int_{\Gamma_\mu^L} \hat{\boldsymbol{u}}_\mu \otimes^s \boldsymbol{v}_\mu^L \, d\Gamma_\mu^L = \mathbf{0} \right\}$$

$$\hat{\boldsymbol{\varepsilon}}_\mu = \mathcal{I}_{\boldsymbol{y}}^L(\hat{\boldsymbol{\beta}}) + \nabla_{\boldsymbol{y}}^s \hat{\boldsymbol{u}}_\mu = \phi_\mu^L(\boldsymbol{y}) \frac{\hat{\boldsymbol{\beta}} \otimes^s \boldsymbol{n}}{\ell_M} + \nabla_{\boldsymbol{y}}^s \hat{\boldsymbol{u}}_\mu; \quad \forall \hat{\boldsymbol{\beta}} \text{ and } \forall \hat{\boldsymbol{u}}_\mu \in \mathcal{V}_\mu^L$$

2.***Hill-Mandel Variational Principle of Macro-Homogeneity:***

$$d\boldsymbol{T} \cdot \hat{\boldsymbol{\beta}} = \frac{\ell_M}{|\Omega_\mu|} \int_{\Omega_\mu} d\boldsymbol{\sigma}_\mu \cdot \hat{\boldsymbol{\varepsilon}}_\mu \, d\Omega_\mu; \quad \forall \hat{\boldsymbol{\beta}} \text{ and } \forall \hat{\boldsymbol{\varepsilon}}_\mu \text{ kinematically admissible}$$

2.a *First consequence of the Hill-Mandel Principle: Failure-Oriented Stress Homogenization Operator:* $\mathcal{H}^L(\bullet)$

$$\mathcal{H}^L(d\boldsymbol{\sigma}_\mu) = \frac{\ell_M}{|\Omega_\mu|} \int_{\Omega_\mu} \left(\boldsymbol{I}^L(\boldsymbol{y}) \right)^T d\boldsymbol{\sigma}_\mu \, d\Omega_\mu = \frac{1}{|\Omega_\mu^L|} \int_{\Omega_\mu^L} d\boldsymbol{\sigma}_\mu \boldsymbol{n} \, d\Omega_\mu^L = d\boldsymbol{T}$$

2.b *Second consequence of the Hill-Mandel Principle: Micro-Equilibrium problem*

Given $\{\boldsymbol{\varepsilon}_R^{(t-dt)}, \boldsymbol{\beta}^{(t-dt)}\}$ and $\{d\boldsymbol{\varepsilon}_R, d\boldsymbol{\beta}\}$; find $d\widetilde{\boldsymbol{u}}_\mu \in \widetilde{\mathcal{U}}_\mu^L$ such that :

$$\int_{\Omega_\mu} d\boldsymbol{\sigma}_\mu \cdot \nabla_{\boldsymbol{y}}^s \hat{\boldsymbol{u}}_\mu \, d\Omega_\mu = 0 \qquad \forall \hat{\boldsymbol{u}}_\mu \in \mathcal{V}_\mu^L$$

4.3. Identification of the localization sub-domain Ω_μ^L in the micro-cell

The so-called *Localization sub-domain* Ω_μ^L has to be identified at $t = t_N$ when the macro-crack nucleation condition is detected. In this Section, we define a criterion to perform this task.

First, we recall that the nucleation criterion of Section 2.2, determining t_N, is based on the existence of a *strain localization-band*, normal to the vector $\boldsymbol{n}$, and the unit vector $\dot{\boldsymbol{\gamma}}_i$ which is parallel to the initial (pseudo-) velocity crack-opening direction. It is presumed that in the interior points of the macro-band, the strain rate component in the direction $(\dot{\boldsymbol{\gamma}}_i \otimes^s \boldsymbol{n})$ increases. On the contrary, in the exterior points of the band, this strain rate component decreases. Then, it is reasonable to postulate that Ω_μ^L can be identified by exploiting this feature. The procedure to define Ω_μ^L is enunciated in the following two steps.

Let be given the set: $\mathbb{S}_N = \{t_N, \boldsymbol{n}, \dot{\boldsymbol{\gamma}}_i\}$ determined at the macro-crack nucleation time t_N:

(i) Apply to the micro-cell, a uniform strain rate given by $(\dot{\boldsymbol{\gamma}}_i \otimes^s \boldsymbol{n})$. Compute the corresponding increments of the strain rate fluctuation, $d\dot{\tilde{\boldsymbol{\varepsilon}}}_\mu$, by solving a similar variational equilibrium problem as it is done in the previous pseudo-time instants, see expression (34). Observe that the *ClaMM* setting is still considered in this step.

(ii) In the micro-cell domain, compute the projection of the micro-strain rate fluctuation in the direction $(\dot{\boldsymbol{\gamma}}_i \otimes^s \boldsymbol{n})$. Then, define Ω_μ^L as follows:

$$\Omega_\mu^L = \left\{ \boldsymbol{y} \in \Omega_\mu,\ d\dot{\tilde{\boldsymbol{\varepsilon}}}_\mu(\boldsymbol{y}) : (\dot{\boldsymbol{\gamma}}_i \otimes^s \boldsymbol{n}) > 0 \text{ for } t = t_N \right\} \tag{66}$$

It is noted that this methodology is exclusively based on a "*kinematical*" criterion and does not take into account the specific constitutive response of points in Ω_μ^L.

The kinematic based rule (66) defining Ω_μ^L, describes a wide range of different situations, as for example those illustrated in Fig. 5 where the shaded dark gray zone identifies the points fulfilling the requirement (66), and thus, it is identified as the strain-localization band Ω_μ^L. Also, in this Figure, the points where the material is described through a constitutive model with softening are denoted: Ω_μ^{Ls}, the additional supra-index "s" indicates softening. Each situation is characterized as follows:

(a) The simpler and more intuitive case is sketched in Fig. 5(a), where the micro-strain localization band, Ω_μ^L, is constituted of materials displaying softening. Evidently, in this case we have: $\Omega_\mu^L \equiv \Omega_\mu^{Ls}$.

(b) Fig. 5(b) shows the case where the points fulfilling the criterion (66) comprise an inclusion of elastic material, Ω_μ^{Le}, which never displays unstable behavior nor softening. Then: $\Omega_\mu^L = \Omega_\mu^{Ls} \cup \Omega_\mu^{Le}$.

(c) Fig. 5(c) shows the case where the micro-structure has voids. In this case, the voids must be thought of being constituted of an extremely flexible elastic material, with the elasticity coefficient going to zero. Then, the void interior points can also be tested through the criterion (66). Those points fulfilling the criterion are denoted: Ω_μ^{Lv}. In this case, the localization sub-domain is defined as: $\Omega_\mu^L = \Omega_\mu^{Ls} \cup \Omega_\mu^{Lv}$.

Even when we cannot formally prove that the present selection of Ω_μ^L guarantees the continuity condition (63) in all conceivable situations, we show in the numerical tests that traction time continuity at $t = t_N$ is fulfilled in the entire range of tested situations, which turns to encompass a wide spectrum of possible failure scenarios. We consider that this issue still remains open in the present *FOMF*.

5. Numerical tests

The variational *FOMF* is implemented into a finite element code. Details of the numerical approximation, as well as several algorithmic aspects of the model, are exposed in Appendix A.

In this Section we show a series of problems that are focused in the analysis of the fundamental aspects of the methodology, that is the nucleation and evolution of strain localized bands in the *RVE* and the "*objectivity*", with respect to the micro-cell size, of the resulting homogenized constitutive response to be transferred to the macro-scale. All the numerical tests share the following characteristics:

- Micro-structures display a simple topology of heterogeneities.
- The sub-domains Ω_μ^L in which strain-localization takes place is pre-induced from the beginning of the analysis by means of the material definition at the micro-level; thus the boundary Γ_μ^L, following the guidelines given in Fig. 5, is also pre-induced (although criterion (66) is employed in its determination).
- In the numerical assessments performed in Sections 5.2, 5.3, 5.4, 5.5, the non-linear macro equilibrium equations are not solved. We define the *RVE* micro-mechanical problem by inserting an arbitrary history of generalized macro-strains given by the successive insertion of $\{d\boldsymbol{\varepsilon}_R, d\boldsymbol{\beta}\}$, at each pseudo-time instant. However, in order to demonstrate that the present approach works as a multiscale formulation, a simple fully coupled (macro–micro) stretching numerical test is addressed in

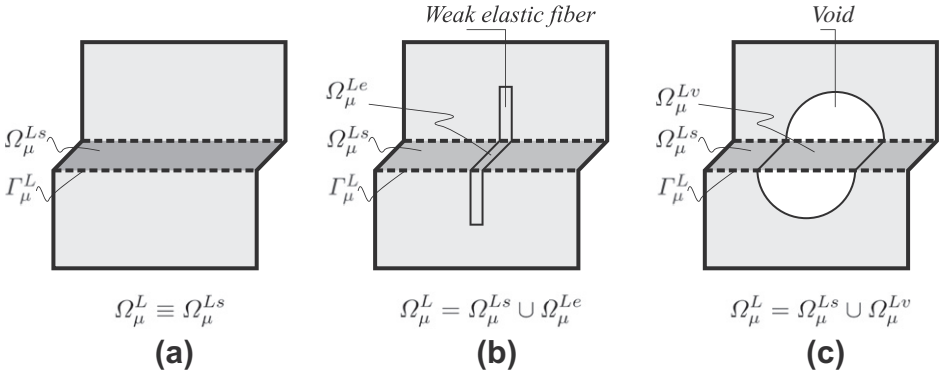

Fig. 5. Localization sub-domain Ω_μ^L for different types of heterogeneous micro-structures: (a) strain-localization sub-domain composed, entirely, of softening-material, (b) strain-localization sub-domain composed of softening-material and elastic fibers, and (c) strain-localization sub-domain composed of softening-material and voids.

Section 5.6. The invariance of the macroscopic solution with respect to the finite element mesh refinement in the micro-scale is also showed in the fully coupled stretching example.

5.1. Preliminaries. General settings

A generic unit system is adopted: the unit of length is represented by $[L]$ and the unit of force by $[F]$.

Two conventional rate-independent constitutive models are used to simulate the material response at the microscopic level:

- A J_2 isotropic elasto-plastic model characterized by the following material parameters: Young's modulus, E_μ, Poisson ratio, ν_μ, yield stress, $\sigma_{\mu Y}$ and fracture energy per unit of surface area, $G_{\mu F}$.
- A scalar isotropic elastic-damage model characterized by: $E_\mu,\ \nu_\mu,\ \sigma_{\mu u},\ G_{\mu F}$, where $\sigma_{\mu u}$ represents the ultimate uniaxial limit strength.

Linear and/or exponential strain softening models are assumed in both material responses, see [36,37] for a detailed description of these conventional constitutive models. Conventional implicit schemes are used for the integration of such constitutive models. A constitutive regularization method based on the concept of *Smeared Crack Approach* (*SCA*) [31], is adopted. Thus, the initial softening modulus $H_{\mu 0}$ which depends, among other parameters, on the micro-structural material characteristic length $\ell_{ch} = E_\mu G_{\mu F}/\sigma^2_{\mu Y}$, is regularized as shown in Table 1. In the following examples, the localization bandwidth, ℓ_μ, is chosen in advance according to the size of the finite element mesh. However, it is noted that in more general problems, this parameter is a result derived from the *RVE* analysis and the evaluation of the localization domain: Ω^L_μ.

Except for the coupled macro–micro problem of Section 5.6, the incremental strains inserted in the micro-cell domain, $\{d\boldsymbol{\varepsilon}_R, \mathcal{I}^L_{\boldsymbol{y}}(d\boldsymbol{\beta})\}$, are parameterized as follows:

$$d\boldsymbol{\varepsilon}_R = d\chi(t)\,(\boldsymbol{\Lambda}\otimes^s\boldsymbol{\Theta}); \quad \boldsymbol{\Lambda} = [\cos(\Lambda), \sin(\Lambda)]^T; \quad \boldsymbol{\Theta} = [\cos(\Theta), \sin(\Theta)]^T \tag{67}$$

$$\mathcal{I}^L_{\boldsymbol{y}}(d\psi(t)\,d\boldsymbol{\beta}) = d\psi(t)\,\phi^L_\mu(\boldsymbol{y})\,\frac{(d\boldsymbol{\beta}\otimes^s\boldsymbol{n})}{\ell_M}; \quad d\boldsymbol{\beta} = [\cos(\beta), \sin(\beta)]^T; \quad \ell_M = \ell_\mu\,\frac{|\Omega_\mu|}{|\Omega^L_\mu|} \tag{68}$$

where Λ, Θ and β are arbitrary angles to be defined in each example, $\phi^L_\mu(\boldsymbol{y})$ is the localization function, given by expression (42), and $\boldsymbol{n} = [\cos(\eta), \sin(\eta)]^T$, with η analytically determined in each case, is the unit vector normal to the macro-cohesive crack $\mathcal{S}$ and parameterized through the angle η. The coefficients $d\chi$ and $d\psi$ define the magnitude of the regular and localized strain increments, respectively.

Sections 5.2–5.5 are devoted to analyze the objectivity of the *RVE* homogenized response with respect to the micro-cell size. Thus, for such numerical examples, we define: (i) a basic heterogeneous micro-structural cell, called RVE_1 (the term *RVE* is used in the sense explained in the remark 2.1 of Section 2), and (ii) two additional micro-cells, named RVE_2 and RVE_3, which are a repetition of the basic heterogeneous cell RVE_1. The homogenized constitutive response is computed and compared for the three micro-cells using two multi-scale approaches:

- The *ClaMM*, described in Section 3, for the complete loading history. No kinematical enrichment ($d\boldsymbol{\beta} \equiv \mathbf{0}\ \forall t$) is incorporated during the complete analysis. The micro-mechanical problem is entirely driven by $d\boldsymbol{\varepsilon}_R$. In this case, a monotonically increasing value of $d\boldsymbol{\varepsilon}_R$ is applied during the loading process.
- The *FOMF*, which consists of the *ClaMM* discussed in Section 3 sequentially coupled at time $t = t_N$ to the *CohMM* (see Section 4). In this case, for $t > t_N$ a change in the macro-kinematics, characterized by $\{d\boldsymbol{\beta}, \boldsymbol{n}\}$, is induced and inserted into the micro-cells. The evolution of these fields is ruled by expression (68). Furthermore, for $t > t_N$, we also control the regular strain increment $d\boldsymbol{\varepsilon}_R$. In some tests we adopt: $d\boldsymbol{\varepsilon}_R = \mathbf{0}$ for $t > t_N$. In other situations, $\boldsymbol{\varepsilon}_R$ is decreased, as it should be expected when the complete macroscopic problem is considered. In any case, for $t > t_N$, the localized inserted strain term, $\{d\boldsymbol{\beta}, \boldsymbol{n}\}$, is dominant compared with $d\boldsymbol{\varepsilon}_R$. Thus, the cohesive homogenized response is not very sensitive to the particular choice about the inserted regular value $d\boldsymbol{\varepsilon}_R$.[1]

For all testes, the "*Minimal Kinematical Restriction*" is considered for the *Standard Boundary Condition "SBC"*, defined in Γ_μ through Eq. (51). For the *Non-Standard Boundary Condition* in Γ^L_μ, see Eq. (52), the "*NSBC-Minimal Kinematical Restriction*" has been adopted, except for the application to situations involving micro-structures with voids (see Sections 5.4 and 5.6) where the "*NSBC-Linear Boundary Condition*" has been applied.[2] Plane strain conditions are considered in all cases.

5.2. Micro-structures with homogeneous strain localization bands

5.2.1. Case 1-(a): horizontal strain localization bands

The first test consists of micro-cells with embedded "*homogeneous*" strain localization bands. The geometry for the basic heterogeneous micro-structure, RVE_1, is shown in Fig. 6(a) where we define: $h = b = 1[L]$ and $\alpha = 0^\circ$. The additional micro-cell domains, RVE_2 and RVE_3, which are used in the *objectivity* analysis, are also shown in Fig. 6(b) and (c). The material M_1 is linear-elastic whereas the material M_2 is characterized by an isotropic elastic-damage relation endowed with linear and exponential strain-based softening models. Table 2 describes the material properties for M_1 and M_2. The localization bandwidth, ℓ_μ, represents the thickness where the micro-strain field localizes. The value $\ell_\mu = 0.091\ [L]$ has been adopted for the three *RVEs*, coinciding with the finite element size in the $\boldsymbol{n}$-direction. The regularized initial softening modulus, $H_{\mu 0}$, is computed from expressions given in Table 1.

Fig. 6(f) shows the RVE_1-mesh which consists of 3 quadrilateral finite elements, while the discrete model for the RVE_2 and RVE_3 contains 6 and 9 elements, respectively.

The first numerical simulation is obtained considering: $\Lambda = \Theta = 90^\circ$, $d\chi = 1e-5$, see Fig. 6(d). Notice that from this

Table 1
Initial softening modulus $H_{\mu 0}$, according to the adopted constitutive model and the *SCA*.

	Linear softening	Exponential softening
J_2-plasticity	$H_{\mu 0} = \frac{E_\mu}{2}\frac{\ell_\mu}{\ell_{ch}}$	$H_{\mu 0} = E_\mu\frac{\ell_\mu}{\ell_{ch}}$
Elastic-damage	$H_{\mu 0} = \frac{1}{2}\frac{\ell_\mu}{\ell_{ch}}$	$H_{\mu 0} = \frac{\ell_\mu}{\ell_{ch}}$

[1] In a fully coupled multi-scale environment, the incremental macro-kinematics $\{d\boldsymbol{\varepsilon}_R, d\boldsymbol{\beta}\}$ will be obtained from the solution of the macro-equilibrium problem.

[2] In the context of *kinematically-based* multi-scale formulations, the application of the *Minimal Kinematical Constraint* is equivalent to imposing an *Uniform Traction Boundary Condition* on the micro-cell boundary. Whenever the stiffness of a micro-constituent intersecting the *RVE*-boundary goes to zero, the uniform traction also goes to zero and so, the minimally constrained multi-scale model provides an invalid homogenized response. The situation is worse if a pore reaches the *RVE*-boundary. In such cases, alternative multi-scale models are preferred. This argument, and taking into account the possibility of finding pores being cut by the strain-localization band Ω^L_μ, justifies the use of the *Linear* multi-scale model that is proposed for the *NSBC*. Independently of the previous comment and after various numerical experiments our conclusion is that, in general, the *Linear Boundary Condition* is an appropriate selection for the *NSBC*.

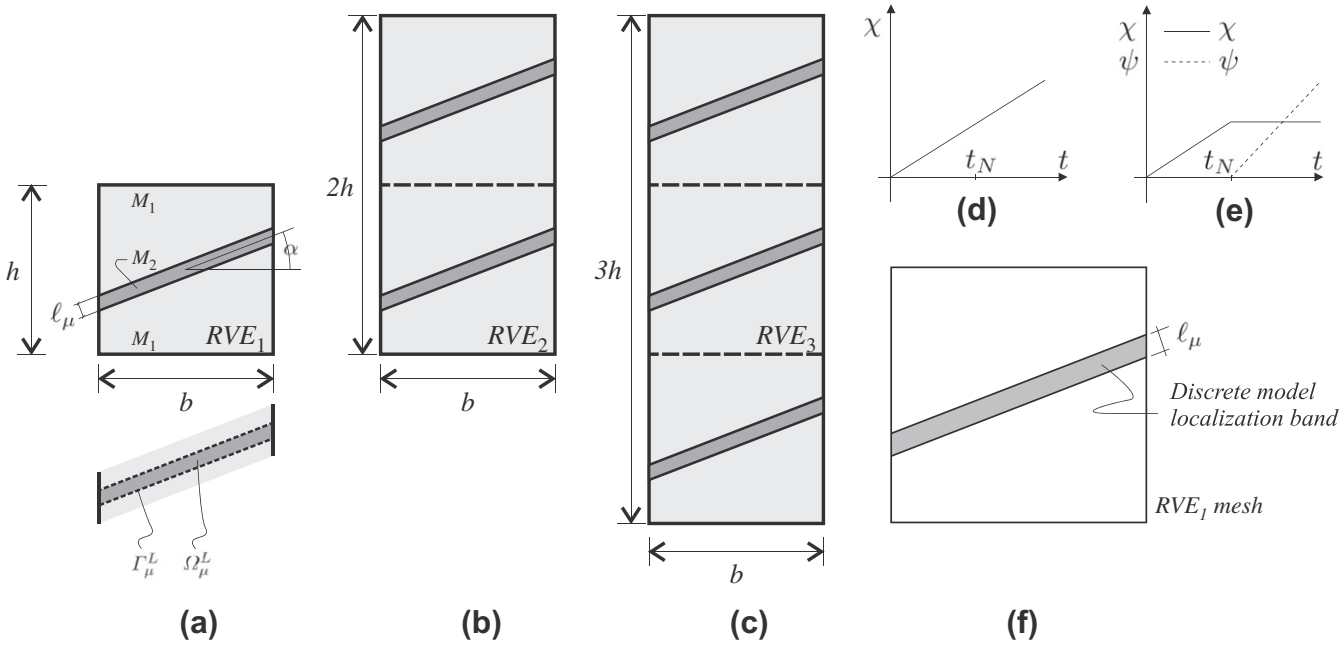

Fig. 6. Micro-structures with homogeneous strain localization bands: (a) RVE_1 (3 finite elements in the discrete model), (b) RVE_2 (6 finite elements in the discrete model), (c) RVE_3 (9 finite elements in the discrete model), (d) χ-function used for the *ClaMM*, (e) χ-function and ψ-function used for the *FOMF*, (f) Finite element discretization for the RVE_1.

Table 2
Material properties for the micro-structures displayed in Fig. 6.

	E_μ [F/L^2]	ν_μ	$\sigma_{\mu u}$ [F/L^2]	$G_{\mu F}$ [F/L]	ℓ_{ch} [L]
Material: M_1	2.1e4	0.2	–	–	–
Material: M_2	2.5e3	0.2	42	0.60	0.85

setting, we model micro-structures with horizontal softening-bands subjected to a purely axial regular strain in the vertical direction, i.e. only $\boldsymbol{\varepsilon}_{Ryy} \neq 0$, see Eq. (67).

Fig. 7(a) and (b) display the homogenized stress–strain constitutive relation in terms of the axial components (σ_{yy} vs. $\boldsymbol{\varepsilon}_{Ryy}$) that are obtained with the *ClaMM* and considering both, linear and exponential, softening models. During the elastic range, indicated as *A*–*B* in these figures, the macro mechanical responses are identical for the three considered *RVE*-sizes. Thus, the constitutive *ClaMM* is objective with respect to this parameter. However, a regular macro-strain increase after crossing the point *B* originates, for different *RVE* sizes, a very marked non-objective mechanical response, as displayed by curves denoted *B*–C_1, *B*–C_2 and *B*–C_3.

Point *B* marks the (pseudo-) time instant in which the *Classical* homogenized response loses objectivity. It agrees with the nucleation time, t_N, obtained using the procedure based on the spectral properties of the Homogenized Tangent Constitutive Tensor, $\boldsymbol{C}$, introduced in Section 2.2. The vector $\boldsymbol{n}$, also given by such a criterion, is consistent with the direction of the softening bands defined in the micro-structure.

Fig. 8 shows the results obtained with the *Cohesive Multi-scale Model (CohMM)* after crossing the point *B* ($t > t_N$). The homogenized *cohesive* responses are depicted in terms of the cartesian components T_y vs. β_y, see Fig. 8(a) and (b). For $t > t_N$, the (incremental) inserted strain localized mode, $\mathcal{I}_{\boldsymbol{y}}^L(d\boldsymbol{\beta})$, is characterized by: $\beta = 90^\circ$, $d\psi = 1.5e-4$ and $\eta = 90^\circ$. In addition, the regular component, $\boldsymbol{\varepsilon}_R$, remains constant and equal to $\boldsymbol{\varepsilon}_R(t_N)$. Fig. 6(e) depicts a schematic representation of the functions $\chi(t)$ and $\psi(t)$ that

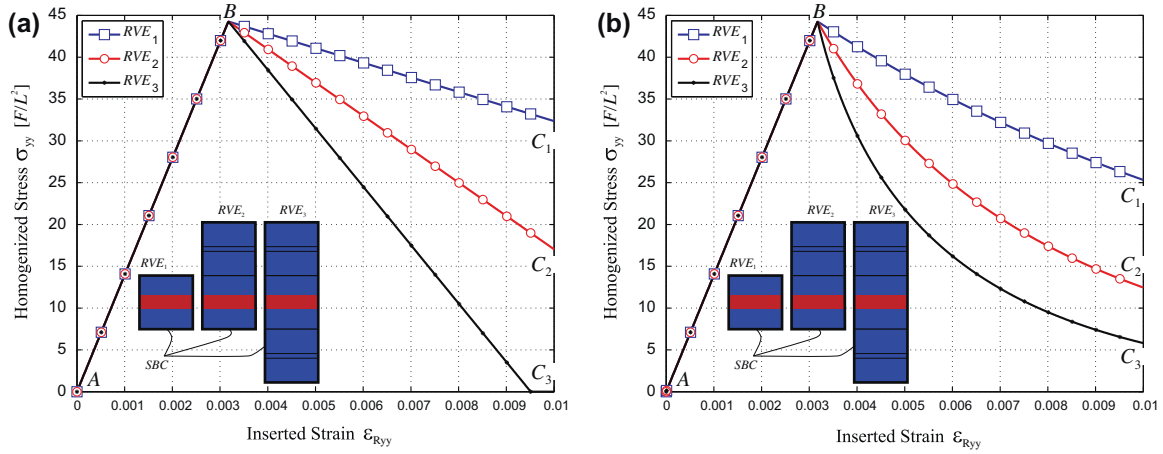

Fig. 7. Homogenized stress–strain relation (σ_{yy} vs. $\boldsymbol{\varepsilon}_{Ryy}$) obtained using the *ClaMM*: (a) linear softening model, (b) exponential softening model.

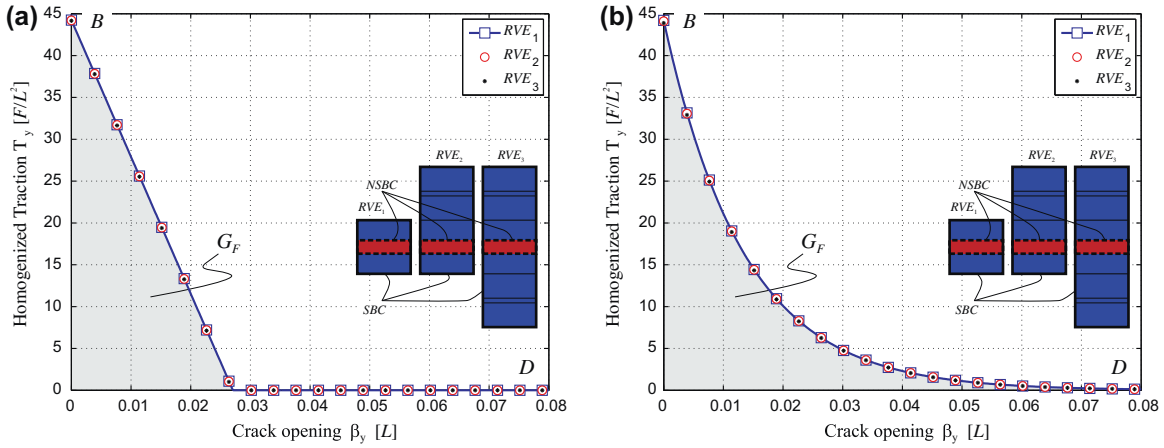

Fig. 8. Homogenized cohesive response (T_y vs. β_y) obtained using the proposed *CohMM* for $t > t_N$: (a) linear softening model, (b) exponential softening model.

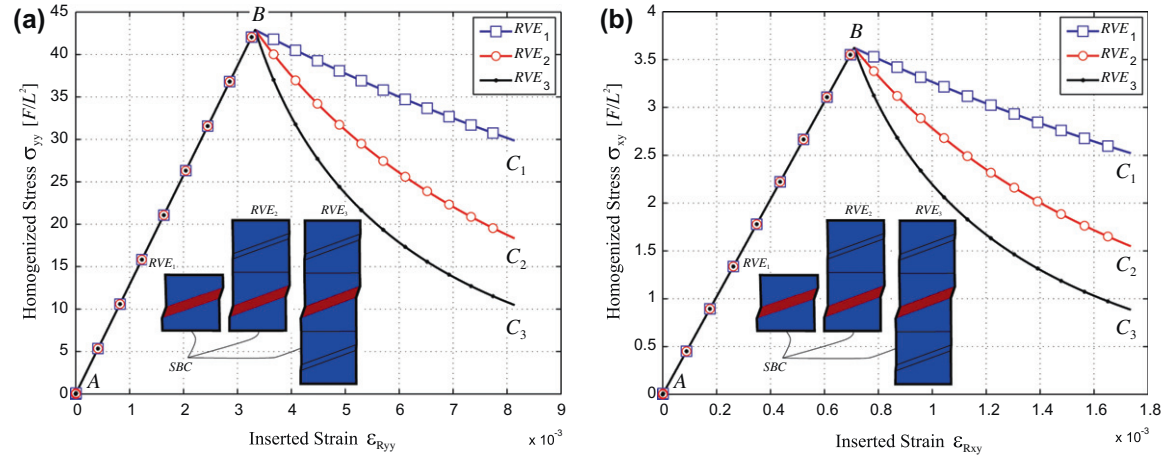

Fig. 9. Homogenized stress–strain response obtained using the *ClaMM*: (a) Axial stress–strain relation (σ_{yy} vs. $\boldsymbol{\varepsilon}_{Ryy}$), (b) Shear stress–strain relation (σ_{xy} vs. $\boldsymbol{\varepsilon}_{Rxy}$).

control the generalized strains during the loading history, from the beginning of the analysis. Note that the selected set of parameters defines a pure Mode I of fracture for the macro-cohesive crack.

Fig. 8 evidences that the *CohMM* provides an objective cohesive response during the post-critical regime. This property holds for both strain-softening damage models, linear and exponential, see the curves denoted as *B–D* in Fig. 8(a) and (b), respectively.

The area under the curve T_y–β_y, i.e. the gray shaded zones in Fig. 8(a) and (b), defines the fracture energy per unit of surface area at macro-level, here denoted as G_F. Note that the new multi-scale cohesive formulation returns an objective measure of G_F, irrespective of the *RVE*-size. In this particular case, due to the simplicity of the test[3], the macro-fracture energy obtained by the integration of the curve T_y–β_y, agrees with the fracture energy defined for the material at the micro-level ($G_F \equiv G_{\mu F}$), for both softening-based damage models.

The whole constitutive response, given by the proposed variational *FOMF*, provides two homogenized responses for different time intervals: (i) the *ClaMM* solution, for $t < t_N$, range *A–B* in Fig. 7, and (ii) the *CohMM* solution, for $t > t_N$, range *B–D* in Fig. 8.

[3] The onset of the non-linear behavior at the micro-scale coincides with the activation of the crack at macro-level and the softening-band is homogeneous in the micro-scale.

5.2.2. Case 1-(b): inclined strain localization bands

A second set of numerical simulations, considering identical material properties for M_1 and M_2, is analyzed. For the sake of simplicity, only an exponential softening rule is adopted. Inclined bands of material with softening, characterized by an angle $\alpha = 20^\circ$, define the topology of the heterogeneous micro-structure.

The increments of regular strains, $d\boldsymbol{\varepsilon}_R$, and the localized component, $\mathcal{I}_{\boldsymbol{y}}(d\boldsymbol{\beta})$, inserted into the micro-scale, are defined by: $\Theta = \beta = 60^\circ$, $\Lambda = 110^\circ$ and η, with η determined with the crack nucleation criterion. As a result, once the cohesive crack is activated at the macro-level, a Mixed Mode of fracture is simulated. Minimal kinematical restriction is applied on the boundary Γ_μ of Ω_μ. Observe that this type of kinematical constraint is consistent with the nucleation and subsequent development of *inclined* softening bands, whereas others types of boundary conditions, such as Linear or Periodic, do not admit such failure pattern.

The coefficients that control the generalized loading history, $d\chi(t)$ and $d\psi(t)$, are similar to those defined in the previous case 1-(a), see Fig. 6(d) and (e).

Numerical results obtained with the *ClaMM* are shown in Fig. 9. Fig. 9(a) depicts the homogenized stress–strain constitutive response in terms of the axial components, σ_{yy} vs. $\boldsymbol{\varepsilon}_{Ryy}$, while Fig. 9(b) displays the curve σ_{xy} vs. $\boldsymbol{\varepsilon}_{Rxy}$. In the pre-critical regime, denoted as *A–B* in the plots, the macro-mechanical response is objective with respect to the *RVE*-size. However, after crossing the point *B*, this property is lost, see the ranges B–C_1, B–C_2 and B–C_3 in the same Figure. Larger *RVE*-sizes provide more brittle

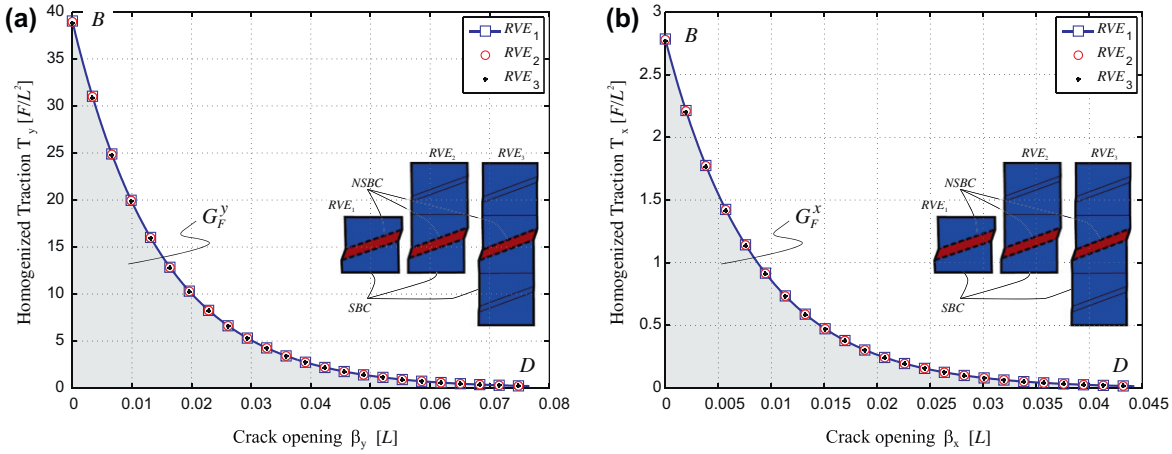

Fig. 10. Homogenized cohesive response obtained using the *CohMM* for $t > t_N$: (a) T_y vs. β_y plot, (b) T_x vs. β_x plot.

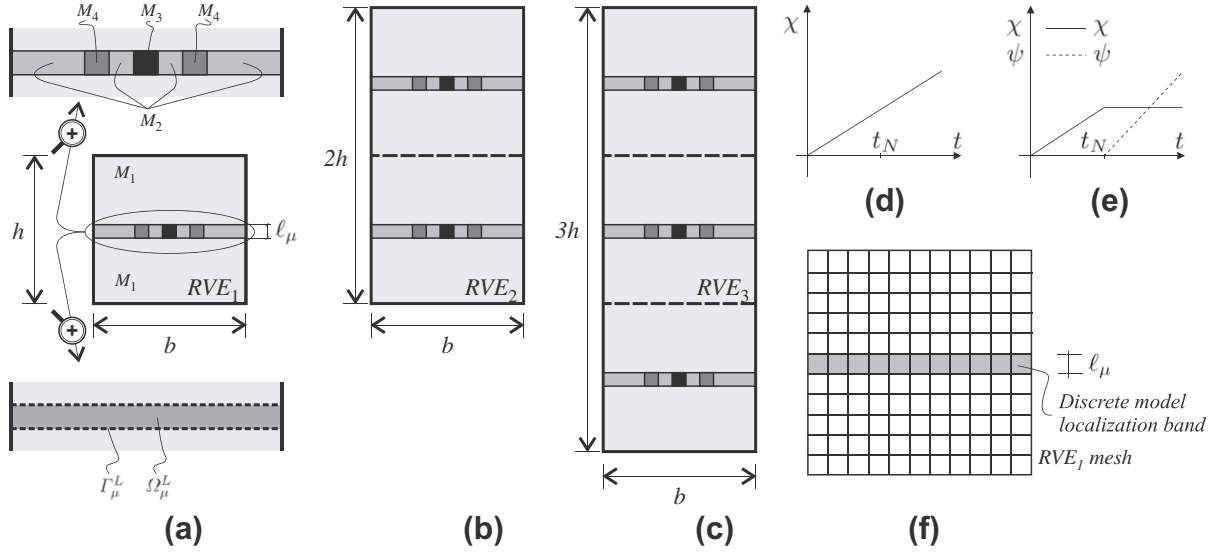

Fig. 11. Micro-structures with non-homogeneous strain localization bands: (a) RVE_1, (b) RVE_2, (c) RVE_3, (d) χ-function used for the *ClaMM*, (e) χ-function and ψ-function used for the *FOMF*, (f) Finite element discretization for the RVE_1.

Table 3
Material properties for the micro-structures depicted in Fig. 11.

	E_μ [F/L²]	ν_μ	$\sigma_{\mu Y}$ [F/L²]	$G_{\mu F}$ [F/L]	ℓ_{ch} [L]
Material: M_1	2.1e5	0.3	–	–	–
Material: M_2	2.0e4	0.3	42e1	3.80	0.43
Material: M_3	2.0e4	0.3	25e1	0.70	0.224
Material: M_4	2.0e4	0.3	48e1	21.00	1.82

homogenized macro-responses. This result proves that the notion of a classical *RVE* is lost in the context of material failure whenever the standard homogenization rules are used.

As explained above and by considering the bifurcation analysis of Section 2.2, the point *B*, as well as the angle η, are automatically detected during the simulations. In this case we obtain $\eta = 110^\circ$ agreeing almost exactly with the angle of the normal to the pre-defined band with strain softening in the *RVE*.

Solutions obtained with the *CohMM* are displayed in Fig. 10. The Fig. 10(a) depicts the homogenized cohesive response in terms of the components T_y vs. β_y and Fig. 10(b) plots the T_x vs. β_x component. Observe that the *CohMM* returns an objective mechanical response, insensitive to the *RVE*-size.

In this case, the fracture energy at the macro level, G_F, is obtained as the addition of the areas under the curves T_y–β_y, here denoted as G_F^y, and T_x-β_x denoted G_F^x, i.e. $G_F = G_F^y + G_F^x$ (see the gray shaded zones in Fig. 10(a) and (b)). Due to the simplicity of the test, the computed value of G_F agrees with the fracture energy adopted for the material M_2: $G_{\mu F} = 0.60$ [F/L].

In summary, the proposed *FOMF*, which includes both the *ClaMM* for $t < t_N$ and the *CohMM* for $t > t_N$, provides an objective mechanical response during the complete loading history.

5.3. Micro-structures with non-homogeneous strain localization bands

The heterogeneous micro-structural pattern modeled in this Section has horizontal strain localization bands composed of *different* softening materials, resembling the presence of obstacles and weaker inclusions during the propagation of the micro-failure mechanisms.

The basic heterogeneous micro-cell geometry, denoted RVE_1, is observed in Fig. 11 as well as the additional micro-cell domains RVE_2 and RVE_3, with the characteristic dimensions: $h = b = 1[L]$. The material M_1 is linear-elastic, whereas the materials $\{M_2, M_3, M_4\}$ which compose the bands, are characterized by

isotropic J_2 elasto-plastic models equipped with linear softening, see in particular the zoomed picture in Fig. 11(a). Table 3 describes the material parameters. Dissimilar values have been assigned to the yield stress ($\sigma_{\mu Y}$) and the fracture energy ($G_{\mu F}$), and thus to ℓ_{ch}, for M_2, M_3 and M_4. Note that the localization bandwidth, $\ell_\mu = 0.091$ [L], coincides with the finite element size in the $\boldsymbol{n}$-direction.

Fig. 11(f) depicts the RVE_1-mesh composed of 121 quadrilateral finite elements. The discrete model for the RVE_2 and RVE_3 contains 242 and 363 elements, respectively.

The increments of generalized strains transferred from the macro to the micro scale, are characterized through the following angles: $\Lambda = \eta$ (η is evaluated with the nucleation criterion, resulting: $\eta = 90^\circ$), $\Theta = \beta = 0^\circ$. For the simulations based on the *ClaMM*, it is adopted $d\chi = 1e-5\ \forall\, t$, see Fig. 11(d). Alternatively, for the *CohMM* formulation, we select: $d\chi = 1e-5$ for $t \leqslant t_N$, $d\chi = 0$ for $t > t_N$ and $d\psi = 5e-4$ for $t > t_N$, see Fig. 11(e). Note that the described set of strain loading parameters, defines a pure shear deformation mode for both, the pre-critical and the post-critical regime.

Fig. 12(a) shows the homogenized stress–strain constitutive response, in terms of the cartesian components σ_{xy} vs. $\boldsymbol{\varepsilon}_{Rxy}$, obtained with the *ClaMM*. Due to the presence of weak material inclusions in the micro-cell domain, material M_3, the non-linear behavior begins at the point denoted A' in the figure, which is significantly below the limit load point. Point B denotes the macro-bifurcation position ($t = t_N$) defined with the criterion of Section 2.2. During the range A'–B, there exist degradation mechanisms with evolution of softening at the micro-level. However, such irreversible processes are not enough to induce material instability at the macro scale. This situation describes a stable energy dissipation regime at the macroscopic level even when softening is taking place in regions of the micro-cell. Observe that the *ClaMM* provides an objective homogenized constitutive response in the whole range A–B, which includes a purely linear elastic behavior (A–A') and an elasto-plastic response due to micro-material softening (A'–B). After crossing the point B, the classical formulation loses constitutive *objectivity* with respect to the *RVE*-size, see the ranges B–C_1, B–C_2 and B–C_3, in Fig. 12(a), which correspond to the solutions of the RVE_1, RVE_2 and RVE_3 micro-cells, respectively.

Point B is correctly detected with the nucleation criterion, which also provides the angle $\eta = 90^\circ$ defining the unit vector $\boldsymbol{n}$ that characterizes the localized macro-deformation mode. In the proposed multi-scale formulation, a macro-cohesive crack, with normal $\boldsymbol{n}$ and displacement jump $\boldsymbol{\beta}$, is nucleated after crossing

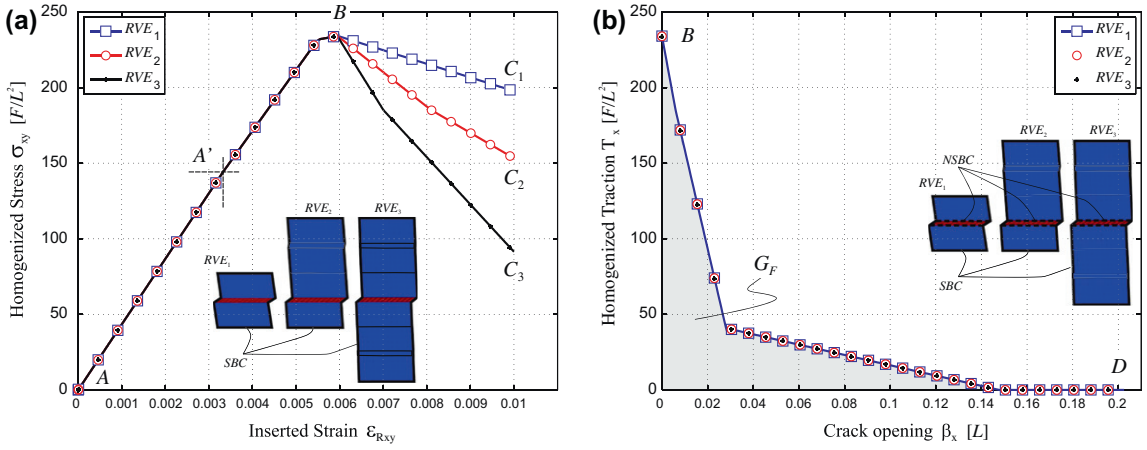

Fig. 12. Homogenized response for micro-structures with non-homogeneous localization bands: (a) σ_{xy} vs. $\boldsymbol{\varepsilon}_{Rxy}$ relation obtained using the *ClaMM*, (b) T_x vs. β_x relation obtained using the *CohMM* for $t > t_N$.

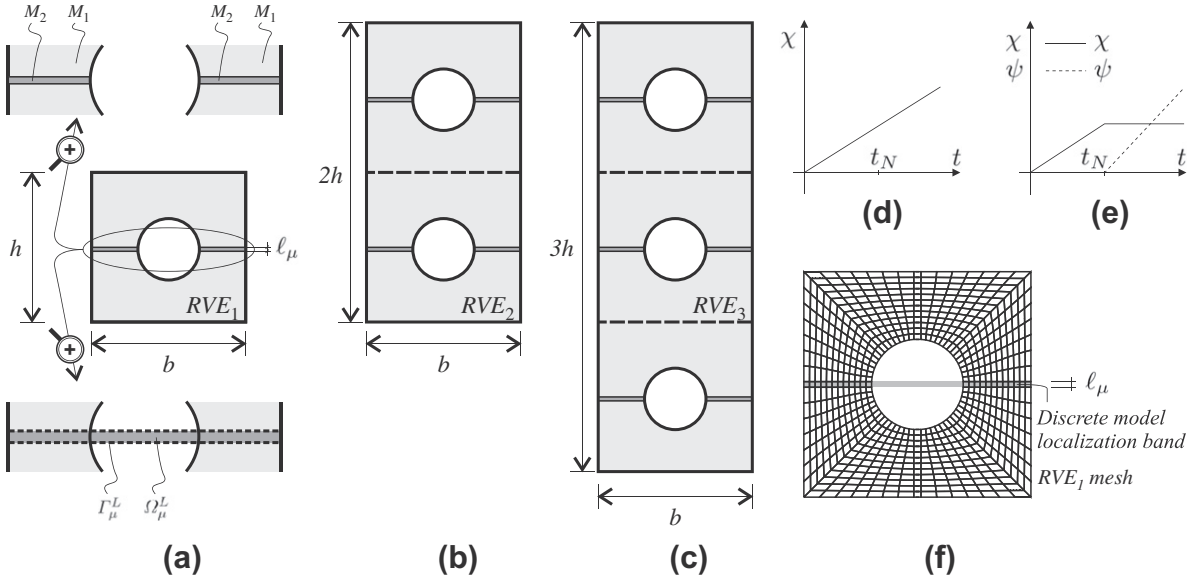

Fig. 13. Micro-structures with voids: (a) RVE_1, (b) RVE_2, (c) RVE_3, (d) χ-function used for the *ClaMM*, (e) χ-function and ψ-function used for the *FOMF*, (f) Finite element discretization for the RVE_1.

the point B. In Fig. 11(a), the definition of the localization sub-domain Ω_μ^L is sketched. Fig. 12(b) displays the homogenized cohesive response, represented in this case through the relation T_x vs. β_x, when the *CohMM* is used. Clearly, a physically admissible and *objective* macro-fracture energy, G_F, is captured, independently of the *RVE*-size, as shown in the range denoted: B-D in Fig. 12(b). Note also that, even though the elasto-plastic relations defined at the micro-level are characterized with linear softening models, the homogenized cohesive response is non-linear. This is a consequence of the *non-homogeneous* degradation mechanisms taking place in the micro-cell.

5.4. Micro-structures with voids

This test is based on a micro-structure containing two types of heterogeneities: (i) micro-voids and (ii) horizontal strain localization bands. Fig. 13 depicts the three considered micro-cell domains: RVE_1, RVE_2 and RVE_3. The characteristic dimensions of the problem are: $h = b = 1$ $[L]$, while the porosity ratio is 0.12. The material M_1 is linear elastic and M_2 is described by a J_2 elasto-plastic relation with an exponential strain softening model, see Fig. 13(a). Table 4 defines the parameters that characterize the material behavior at the micro-scale. In this case, the localization bandwidth is: $\ell_\mu = 0.025$ $[L]$.

For the RVE_1, Fig. 13(f) displays the finite element mesh used in the numerical simulation, which is composed of 720 quadrilateral elements. The discrete model for the RVE_2 and RVE_3 contains 1440 and 2160 elements, respectively.

The increments of the generalized macro-strains, inserted in the micro-cell, are defined through the angles $\Lambda = 90°$, $\Theta = \beta = 0°$, whereas the angle η is evaluated with the nucleation criterion of Section 2.2, resulting: $\eta = 90°$. These data agrees with a pure shear deformation mode applied to the *RVE* for both, the pre-critical and the post-critical regimes.

The first numerical simulation is performed using the *ClaMM*. We adopt a monotonically increasing regular macro-strain $\boldsymbol{\varepsilon}_R$, which is controlled by the incremental coefficient $d\chi = 2e - 5 \;\forall\, t$, see Fig. 13(d) and Eq. (67). Fig. 14(a) shows the homogenized stress–strain response: σ_{xy} vs. $\boldsymbol{\varepsilon}_{Rxy}$. Point B corresponds with the macro bifurcation time. *Objectivity* with respect to the *RVE*-size is observed only for the range denoted: A–B. After crossing the point B, the macro constitutive response becomes strongly dependent on the micro-cell size, see the ranges B–C_1, B–C_2 and B–C_3 in the same Figure.

Let us now consider the numerical results obtained with the *CohMM*. In this case, the (strain-driven) loading history is characterized by: $d\chi = 2e - 5$ for $t \leqslant t_N$, $d\chi = 0$ for $t > t_N$ and $d\psi = 6e - 4$ for $t > t_N$, see the plot of $\chi(t)$ and $\psi(t)$ in Fig. 13(e) and expression (68). Fig. 14(b) plots the homogenized cohesive response in terms of the components T_x vs. β_x. A physically admissible *objective* solution is computed for the three *RVE* micro-cells, see the range denoted: B–D in the same figure.

Fig. 13(a) shows the topology of the localization sub-domain Ω_μ^L evaluated with the methodology discussed in Section 4.3. Note that Ω_μ^L includes a portion of the void. Observe also that the proposed identification of Ω_μ^L ensures: (i) an *objective* constitutive behavior and (ii) the traction continuity condition between the *ClaMM* and the *CohMM* at the nucleation time, t_N, as can be seen by comparing the points denoted B in Fig. 14(a) and (b), respectively.

5.5. Macro-cohesive response undergoing a loading–unloading process

Loading–unloading strain-driven processes are evaluated during the macroscopic post-critical regime ($t > t_N$). For this purpose we analyze the problem presented in Section 5.2.2, Case 1-(b), with an isotropic exponential softening model.

The incremental strain history applied after the nucleation time ($t > t_N$) consists of: (i) removing quickly, the strain component $\boldsymbol{\varepsilon}_R$, simulating a sudden regular unloading mechanism at the macro-scale and (ii) controlling the inserted generalized strain, $\mathcal{I}_{\mathbf{y}}^L(d\boldsymbol{\beta})$, through a coefficient $d\psi = 1.5e - 4$ and inserting three unloading processes, which are simulated by changing, alternatively, the sign of $d\psi$.

The homogenized cohesive responses determined with the *CohMM* are shown in Fig. 15. The homogenized traction vs. crack opening relation is presented, for both cartesian components, in Fig. 15. The intrinsic mechanical response of the underlying micro-scopic damage model, is inherited at the macroscopic level. In this sense, subsequent unloading branches are characterized by a degraded elastic response related with the damage level taking place in the localized strain softening bands.

Considering three different micro-cell sizes, RVE_1, RVE_2 and RVE_3, the *CohMM* provides an *objective* homogenized cohesive

Table 4
Material properties for the micro-structures displayed in Fig. 13.

	E_μ $[F/L^2]$	ν_μ	$\sigma_{\mu Y}$ $[F/L^2]$	$G_{\mu F}$ $[F/L]$	ℓ_{ch} $[L]$
Material: M_1	2.1e5	0.3	–	–	–
Material: M_2	2.0e4	0.3	42e1	5.25	4.54

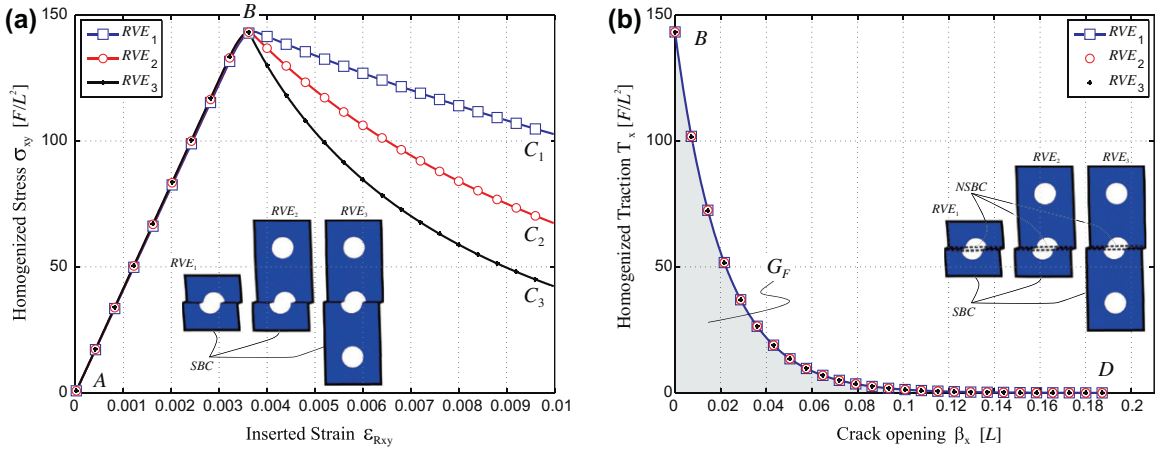

Fig. 14. Homogenized response for porous micro-structures with horizontal strain localization bands: (a) σ_{xy} vs. $\boldsymbol{\varepsilon}_{Rxy}$ relation obtained using the *ClaMM*, (b) T_x vs. β_x relation obtained using the *CohMM* for $t > t_N$.

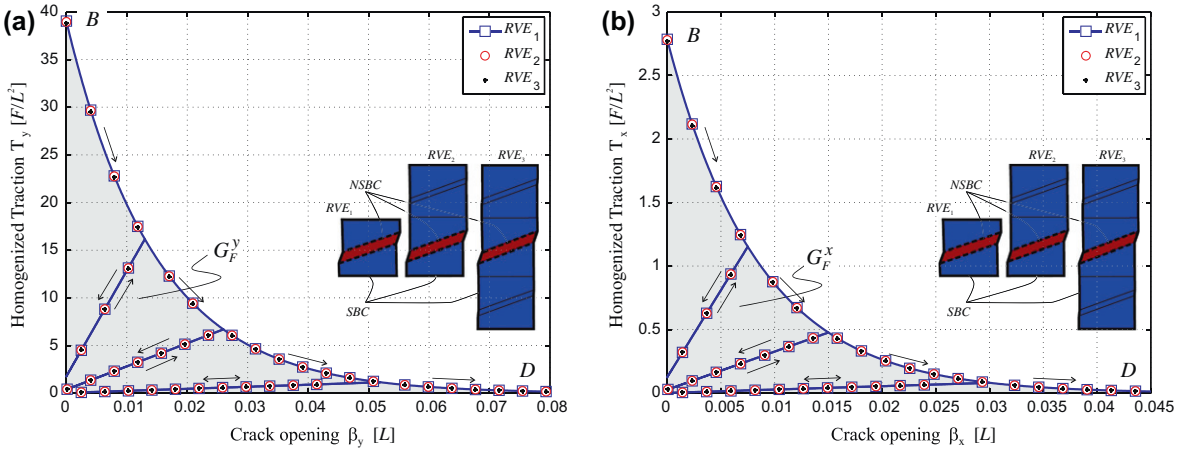

Fig. 15. Micro-structures with inclined strain localization bands subjected to loading–unloading processes. Homogenized cohesive response obtained with the *CohMM* for $t > t_N$: (a) T_y–β_y relation, (b) T_x–β_x relation.

response for both: loading and unloading regimes. The obtained macro-fracture energy G_F $(= G_F^y + G_F^x)$ is *objective* and agrees with the material property, $G_{\mu F}$, assigned to the damage-based material M_2, in the micro-scale.

5.6. A simple fully coupled macro–micro material failure simulation

This numerical experiment is devoted to show key additional aspects concerning the present multi-scale formulation, such as: (i) the numerical response of a fully coupled (macro–micro) simulation of the material failure at macro-scale as a result of strain localization at the micro-scale and (ii) the invariance of the homogenized macro-mechanical response with respect to finite element mesh refinement in the micro-scale. Objectivity with respect to *RVE*-size has been widely proved through the examples of Sections 5.2, 5.3, 5.4, 5.5, so it is not considered here.

In order to keep the presentation as simple as possible, a 1D stretching test is proposed. Fig. 16(a) schematizes the model at both physical scales. The problem geometry is defined through the following characteristic dimensions: $b = 180$ $[L]$ and $b_\mu = b/100$ $[L]$. At the macroscopic level, the specimen left end is clamped while its right end is stretched with a prescribed (monotonically increasing) displacement value: $\boldsymbol{u}_D$. The macro-structure is composed of two different materials: (i) a homogeneous elastic material, called M_1, modelled by means of a standard phenomenological linear-elastic law and (ii) an inelastic material located at the center of the specimen, which is equipped with a heterogeneous micro-structure and modelled using the proposed multi-scale for-

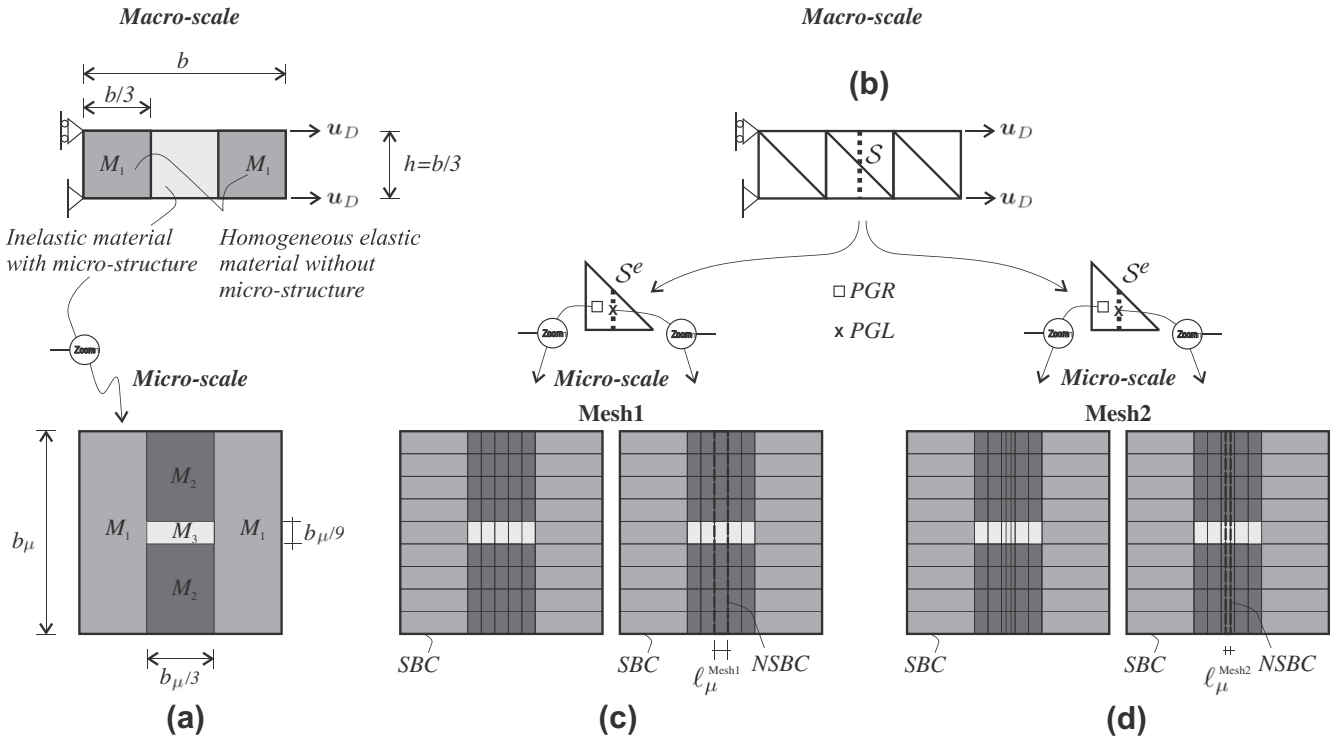

Fig. 16. 1D stretching test: (a) physical model description at the macro and micro scale levels, (b) macro-scale finite element model, (c) micro-scale finite element model: Mesh_1, (d) micro-scale finite element model: Mesh_2.

mulation, refer to Fig. 16(a). As can be seen in the sketch, the micro-scale also comprises dissimilar material behaviors, that is: (i) an elastic material M_1, (ii) a damage material M_2 with linear softening and (iii) the material M_3 which, in a first simulation (Sim_1), it is considered identical to M_2 and later, in a second simulation (Sim_2), it represents a void. Evidently, Sim_1 corresponds to a homogeneous softening band in the micro-scale. In Table 5, the material properties are described. They have the same physical meaning given in the previous examples. In addition, the same softening regularization formulas defined in Table 1 are considered.

The problem is numerically solved by applying the *FOMF* framework. Fig. 16 (right) show the finite element meshes used in the simulations. At the center of the macro-specimen, triangular finite elements with embedded strong discontinuities are considered (refer to Fig. 16 (b)) once the bifurcation condition (6) is reached in the corresponding *RVEs* (i.e. $\forall\ t > t_N$). Henceforth, and within the finite element technology context explained in the Appendix A, two integration points are activated (*PGR* and *PGL*) in order to impose the incremental traction equilibrium across the nucleated macro-cohesive crack. Note that *PGR* is linked to a classical *RVE* while *PGL* is linked to a *localized RVE* where to so-called *NSBC* has been included on Γ_μ^L. Thus, the homogenized response for *PGR* (in terms of "*stresses*") is obtained by applying the *ClaMM* and the homogenized response for *PGL* (in terms of "*cohesive tractions*") arises from the proposed *CohMM*.

In the micro-scale, two meshes of bi-linear quadrilateral finite elements are used, here referred to as: $Mesh_1$ and $Mesh_2$, see Fig. 16(c) and (d), respectively. The softening regularization is tackled by means of the smeared crack approach. Thus, the thickness of the localization band in the *RVE*-discrete model is ruled by the finite element size. In this context we have: $\ell_\mu^{Mesh_1} = b_\mu/15$ and $\ell_\mu^{Mesh_2} = b_\mu/45$, which correspond to the minimum size of the finite element in Mesh 1 and in Mesh 2, respectively.

All numerical simulations are carried out using *Minimal Kinematical Restriction* for the *SBC* and *Linear Boundary Conditions* for the *NSBC*. Plane strain conditions are assumed at both scales.

Table 5
Material properties for the 1D stretching test.

	E_μ $[F/L^2]$	ν_μ	$\sigma_{\mu Y}$ $[F/L^2]$	$G_{\mu F}$ $[F/L]$	ℓ_{ch} $[L]$
Material: M_1	3.0e4	0.0	–	–	–
Material: M_2	1.5e4	0.0	10.0	0.40	60.0
Material: M_3 (Sim_1)	1.5e4	0.0	10.0	0.40	60.0
Material: M_3 (Sim_2)	0.0	0.0	–	–	–

First, let us consider the case referred to as Sim_1. Fig. 17(a) shows the macroscopic Load–Displacement curve (P_x vs. u_D) on the right end of the specimen, while Fig. 17(b) displays the homogenized *cohesive* response of the macro-crack, in terms of the cartesian components T_x vs. β_x. For this 1D test, due to fact that the softening band is homogeneous in the *RVE*, the onset of the post-critical non-linear behavior at the micro-level coincides with the crack nucleation at the macro-level. The dissipation process takes place, exclusively, in the macro-cohesive crack; there is no *volumetric* dissipation at the macro-scale. Thus, both responses: the area under the Load–Displacement curve (per unit of cross sectional area) and the area under the Traction-Separation curve (T_x–β_x), provide the homogenized macro-fracture energy: $G_F = 0.40\ [F/L]$. As expected, the so obtained magnitude of effective fracture energy coincides with the value defined at the micro-scale, $G_{\mu F}$, for $M_2 \equiv M_3$. Note that the numerical results are insensitive to mesh refinement in the micro-cell.

For the Sim_2 case, a pore is included in the micro-cell definition. Fig. 18(a) shows the macroscopic Load–Displacement curve on the right end of the specimen. In this case, there is a *volumetric* stable dissipation period at the macro-level because inhomogeneous softening takes place in the *RVE*, see the range *A*-*B* in Fig. 18(a). When the damage reaches a critical level in the material M_2 (at the micro-scale), the bifurcation condition, given by Eq. (6), is satisfied and a macro-crack is nucleated. Henceforth, the dissipation only takes place in the cohesive interface. Fig. 18(b) displays the homogenized *cohesive* response of the macro-crack after crossing the bifurcation point ($t > t_N$), in terms of T_x vs. β_x. The area under the T_x-β_x curve gives the effective fracture-energy: $G_F \approx 0.35\ [F/L]$ which, as expected, is smaller than the fracture energy defined for the material M_2 ($G_{\mu F} = 0.40[F/L]$), in the micro-scale. In this case, the area under the macroscopic Load–Displacement curve is not directly related to the effective fracture energy, since it also includes mechanisms of stable *volumetric* dissipation. Note that, once again, the numerical results are insensitive to mesh refinement in the micro-cell.

Even though the presented stretching test is simple, the problem involves all the fundamental ingredients characterizing the *FOMF*, which have been implemented into a finite element code, such as: (i) a criterion to detect macroscopic bifurcation using homogenized information from the micro-scale, (ii) crack nucleation at the macro-scale, (iii) specific macro-kinematic insertion into the *RVE*-domain, (iv) generalized homogenization for stresses (v) imposition of *Standard* as well as *Non-Standard Boundary Conditions* in the micro-cell, among other rather conventional techniques. The numerical results at the macro-scale level are

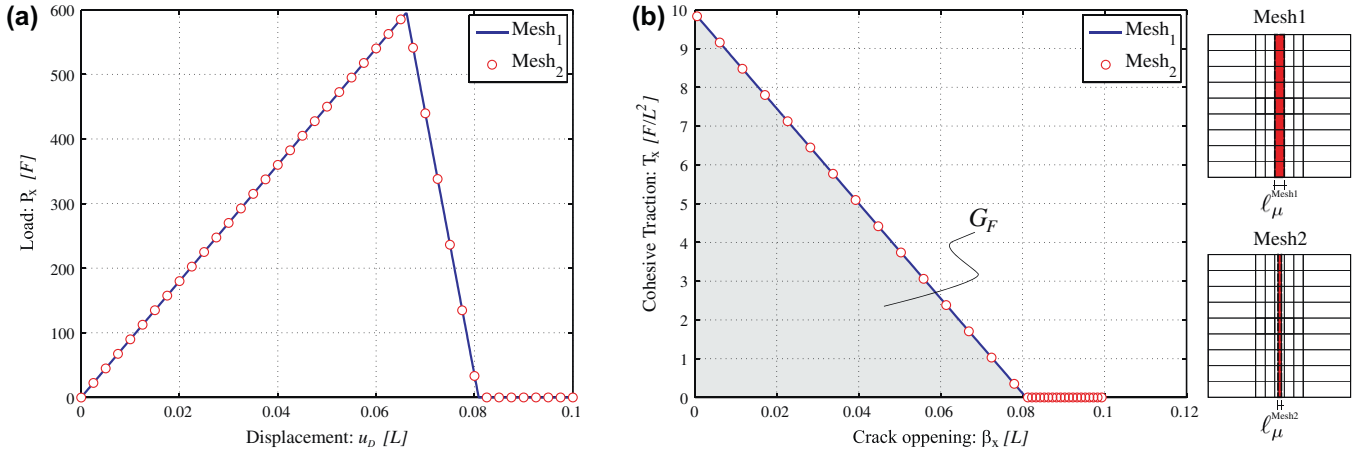

Fig. 17. 1D stretching test – Sim_1 (homogeneous softening band in the micro-scale): (a) macroscopic Load–Displacement curve P_x–u_D, (b) homogenized cohesive response T_x–β_x.

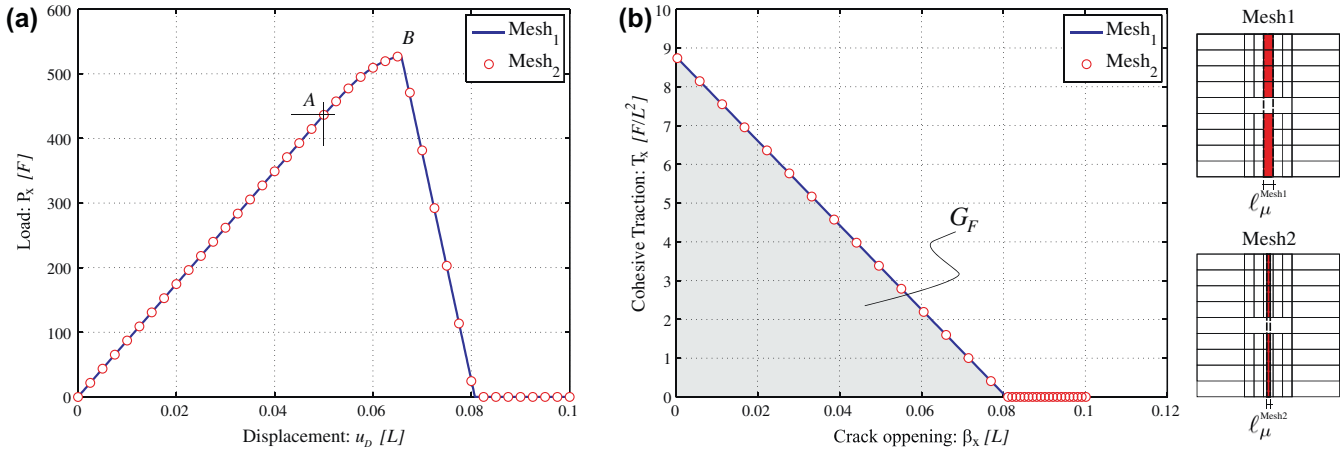

Fig. 18. 1D stretching test – Sim_2 (inhomogeneous softening band in the micro-scale): (a) macroscopic Load–Displacement curve P_x–u_D, (b) homogenized cohesive response T_x–β_x.

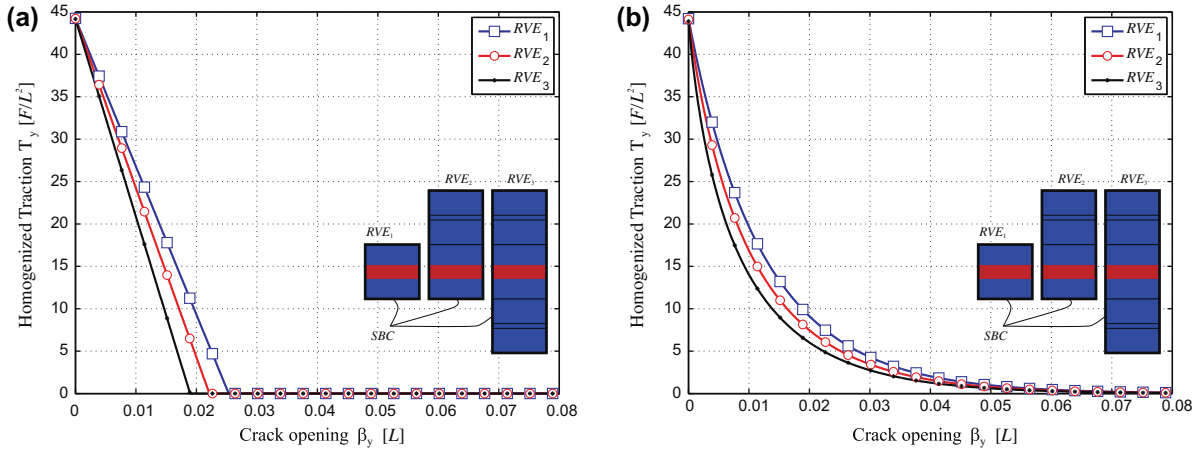

Fig. 19. Example N°1, Case 1-(a). Micro-structures with horizontal localization bands. Homogenized cohesive response obtained removing from the *Failure-Oriented Multi-scale Formulation* the additional *Non-Standard Boundary Condition (NSBC)* applied over the boundary of the localization sub-domain: (a) linear softening, (b) exponential softening.

physically consistent and insensitive to mesh refinement in the micro-scale.

6. Additional discussions

Regarding the *FOMF*, in this Section we investigate the effect that the removal of the *Non-Standard Boundary Condition (NSBC)* has on the *objectivity* of the cohesive response with respect to the *RVE*-size. Except for the *NSBC* removal, all the remaining kinematical and mechanical ingredients are preserved. Such a fictitious model is conceptually characterized by the collection of elements $\{\mathcal{I}^L_{\boldsymbol{y}}(\bullet), \mathcal{H}^L(\bullet), \widetilde{\boldsymbol{\mathcal{U}}}_\mu, \boldsymbol{\mathcal{V}}_\mu\}$ meaning that, in Box 3, we change $\widetilde{\boldsymbol{\mathcal{U}}}^L_\mu$ and $\boldsymbol{\mathcal{V}}^L_\mu$ by $\widetilde{\boldsymbol{\mathcal{U}}}_\mu$ and $\boldsymbol{\mathcal{V}}_\mu$, respectively. With this modified model, we evaluate the homogenized cohesive-response, via numerical simulations.

The proposed numerical test is based on the Case 1-(a) of Section 5.2.1. Fig. 19 shows the homogenized cohesive response, in terms of the components T_y vs. β_y, during the post-critical regime ($t > t_N$), for linear and exponential damage models. Note that, for the selected arbitrary strain-driven loading path, the *objectivity* of the constitutive response, with respect to the *RVE*-size, is lost. This result clearly evidences, even for this simple application, the fundamental role played by the *Kinematical Admissibility* concept along with the "*two*" derived *Kinematical Constraints*, i.e. the *Standard* and also the *Non-Standard Boundary Condition*, in order to obtain a mechanically well-posed (*objective*) homogenized response. Similar conclusions are obtained for all the tests in Section 5, when the *NSBC* is removed.

7. Conclusions

Throughout this work, two main contributions have been exposed in the context of *RVE-based Multi-scale Formulations*.

First, following a variational and kinematical based approach, the introduction of the so-called *Insertion Operator* $\mathcal{I}_{\boldsymbol{y}}(\bullet)$ allows us to generalize the Classical Multi-scale formulations. We showed that this operator determines the stress homogenization procedure which emerges from a duality relation with $\mathcal{I}_{\boldsymbol{y}}(\bullet)$ through the Hill–Mandel Variational Principle of macro-homogeneity. The equilibrium problem at the micro level and the stress homogenization procedure are direct consequences of the formulation, once the operator $\mathcal{I}_{\boldsymbol{y}}(\bullet)$ and the *Kinematical Admissibility* concept have been properly defined.

Second, we presented the *Failure-Oriented Multi-scale Formulation* (*FOMF*) that models heterogeneous materials whose micro-structure undergoes softening, nucleation of strain-localization bands and degradation phenomena. This formulation has been envisaged for situations in which micro-failure mechanisms are

eventually manifested through the nucleation and evolution of a macro cohesive crack. The *FOMF* includes two multi-scale sub-models that are consistently coupled: (i) a *Classical Multi-scale Model* (*ClaMM*) valid for the macro-scale stable constitutive response and (ii) a *Cohesive Multi-scale Model* (*CohMM*) that characterizes the cohesive crack evolution. In this sense, the model provides a standard *Stress–Strain Homogenized* response for the continuum part of the solid as well as a *Cohesive Homogenized Constitutive Relation* for the macro-crack.

The *FOMF* is based on a change of the *macro-to-micro* kinematical information transference after crossing a specific (pseudo-) time in the loading history, denoted in this article as the nucleation time t_N. A criterion based on the spectral properties of the *Homogenized Localization Tensor* was proposed to detect the nucleation time. After crossing this critical time, the macro-kinematics is generalized, accounting for strains and displacement discontinuities. Such a generalized macro-kinematics is consistently inserted in the micro-cell domain by means of a proper definition of the *Insertion Operator* $\mathcal{I}^L_{\boldsymbol{y}}(\bullet)$, jointly with the *Kinematical Admissibility* concept, related to it. In this context, two *Strain Homogenization Procedures* are obtained imposing, respectively, two constraint equations in the micro-cell kinematics: (i) the classical family of boundary conditions in the multi-scale formulations, on the micro-cell boundary and (ii) an additional new kinematical (non-standard) constraint on the boundary of the localization sub-domain.

The incorporation of the *Non-Standard Boundary Condition* (*NSBC*) guarantees the mechanical objectivity of the new formulation with respect to the *RVE*-size and also physically consistent results. Making use of such kinematics based ingredients and introducing the Hill–Mandel Principle of energetic equivalence, both the Stress Homogenization Operator $\mathcal{H}^L(\bullet)$ and the variational equilibrium problem to be solved at the micro-level, are consistently derived.

A criterion to detect the localization sub-domain Ω^L_μ, at the *RVE*-level, has also been presented. This strategy is fully consistent with the nucleation criterion of Section 2.2, and postulates that every point in the micro-cell in which the increment of strain fluctuation field tends to localize after the nucleation instant, should be included in the definition of Ω^L_μ. Such a methodology is quite general and it is not restricted to points in the micro-cell displaying unstable constitutive response. It represents a purely kinematics based criterion which, eventually, can include points that belong to materials still in a stable regime, weak elastic inclusion or, as a limit case, parts of voids that are crossed by the strain localization bands. The criterion allows to solve a problems of micro-structures with voids porous micro-structure problem (see Section 5.4), as also, opens a research area to future applications considering micro-structures composed of a softening matrix endowed with weak elastic materials (inclusions, fibers, etc). The correct definition of Ω^L_μ is a fundamental ingredient of the proposed *Failure-Oriented* multi-scale technique.

Within the proposed multi-scale approach, a length parameter ℓ_μ, has been introduced representing the thickness where strain-localization takes place in the *RVE*. From a strictly mechanical point of view, ℓ_μ has a clear physical meaning as a material property of the micro-constituents in the *RVE*. However, from the modelling point of view, ℓ_μ is not necessarily related to the Irwin's characteristic material length parameter ℓ_{ch}, and depends on the model that is used to regularize the material softening. Then, the effective fracture energy of the macro-crack, G_F, depends on ℓ_{ch}, the topology of the localization sub-domain Ω^L_μ, and the loading history, but not on ℓ_μ. On the other hand the characteristic length ℓ_M, present in the formulation, is immaterial and must be considered as a subsidiary parameter, which does not play any role. In fact, it is completely removed from the equations governing the problem.

The *FOMF* allows to tackle the question about the existence of a *RVE* domain when softening materials are considered.

Several numerical examples have been presented showing the capabilities of the formulation and the objectivity of the homogenized constitutive response with respect to the micro-cell size. We claim that the proposed methodology provides not only a well-posed variational and mechanical framework but also a computationally viable technique for modelling material failure in a multi-scale environment. Future works will address specific applications of the theory in order to incorporate large deformations, the analysis of complex heterogeneous micro-structures for real technological problems, as well as the use of more elaborated regularized constitutive models defined at the micro-scale level.

8. Acknowledgments

The first and third authors acknowledge the financial support from ANPCyT of Argentina through grant PICT 2008–1228 and from CONICET (PIP 2010–2012). The second and the fourth authors acknowledge the financial support from the Brazilian agencies CNPq and FAPERJ.

In addition, the authors wish to acknowledge to professor S.M. Giusti, from UTN-FRC-CONICET, for motivating discussions during the early development of the ideas behind this contribution. Computational support offered by S. Toro, from CIMEC-INTEC-UNL-CONICET, is also gratefully acknowledged.

Appendix A. Numerical implementation of the *FOMF*

A brief description of the numerical techniques used and developed for the computational implementation of the *FOMF*, within the context of a finite element code, is presented. We only highlight the *non-conventional* numerical aspects that must be developed in order to demonstrate the computational viability of this methodology.

A.1. The finite element technique

The *FOMF* is particularly adequate to be numerically tackled using the finite element method. Two different techniques are used: (i) one is that adopted for simulating the macro scale, where a strong discontinuity kinematics is assumed in the model, and (ii) an alternative technique is used to solve the *RVE*-problem. Considering that material softening is assumed in the micro-scale, the use of a mathematically well-posed approach becomes imperative in order to regularize the constitutive model and obtain mesh independent results.

A.1.1. Macro-scale finite element modeling with embedded strong discontinuities

A non-symmetric formulation with a kinematic enrichment, the addition of a new shape function which has one element support, such as that described in [27] and denoted *E-FEM* technique, is here adopted. This formulation introduces additional displacement modes which specifically capture the strong discontinuity kinematics, or macro-crack, defined by Eq. (8). Triangular elements with constant regular strain are used as the underlying FE technology. The enhanced shape function is discontinuous and the strong discontinuity mode is characterized by a constant displacement jump inside every finite element crossed by the crack, see Fig. 20(a). An advantageous characteristic of this technique is that the macro-crack could intersect the finite element in any arbitrary direction.

Fig. 20(b) depicts the most salient characteristic of this element. Two integration points (named *PGR* and *PGL*) are used to satisfy the additional traction incremental continuity condition across the discontinuity surface $\mathcal{S}^e$, given by the equation:

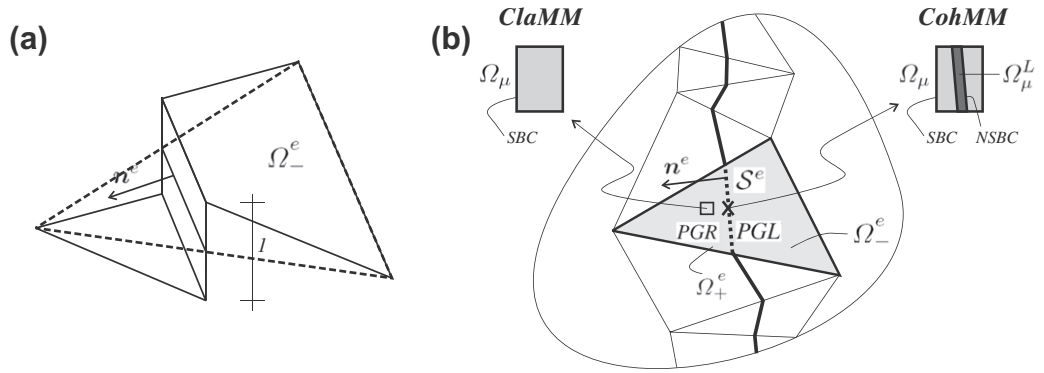

Fig. 20. Finite element technique with embedded strong discontinuities in the macro-scale: (a) shape function for the enhanced discontinuous mode, (b) a body discretized with a finite element mesh using the *E-FEM* methodology.

$$\underbrace{d\boldsymbol{\sigma}}_{PGR}\,\boldsymbol{n}^e = \underbrace{d\boldsymbol{T}}_{PGL} \tag{69}$$

where $\boldsymbol{n}^e$ is the unit vector normal to the cohesive interface $\mathcal{S}^e$ embedded into the finite element "*e*". Each Gauss point is linked to their corresponding *RVE*. Prior to the macroscopic bifurcation, both *RVEs* evolve identically, since a constant regular-strain triangle is adopted. Thus Eq. (69) is trivially fulfilled. After crossing the bifurcation point, each *RVE* evolves following different branches, as it is explained next.

The integration point *PGR* (square-symbol in Fig. 20(b)) is related with the regular component of the strain, $\boldsymbol{\varepsilon}_R$, see Eq. (10). Since $\boldsymbol{\beta}$, the displacement jump, is constant into the finite element, the second term in this expression vanishes. The *Classical Multi-scale Model* (*ClaMM*), defined in Section 3 and Box 2, is used for the stress homogenization procedure in the point *PGR*, during the complete loading history. Thus the corresponding incremental strain, $d\boldsymbol{\varepsilon}^e_R$, is homogenously inserted into the *RVE* and so, the increment of the homogenized stress, $d\boldsymbol{\sigma}^e$, is obtained. After detecting the macro-bifurcation condition, an elastic evolution is imposed in every point of this *RVE* forcing, in that way, an homogenized elastic unloading process in the regular Gauss point.

The integration point *PGL* (*x*-symbol in Fig. 20(b)) is related with the strain-localization phenomenon taking place in the micro-scale. The *Cohesive Multi-scale Model*, defined in Section 4 and Box 3, is used for homogenizing the traction in the point *PGL*, after bifurcation. Making use of the *Insertion Operator* (see Eq. (42)), the incremental generalized kinematics, characterized by $\{d\boldsymbol{\varepsilon}^e_R, \boldsymbol{\beta}^e, \boldsymbol{n}^e\}$, is inserted into the *RVE*. Note that both, the *Standard* as well as the *Non-Standard Boundary Conditions* (*SBC* and *NSBC*) are imposed to this *RVE*. The increment of the homogenized traction vector, $d\boldsymbol{T}^e$, is then obtained by using the generalized *Homogenization Operator*, given by expression (61).

A.1.2. Micro-scale (RVE) modeling

A smeared crack approach is used at the *RVE*-level. We do not give additional details about its numerical implementation because it is a rather standard technique, see for example [31]. The only requirement to be carefully implemented, is the re-definiton given to the continuum softening modulus, as it was shown in Table 1 and in each of the numerical examples.

A.1.3. Numerical treatment of the boundary conditions in the RVE

The algorithmic treatment given to the incremental displacement fluctuations of the *RVE*-boundary nodes, $\Delta\tilde{\boldsymbol{U}}_\mu$, to satisfy the required boundary conditions in different multi-scale models, deserves further explanation. Note that we introduce the notation $\Delta\tilde{\boldsymbol{U}}_\mu$, instead of $d\tilde{\boldsymbol{u}}_\mu$, to represent "*discrete incremental nodal displacement fluctuations*".

A.1.3.1. Standard Boundary Conditions (SBC) over the boundary Γ_μ.

Displacement restrictions arising either, in the minimum kinematical constraint defined through Eq. (25), in the periodic boundary model or in any other model, are satisfied by adding additional *linear* equations to the standard system of equations governing the micro-equilibrium problem. One equation for every specific constraint. In what follows, we define "*c*" being the list of degrees of freedom (d.o.f.) with imposed kinematical constraints and "*f*" the d.o.f. list without restrictions. Sub-index "*c*" (constrained) and "*f*" (free) denote the belonging of each d.o.f. in the FE model. Thus the vector of nodal incremental displacement fluctuations can be expressed as: $\Delta\tilde{\boldsymbol{U}}_\mu = [\Delta\tilde{\boldsymbol{U}}_{\mu(f)}\ \Delta\tilde{\boldsymbol{U}}_{\mu(c)}]^T$. We can write the restrictions arising in every multi-scale models through the linear restriction matrix $\mathbf{L}^{\text{ClaMM}}_\mu$, such that: $\Delta\tilde{\boldsymbol{U}}_{\mu(c)} = \mathbf{L}^{\text{ClaMM}}_\mu\,\Delta\tilde{\boldsymbol{U}}_{\mu(f)}$. With the previous definition at hand, for each current iteration "*k*" in the Newton–Raphson procedure at the micro-scale level, the incremental displacement fluctuation is obtained via static condensation, using the following expressions:

$$\Delta\tilde{\boldsymbol{U}}^{(k)}_{\mu(f)} = -\left[\mathbb{K}^{(k-1)}_\mu\right]^{-1}\Delta\mathbb{R}^{(k-1)}_\mu \tag{70}$$

$$\Delta\tilde{\boldsymbol{U}}^{(k)}_{\mu(c)} = \mathbf{L}^{\text{ClaMM}}_\mu\,\Delta\tilde{\boldsymbol{U}}^{(k)}_{\mu(f)} \tag{71}$$

$$\mathbb{K}^{(k-1)}_\mu = \mathbf{K}^{(k-1)}_{\mu(ff)} + \mathbf{K}^{(k-1)}_{\mu(fc)}\,\mathbf{L}^{\text{ClaMM}}_\mu + \left[\mathbf{L}^{\text{ClaMM}}_\mu\right]^T\mathbf{K}^{(k-1)}_{\mu(cf)} + \left[\mathbf{L}^{\text{ClaMM}}_\mu\right]^T\mathbf{K}^{(k-1)}_{\mu(cc)}\,\mathbf{L}^{\text{ClaMM}}_\mu \tag{72}$$

$$\Delta\mathbb{R}^{(k-1)}_\mu = \Delta\mathbf{R}^{(k-1)}_{\mu(f)} + \left[\mathbf{L}^{\text{ClaMM}}_\mu\right]^T\Delta\mathbf{R}^{(k-1)}_{\mu(c)} \tag{73}$$

where $\Delta\mathbf{R}_\mu$ represents the nodal incremental *Residue* vector of the micro-equilibrium problem, and $\mathbf{K}_\mu$ is the *Stiffness* operator defined as: $\mathbf{K}_\mu = \frac{\partial\Delta\mathbf{R}_\mu}{\partial\Delta\tilde{\mathbf{U}}_\mu}$.

Note that for the *SBC*, $\mathbf{L}^{\text{ClaMM}}_\mu$ should be evaluated once, since it does not change during the entire simulation. The formal construction of the linear restriction matrix $\mathbf{L}^{\text{ClaMM}}_\mu$ and the proper selection of the constrained d.o.f. of $\Delta\tilde{\boldsymbol{U}}_\mu$, have to be done in accordance with the particular class of multi-scale model under consideration, see Remark (3.2). This subsidiary issue is not additionally tackled in this contribution (refer to [12] and also [29] for specific implementation details).

A.1.3.2. Non-Standard Boundary Conditions (NSBC) over the boundary Γ^L_μ.

The numerical treatment given to the constraints on the incremental displacement fluctuations, $\Delta\tilde{\boldsymbol{U}}_\mu$, arising over the boundary nodes of Ω^L_μ (the so called *NSBC*), follows an identical procedure to that given for the *SBC*. The only difference lies on the fact that

NSBC are imposed once the bifurcation condition has been detected, at the macroscopic level, i.e. during the evolution of the mechanical problem.

From the algorithmic point of view and considering the strategy described in the previous section, the simultaneous imposition of the *SBC* and *NSBC* requires, at $t = t_N$, an update of the list "*c*" of d.o.f. with kinematical constraints including proper d.o.f. belonging to the boundary Γ_μ^L (consistently the list "*f*" is also updated). A unique reevaluation of the linear restriction matrix is also required which, in this context, is named $\mathbf{L}_\mu^{\text{CohMM}}$ including both the *SBC* and the *NSBC*. Then, the same expressions (70)–(72) are used to find $\Delta\tilde{\boldsymbol{U}}_\mu^{(k)}$ for each *k*-iteration, but replacing $\mathbf{L}_\mu^{\text{ClaMM}}$ by $\mathbf{L}_\mu^{\text{CohMM}}$:

$$\Delta\tilde{\boldsymbol{U}}_{\mu(f)}^{(k)} = -\left[\mathbb{K}_\mu^{(k-1)}\right]^{-1}\Delta\mathbb{R}_\mu^{(k-1)} \tag{74}$$

$$\Delta\tilde{\boldsymbol{U}}_{\mu(c)}^{(k)} = \mathbf{L}_\mu^{\text{CohMM}}\,\Delta\tilde{\boldsymbol{U}}_{\mu(f)}^{(k)} \tag{75}$$

$$\mathbb{K}_\mu^{(k-1)} = \mathbf{K}_{\mu(ff)}^{(k-1)} + \mathbf{K}_{\mu(fc)}^{(k-1)}\mathbf{L}_\mu^{\text{CohMM}} + \left[\mathbf{L}_\mu^{\text{CohMM}}\right]^T\mathbf{K}_{\mu(cf)}^{(k-1)} + \left[\mathbf{L}_\mu^{\text{CohMM}}\right]^T\mathbf{K}_{\mu(cc)}^{(k-1)}\mathbf{L}_\mu^{\text{CohMM}} \tag{76}$$

$$\Delta\mathbb{R}_\mu^{(k-1)} = \Delta\mathbf{R}_{\mu(f)}^{(k-1)} + \left[\mathbf{L}_\mu^{\text{CohMM}}\right]^T\Delta\mathbf{R}_{\mu(c)}^{(k-1)} \tag{77}$$

A.2. Determination of the bifurcation condition at the macro-scale

After the Newton–Raphson iterative procedure converges, at the macro-scale level, the bifurcation condition (6) is evaluated as follows. The homogenized constitutive tangent tensor, $\boldsymbol{C}$, is determined in every quadrature point (see Section 3.4), and thus we can compute $\boldsymbol{Q}$ (the localization tensor). Then, using a swept algorithm, we find the minimum value:

$$\omega = \min_{\theta=0:\Delta\theta:\pi}\det\left(\mathbf{Q}(\theta)\right) \tag{78}$$

by typically predefining an angle increment: $\Delta\theta$.

When the condition $\omega \leqslant 0$ is found for the first time, the flag indicating the bifurcation state of that quadrature point is set to "TRUE" (the nucleation time t_N is obtained). Both solutions (θ_1, θ_2) provided by (78) determine the unit normal vector to the crack $\boldsymbol{n}$ and $\dot{\gamma}$, used in Eq. (66).

References

[1] G. Barenblatt, The mathematical theory of equilibrium of cracks in brittle fracture, Adv. Appl. Mech. 7 (1962) 55–129.
[2] Z. Bazant, J. Planas, Fracture and Size Effect in Concrete and Other Quasibrittle Materials, CRC Press, Boca Raton, FL, 1998.
[3] T. Belytschko, H. Chen, J. Xu, G. Zi, Dynamic crack propagation based on loss of hyperbolicity and a new discontinuous enrichment, Int. J. Numer. Methods Engrg. 58 (2003) 1873–1905.
[4] T. Belytschko, S. Loehnert, J.H. Song, Multiscale aggregating discontinuities: a method for circumventing loss of material stability, Int. J. Numer. Methods Engrg. 73 (2008) 869–894.
[5] R. Christensen, K. Lou, Solutions for effective shear properties in three phase sphere and cylinder models, J. Mech. Phys. Solids 27 (1979) 315–330.
[6] E. Coenen, V. Kouznetsova, M. Geers, Novel boundary conditions for strain localization analyses in microstructural volume elements, Int. J. Numer. Methods Engrg., 90 (2012) pp. 1–21.
[7] D. Dugdale, Yielding of steel sheets containing slits, J. Mech. Phys. Solids 8 (1960) 100–108.
[8] J. Eshelby, The determination of the field of an ellipsoidal inclusion and related problems, Proc. R. Soc. Lond. A 241 (1957) 376–396.
[9] F. Feyel, J. Chaboche, *Fe*^{2} multiscale approach for modelling the elastoviscoplastic behaviour of long fibre SiC/Ti composite materials, Comput. Methods Appl. Mech. Engrg. 183 (2000) 309–330.
[10] J. Fish, Q. Yu, K. Shek, Computational damage mechanics for composite materials based on mathematical homogenization, Int. J. Numer. Methods Engrg. 45 (1999) 1657–1679.
[11] I. Gitman, H. Askes, L. Sluys, Representative volume: existence and size determination, Eng. Fract. Mech. 74 (2007) 2518–2534.
[12] S. Giusti, P.J. Blanco, E. de Souza Neto, R.A. Feijóo, An assessment of the Gurson yield criterion by a computational multi-scale approach, Eng. Comput.: Int. J. Comput.-Aid. Eng. Softw. 26 (3) (2009) 281–301.
[13] Z. Hashin, S. Shtrikman, A variational approach to the theory of the elastic behaviour of multiphase materials, J. Mech. Phys. Solids 11 (1963) 127–140.
[14] R. Hill, A self-consistent mechanics of composite materials, J. Mech. Phys. Solids 13 (1965) 213–222.
[15] A. Hillerborg, M. Modeer, P. Petersson, Analysis of crack formation and crack growth in concrete by means of fracture mechanics and finite elements, Cement Concrete Res. 6 (1976) 163–168.
[16] V. Kouznetsova, Computational homogenization for the multi-scale analysis of multi-phase materials, Ph.D. Thesis, Technische Universiteit Eindhoven, Netherlands, 2002.
[17] V. Kouznetsova, M. Geers, W. Brekelmans, Multi-scale constitutive modelling of heterogeneous materials with a gradient-enhanced computational homogenization scheme, Int. J. Numer. Methods Engrg. 54 (2002) 1235–1260.
[18] V. Kouznetsova, M. Geers, W. Brekelmans, Multi-scale second-order computational homogenization of multi-phase materials: a nested finite element solution strategy, Comput. Methods Appl. Mech. Engrg. 193 (2002) 5525–5550.
[19] M. Kulkarni, P. Geubelle, K. Matous, Multi-scale modeling of heterogeneous adhesives: effect of particle decohesion, Mech. Mater. 41 (2009) 573–583.
[20] K. Matous, M. Kulkarni, P. Geubelle, Multiscale cohesive failure modeling of heterogeneous adhesives, J. Mech. Phys. Solids 56 (2008) 1511–1533.
[21] J. Michel, H. Moulinec, P. Suquet, Effective properties of composite materials with periodic microstructure: a computational approach, Comput. Methods Appl. Mech. Engrg. 172 (1999) 109–143.
[22] C. Miehe, A. Koch, Computational micro-to-macro transition of discretized microstructures undergoing small strain, Arch. Appl. Mech. 72 (2002) 300–317.
[23] C. Miehe, J. Schroder, M. Becker, Computational homogenization analysis in finite elasticity: material and structural instabilities on the micro- and macro-scales of periodics composites and their interaction, Comput. Methods Appl. Mech. Engrg. 191 (2002) 4971–5005.
[24] T. Mori, K. Tanaka, Average stress in the matrix and average energy of materials with misfitting inclusions, Acta Metall. 21 (1973) 571–574.
[25] S. Nemat-Nasser, M. Hori, Micromechanics: Overall Properties of Heterogeneous Materials, Elsevier, 1999.
[26] V. Nguyen, O. Valls, M. Stroeven, L. Sluys, On the existence of representative volumes for softening quasi-brittle materials – a failure zone averaging scheme, Comput. Methods Appl. Mech. Engrg. 199 (2010) 3028–3038.
[27] J. Oliver, A.E. Huespe, Theoretical and computational issues in modelling material failure in strong discontinuity scenarios, Comput. Methods Appl. Mech. Engrg. 193 (2004) 2987–3014.
[28] J. Oliver, A.E. Huespe, J. Cante, G. Díaz, On the numerical resolution of the discontinuous material bifurcation problem, Int. J. Numer. Methods Engrg. 83 (2010) 786–804.
[29] D. Perić, E. de Souza Neto, R.A. Feijóo, M. Partovi, A.C. Molina, On micro-to-macro transitions for multi-scale analysis of non-linear heterogeneous materials: unified variational basis and finite element implementation, Int. J. Numer. Methods Engrg. 87 (2011) 149–170.
[30] J. Rice, The localization of plastic deformation, in: W. Koiter (Ed.), Theoretical and Applied Mechanics, 14th IUTAM Congress, Amsterdam, North-Holland, 1976, pp. 207–220.
[31] J. Rots, Computational modelling of concrete fracture, Ph.D. Thesis, Delft University. Netherlands, 1988.
[32] J. Rudnicki, J. Rice, Condition for the localization of deformations in pressure sensitive dilatant materials, J. Mech. Phys. Solids 23 (1975) 371–394.
[33] K. Runesson, N. Ottosen, D. Peric, Discontinuous bifurcations of elastic-plastic solutions at plane stress and plane strain, Int. J. Plasticity 7 (1991) 99–121.
[34] P.J. Sanchez, P.J. Blanco, A.E. Huespe, R.A. Feijóo, Failure-Oriented multi-scale variational formulation for softening materials, Technical Report P&D No. 6, LNCC-MCTI Laboratório Nacional de Computação Científica, 2011.
[35] E. Sanchez-Palencia, Non-homogeneous media and vibration theory, Lecture Notes in Physics, vol. 127, Springer-Verlag, Berlin, 1980.
[36] J. Simo, T. Hughes, Computational Inelasticity, Springer-Verlag, 1998.
[37] J. Simo, J. Ju, Strain- and stress-based continuum damage models – Part II: Formulation, Int. J. Solids Struct. 23 (1987) 841–869.
[38] J. Simo, J. Oliver, A new approach to the analysis and simulation of strain softening in solids, in: Z. Bazant, Z. Bittnar, M. Jirásek, J. Mazars (Eds.), Fracture and Damage in Quasi-Brittle Structures, E & FN Spon, 1994, pp. 25–39.
[39] J.H. Song, T. Belytschko, Multiscale aggregating discontinuities method for micro–macro failure of composites, Compos. Part B 40 (2009) 417–426.
[40] E. de Souza Neto, R.A. Feijóo, Variational foundation on multi-scale constitutive models of solids: small and large strain kinematical formulation, LNCC Research & Development Report No. 16, 2006.
[41] E. de Souza Neto, R.A. Feijóo, On the equivalence between spatial and material volume averaging of stress in large strain multi-scale solid constitutive models, Mech. Mater. 40 (2008) 803–811.
[42] C. Verhoosel, J. Remmers, M. Gutiérrez, R. de Borst, Computational homogenization for adhesive and cohesive failure in quasi-brittle solids, Int. J. Numer. Methods Engrg. 83 (2010) 1155–1179.
[43] J. Willis, Variational and related methods for the overall properties of composites, Adv. Appl. Mech. 21 (1981) 1–78.